2-1-2013

Assembly Of Surface Engineered Nanoparticles For Functional Materials

Xi Yu
University of Massachusetts - Amherst, xyu@chem.umass.edu

ASSEMBLY OF SURFACE ENGINEERED NANOPARTICLES FOR FUNCTIONAL MATERIALS

A Dissertation Presented

by

Xi Yu

Submitted to the Graduate School of the
University of Massachusetts Amherst in partial fulfillment
of the requirements for the degree of

DOCTOR OF PHILOSOPHY

February 2013

Chemistry

ASSEMBLY OF SURFACE ENGINEERED NANOPARTICLES FOR FUNCTIONAL MATERIALS

A Dissertation Presented

by

Xi Yu

Approved as to style and content by:

_____
Vincent M. Rotello, Chair

_____
Ricardo Metz, Member

_____
Nathan Schnarr, Member

_____
Alfred J. Crosby, Member

_____
Craig T. Martin, Department Head
Department of Chemistry

DEDICATION

To my family and people who contributed to this research

ACKNOWLEDGMENTS

First, I would like to thank my advisor, Prof. Vincent M. Rotello, for his encouragement, support and guidance. I have learned a lot from him. Over the past six years, he not only trained me how to design and perform an experiment, but also taught me how to be a scientist. I appreciate the kind of freedom he gave me to try something new.

I am grateful for the input and advice offered by my committee member, Prof. Ricardo Metz, Prof. Nathan Schnarr and Prof. Alfred J. Crosby during my studies. I would like to acknowledge their constructive comments throughout my research.

I really owe a lot to all the present and past members of the Rotello group. I have done most of my research in collaboration with group members. The friendly and collaborative environment in the lab was a real treat to work. Although every member helped me with more or less, I must mention some names, like Hao, Bappa, Chandra, Brian, Subinoy, Vikas, Ryan, Debu, Yi-cheun and Qian for their enormous help.

I would like to give special thanks to my collaborators, Dr. Boqian Yang, Dr. Serkan Eymur, Jonathan Pham and Dr. Vijay Singh for their great help in the experiment. Prof. Michael Barnes, Prof. Paul Lahti and Prof. DV provided their invaluable help from quantum mechanics to organic chemistry. Without them, I certainly cannot finish my research.

I want to express my gratitude to my family, relatives and friends. Without their hope, love and support this work would have been impossible. My family was always a support for me. My friends were always with me in fun as well as difficult times.

Most specially, I would like to thank my friends, Jian, Zhaochang, Zhun, Hao, Ying and Zhongjin. It is them who help me find out the ultimate significance of my work and how should I do to make my research more meaningful.

ABSTRACT

ASSEMBLY OF SURFACE ENGINEERED NANOPARTICLES FOR FUNCTIONAL MATERIALS

FEBRUARY 2013

XI YU

B.A., JILIN UNIVERSITY

M.A., JILIN UNIVERSITY

Ph.D., UNIVERSITY OF MASSACHUSETTS AMHERST

Directed by: Professor Vincent M. Rotello

Nanoparticles are regarded as exciting new building blocks for functional materials due to their fascinating physical properties because of the nano-confinement. Organizing nanoparticles into ordered hierarchical structures are highly desired for constructing novel optical and electrical artificial materials that are different from their isolated state or thermodynamics random ensembles. My research integrates the surface chemistry of nanoparticles, interfacial assembly and lithography techniques to construct nanoparticle based functional structures. We designed and synthesized tailor-made ligands for gold, semiconductor and magnetic nanoparticle, to modulate the assembly process and collective properties of the assembled structures, by controlling the key parameters such as particle-interface interaction, dielectric environments and inter-particle coupling etc. Top-down technologies such as micro contact printing, photolithography and nanoimprint lithography are used to guide the assembly into arbitrarily predesigned structures for potential device applications.

TABLE OF CONTENTS

Page

LIST OF TABLES

Table Page

LIST OF FIGURES

Figure Page

CHAPTER 1

ASSEMBLY OF SURFACE ENGINEERED NANOPARTICLES: FROM ARTIFICIAL ATOMS TO ARTIFICIAL MATERIALS

1.1 Nanoparticles

1.1.1 Introduction

Nanoparticles (NP) are nanometer scale clusters of metals, semiconductors, and magnetic material consisting of hundreds to thousands of atoms.[1, 2, 3] They represent hybrid systems intermediate between small molecular systems and macroscopic materials and exhibit a number of unique physical and chemical properties distinct from bulk material.

The novel properties of NPs arise in one hand from their enormous surface area, showing a dominance of the surface properties over bulk properties. On the other hand, they possess fascinating physical properties because of nano-confinement. The electronic structure, optical, and magnetic properties of materials can be tuned by varying the physical size of the crystal, leading to new phenomena, such as superparamagnetism of magnetic NPs,[4] surface plasmon resonance in Au and Ag nanoparticles,[5] and the size dependent band gap of semiconductor NPs.[6] The properties of NPs are tunable based on their component, size, shape, functionalized surface, and chemical surroundings. The unique properties of NPs have attracted great interest in the scientific community and have been utilized in various applications in chemistry, biology and material science, such as catalysis,[7] chemical and biological sensing,[8, 9] cell labeling and imaging, and optoelectronic device[10].

To date, a variety of nanoparticles were synthesized including metallic materials such as gold,[11] silver,[12] semiconductor materials such as cadmium selenide,[13] and magnetic materials such as $CoPt_3$ [14] and iron platinum [15] (Figure 1.1). Besides spherical nanocrystals, more complex

geometries such as rods, cylinders, prisms, cubes, tetrapods and hybrid compositions were also reported.[16]

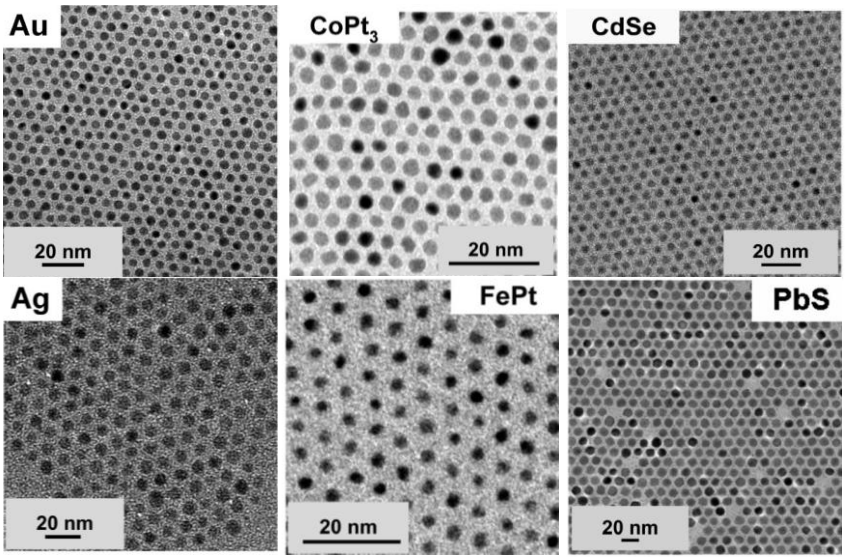

Figure 0.1 TEM images of metal (Au, Ag), magnetic ($CoPt_3$, FePt) and semiconductor (CdSe, PbS) nanoparticles. (reproduced from reference10)

1.1.2 Fabrication of monolayer-protected nanoparticles

NPs are usually synthesized through solution based colloidal chemistry method, formed by solution phase nucleation and growth process following precursors activation. The size and shape of NPs can be controlled by precursor concentration, temperature, and the capping ligand (type and concentration).[17] The organic ligand played a critical role in the colloidal nanoparticle preparation process as capping chemical to control the grow dynamics and they also serve to reduce enormous surface energy of bare nanoparticles, protecting them from agglomeration and improving their solubility. Since colloidal NPs synthesized in this way are covered by a self-assembled monolayer of organic ligands, they are sometimes called monolayer protected nanoparticles.[18]

Although the organic ligands are initially used as capping agent in the NP synthesis process, they have shown much more than simply protecting effect. It has been found that ligands can modulate the physical properties of NPs by ligand particle interaction. For example, ligands can modulate

the surrounding dielectric environment, [19] the electron energy level of the NP, [20, 21] or squeeze/expand the electron wavefunction of the NPs[21]. The ligands can also functionalize the surface of the particles that can be used in controlled catalysis,[22] sensing[23] and drug delivery[24] utilizing the special surface effect of the NPs (Figure 1.2).

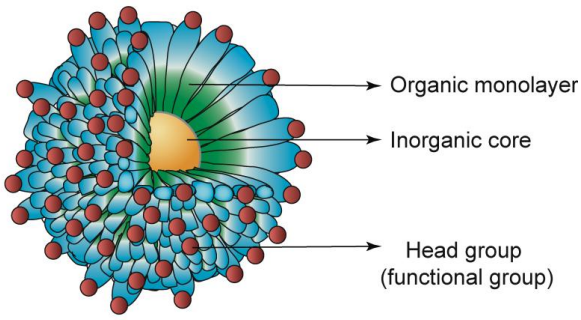

Figure 0.2 Schematic representing monolayer-protected nanoparticles, the inorganic core protected by an organic monolayer that can feature chemically different end group for myriad of applications

Table 0-1 Characteristics, ligands and representative applications for various metal and semiconductor and magnetic nanoparticles. (reproduced from reference 25)

Core material	Characteristics	Applications	Tail of Ligand(s)
Au	Optical absorption, fluorescence and fluorescence quenching, stability	Biomolecular recognition, delivery, sensing, thermal therapy	Thiol, disulfide, phosphine, amine
Pt	Catalytic property	catalyst, photocatalyst, sensing	Thiol, dithiol, phosphine, amine, isocyanide
Ag	Surface-enhanced fluorescence	Sensing	Thiol, disulfide
CdSe, CdS	Luminescence, photo-stability	Imaging, sensing	Thiol, phosphine, pyridine
Fe_2O_3/ Fe_3O_4	Magnetic property	MR imaging and biomolecule purification, Hyperthermia, opto-electronics electronic, magnetic devices.	Diol, dopamine derivative, amine, alkoxysilane, carboxylate
FePt, FePd	large uniaxial magnetocrystalline anisotropy	Magnetic recording	Thiol, Dopamine, carboxylate
SiO_2	Biocompatibility	Biocompatible by surface coating	Alkoxysilane

Various functionalized ligand can be introduced to the surface of the NPs by place-exchange process initially described by Murry for gold NP system.[18] Similar place-exchange reactions exist for other core materials, given the proper choice of ligands and exchange conditions. Table 1.1 listed various nanoparticles with different ligands and their applications.[25]

1.2 Nanoparticle Assemblies

NPs are often called artificial atoms due to their atomic-like behaviors. Since their sizes are comparable with characteristic wavelengths of electrons, electrons of the NPs can also exhibit a discrete, atomic-like spectrum of energies due to quantum confinement. Furthermore, this analogy can be extended to artificial nanocrystal solid, as well-defined groupings of plasmonically or electronically coupled NPs (Figure 1.3).[26, 27] Just as a gold crystal has properties distinct from single gold atom, or hydrogen molecule has properties different from two uncoupled hydrogen atoms, nanocrystal assemblies exhibit properties altered from those of the component nanoparticles due to organized structures and inter-particle coupling.[28] For example when Ag or gold nanoparticles aggregate into close packed network, their plasmon peak is shifted towards low energy and an increase in the bandwidth is observed due to coupled plasmon effect.[29]

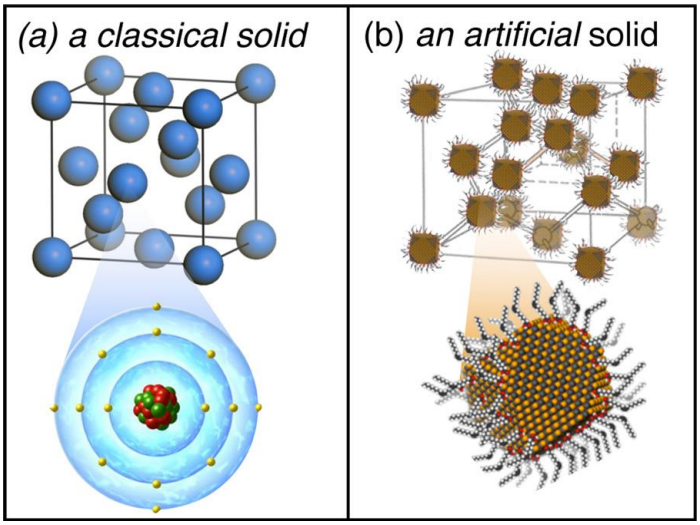

Figure 0.3 Schematic illustration of (a) classical solid comprised of atoms (i.e., carbon atoms in a diamond lattice) and (b) analogous artificial solid comprised of NQD as artificial atoms. (reproduced from reference 28)

Thus, organizing nanoparticles into desired structures and tuning their electronic coupling are of great importance for constructing novel optical and electrical artificial materials that are different from their isolated state or thermodynamics random ensembles.[30]

There is an intense search for strategies to organize NPs through self-assembly processes. NPs self-assembly refers to the process by which NPs, may with other discrete components, spontaneously organize by inherent or external interactions to reach a thermodynamic equilibrium aggregation state.[31, 32, 33]The assembly is driven by various type of inter particle forces, such as van der Waals, electrostatic, molecular, entropy, and surface tension,[34] or with the assistant of external forces, such as electric or magnetic field.[35, 36] Each of the interaction has its own magnitude and length scale (Figure 1.4).[37] A successful assembly depends on the delicate balance of various forces and can be used to construct hierarchical structures possessing orders at multi-scales. The interactions can be tuned by engineering the inorganic core (e.g. vdW) and applying appropriate surface chemistry. The dynamic nature of the non-covalent interactions can also be exploited to construct reversible and stimuli responsive assembly structures.

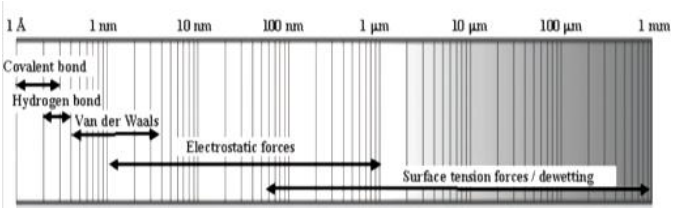

Figure 0.4 Interactions working at different length scales. (reproduced from reference 37)

Depending on the relative importance of different interactions, and also considering the purposes of different researches, assemblies can be generally categorized based on the assembly environment into three types: (i) assembly in bulk (ii) assembly at surfaces (iii) assembly at the interfaces.

1.2.1 Assembly in bulk

Self-assembly of NPs in bulk solution depends on homogeneous inter-particle interactions such as the vdW and magnetic forces of particles and intermolecular interactions such as hydrogen bonding, molecular dipole interactions. Thermo fluctuation in solution by solvent molecules also facilitates the assembly system to overcome local energy barriers to reach the thermodynamically most stable state.

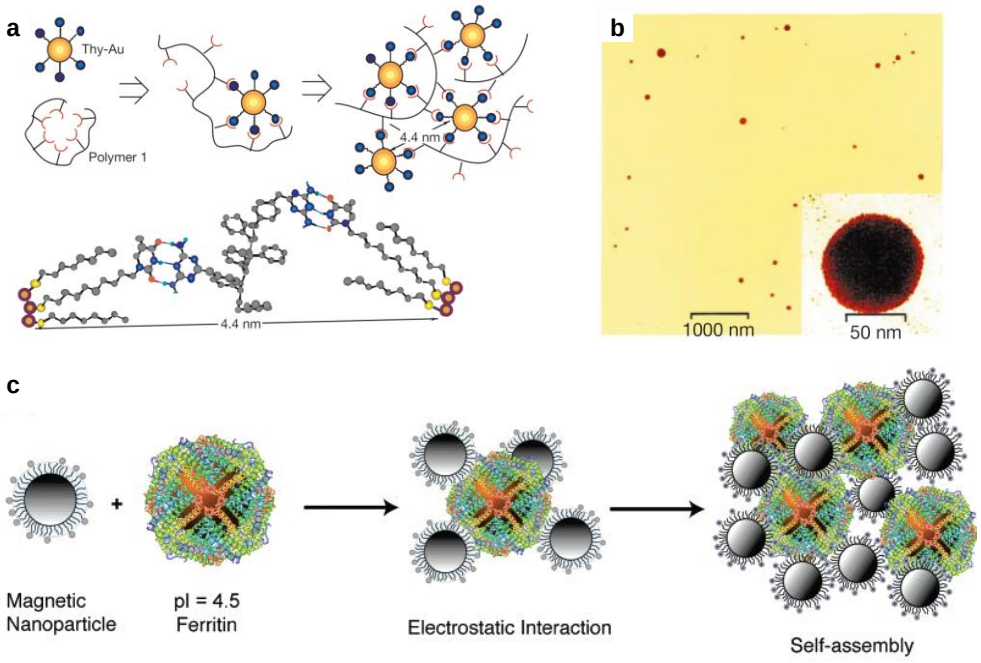

Figure 0.5 (a) "Bricks and mortar" assembly of Au NPs and polymer. (b) TEM images of the aggregates. (c) Magnetic Nanoparticles Assembled with Ferritin via Electrostatic Interaction (Reproduced from reference 39 and 40)

Exploitation of the spontaneous and directed assembly of surface functionalized NPs with synthetic macromolecules, polymers, dendrimers, and biomolecule through well controlled molecular interactions has been well investigated. Rotello group pioneered the use of "bricks and mortar" concept for organizing NPs into structured assemblies.[38] In earlier work, we have demonstrated the assembly of thymine functionalized Au NPs with diaminotriazine functionalized polystyrene via three point hydrogen bonding interaction (Figure 1.5a).[39] This method has been shown to generate discrete aggregation with network structure (Figure 1.5b). In

another work, ferritin and magnetic FePt NPs are assembled into bionanocomposites magnetic materials via electrostatic interaction (Figure 1.5c).[40] The ferritin provides added magnetic volume fraction to the magnetic nanocomposite and the assemblies showed different blocking temperature, net magnetic moment, coercivity, and remnance comparing to both of the components.

Assembly of 3D ordered colloidal aggregates is of great importance for the development of new solid materials with potential application in optoelectronic devices. Surface ligands are the key to control the precise balance between particle interaction and molecular interactions. Mirkin and coworkers used DNA modified NPs to assemble NPs lattices. They demonstrated that DNA

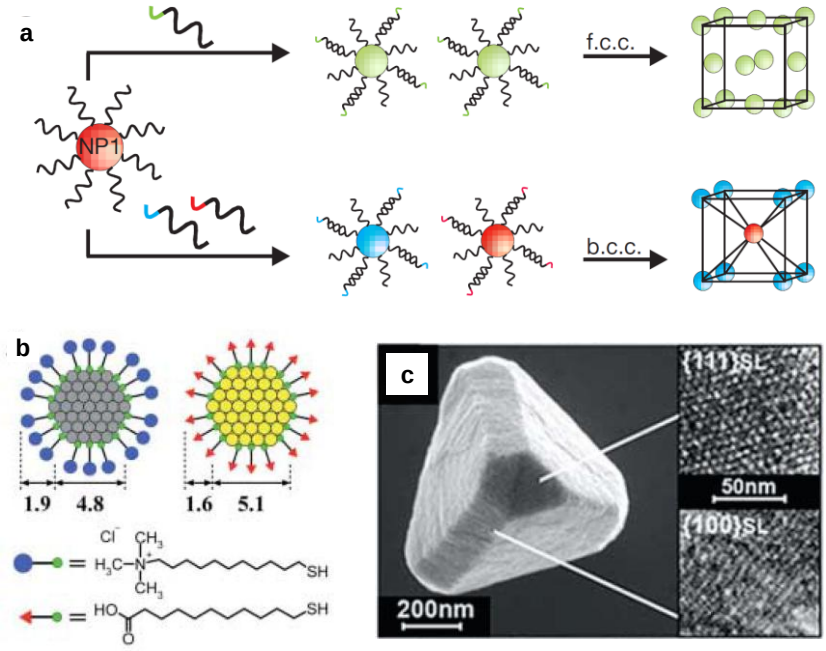

Figure 0.6 (a) Schematic of NPs used for electrostatic assembly (b) Au-Ag NPs macroscopic crystals formed after assembly. (c) Au NPs-DNA conjugate programmed for crystallization of NPs. (Reproduced from reference 41 and 42)

guided self-assembly of Au NPs can produce different crystalline states such as face-centered-cubic or body-centered-cubic crystal structures of NPs (Figure 1.6a) by changing the sequence of the DNA linker.[41] Similarly, Grzybowski et al fabricate crystals of diamond like lattice via

electrostatic interaction of NPs.[42] In their study they used oppositely charged metallic NPs of similar size for self-assembly (Figure 1.6b). Crystallization of NPs into a diamond-like structure (Figure 1.6c) is mediated by screened electrostatic interactions, where the particles interact by short-range electrostatic potentials.

1.2.2 Assembly at interface

Assembly at interface, liquid-air or immiscible liquids, is based on non-balanced intermolecular interactions at phase boundary.[33, 43] NPs are driven to the interface to decrease the surface energy of the system. Therefore the surface energies (surface tensions) between particle and two phases are critical parameters in the process, as shown in Figure 1.7. A detailed energy analysis showed that the decrease of the system energy by moving a particle to the interface is related to the effective radius (r) of the particle and the surface tension of the particle (p) with respect to oil (o) and water (w) by equation 1,

$$\Delta E = -\frac{\pi r^2}{\gamma_{o/w}}\left[\gamma_{o/w} - \left(\gamma_{p/w} - \gamma_{p/o}\right)\right]^2 \qquad (1)$$

through which we can conclude that big particles with equal wettability with water and oil are more stable at the interface.

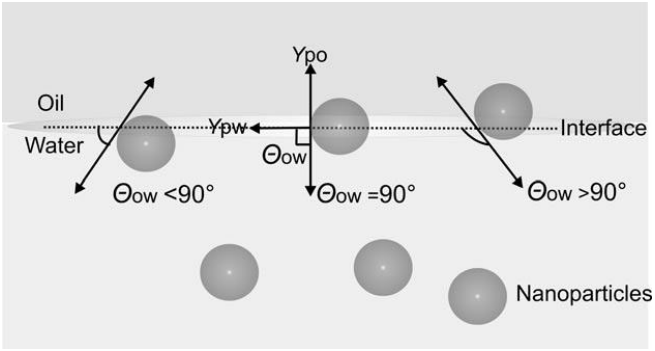

Figure 0.7 Interfacial assembly is governed by the surface tension of the particle (p) with respect to oil (o) and water (w) and the oil-water surface tension. Energy balance of particle assembly at interfaces is given by Equation 1. Particles with equal wettability with water and oil are more stable at interface, where contact angle Θ=90°.

Interface offers a naturally two dimension confined environment for assembly of 2D NP film, and surface chemistry is the key to modulate the wetting property of the NPs for a successful assembly. Duan and Mohwald et al prepared 2,2'-dithiobis[1-(2-bromo-2-methyl-propionyloxy)ethane] (DTBE) modified gold nanoparticle and 2-bromo-2-methylpropionic acid (BMPA) modified iron oxide nanoparticles (Figure 1.8).

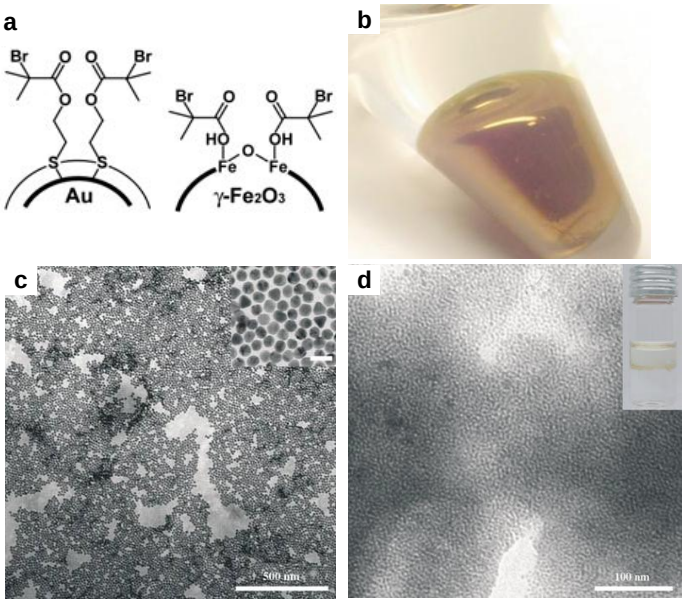

Figure 0.8 a) Schematic illustration of the structures of Au NP with DTBE (left) and Fe_2O_3 nanoparticles (right). b) Photograph of the self-assembled Au NP with DTBE nanoparticles at the water/toluene interface in a plastic Eppendorf tube. c) TEM image of the monolayer of 12-nm Au NP with DTBE nanoparticles, formed at the water/toluene interface; inset: high-magnification TEM picture, the scale bar is 25 nm. d) TEM image of the thin film of 4-nm Fe_2O_3 NP with BMPA nano-particles formed at the water/toluene interface. The yellow layer formed at the water/toluene interface is clearly visible in the photo- graph shown in the inset. (reproduced from reference 44)

The terminal 2-bromopropionate group of these ligands may render the contact angles of the nanoparticles at the water/oil interface close to 90°, driving nanoparticles to the water/oil interface and to self-assemble into closely packed arrays. Meanwhile, the possibility to form nanoalloy films at interfaces has also been demonstrated by co-assembly of silver and gold nanoparticles.[44] Hierarchical assembled structures can be obtained when combing other template

technique. For example, Russell et al combine self-assemble CdSe nanoparticles at the polymer solution–water droplet interface with the well-ordered hexagonal array breath figures that are made by the condensation of micrometer-sized water droplets on the surface of a polymer solution. Droplet array is the first level order and NPs film is the second in this structure.[45]

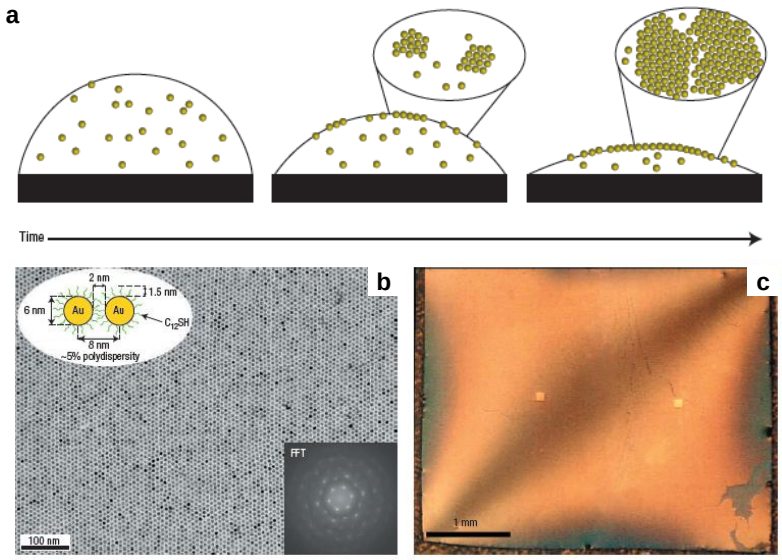

Figure 0.9 a) schematic diagram of the self-assembly process during the early stages of drying, showing how NPs are captured by a quickly receding liquid–air interface. b) micrograph of a typical monolayer dodecanethiol-ligated 6-nm gold NPs. The upper left inset schematically shows the arrangement of two neighboring NPs in the monolayer. The lower right inset is a fast Fourier transform of the image. c) top view of a fully formed, compact nanocrystal monolayer on the top surface of a thin liquid droplet. (reproduced from reference 46)

Interfacial assembly also proved to be an idea strategy for self-organization of NPs due to the dynamic nature, where continuous adjustment of the position of particles at the interface provides error-correction ability for ordered structure. NP at interface can move as random walk and aggregate, forming 2D aggregation with amorphous liquid like state or even 2D crystals, following similar nucleation and growth mechanism as crystallization in 3D. Nanoparticle assembly at liquid-air interface in the drying process has been approved an amazingly easy way to get ordered NPs 2D layer. Jaeger et al. reported the highly ordered gold NP monolayer formed at toluene-air interface in the evaporation process (Figure 1.9).[46] They found the ordered

monolayer of NPs is controlled by evaporation kinetics and particle interactions with the liquid–air interface. In the presence of an attractive particle–interface interaction, rapid early-stage evaporation dynamically produces a two-dimensional solution of nanoparticles at the liquid–air interface, from which nanoparticle islands nucleate and grow. Their theoretical model also predicts that controlling the interaction between the particles and the liquid–air interface is the key to the realization of highly ordered NP monolayer.

Another form of NP assembly at interface is NP stabilized emulsion, which is also called Pickering emulsions.[47] As has been shown in equation 1, adsorption of NP at the interface decreases the system free energy. This effect, combined with the inter-particle vdW attraction interaction, stabilized the emulsion droplets. Further stabilization of the emulsion has been achieved by incorporating other interactions by surface functionalization of NPs. Electrostatic, coordination chemistry etc. have been utilized through tailor-made ligands possessing charges[48] or coordination group such as terpyridine.[49]

Nanoparticles can also be used to assemble at the interface that instantaneously forms in the transition process from homogenous state to phase separation state of a mixed binary liquid system. The bicontinuous interface formed in the demixing process via spinodal decomposition can be stabilized by NPs that are neutrally wetted by both liquids. This so called bijel material would have many potential applications, for example, as micro-reaction media considering the semi-permeable property of the interface (Figure 1.10).[50, 51]

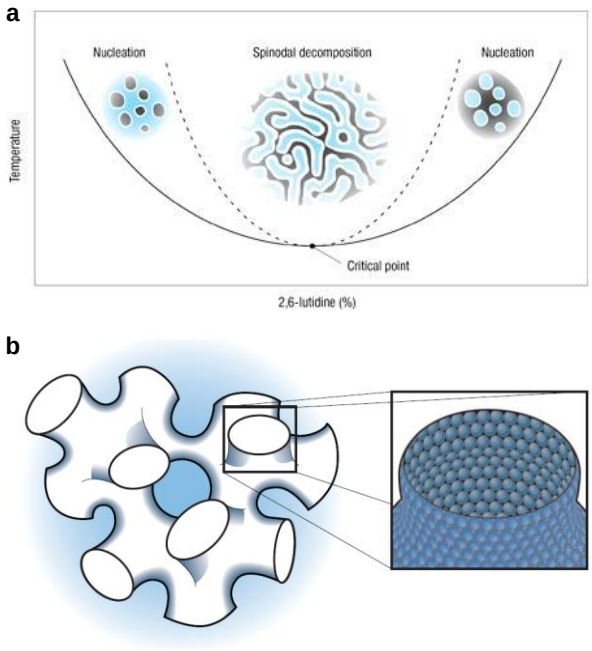

Figure 0.10 a) schematic phase diagram for a mixture of two fluids, water and 2,6-lutidine. At certain ratio, on heating, spinodal decomposition occurs, forming bicontinuous phase separation. b) bicontinuous structure stabilized by a sing layer of nanoparticles at interface. (reproduced from reference 50)

1.2.2 Assembly at surface

The purpose of assembly on surface focus more on the potential device applications, where the NPs have to be precisely organized on a solid substrate for outlet micro electrode connection. The assembly can be combined with top-down lithography techniques, such as micro contact printing, photo lithography, dip-pen lithography and nanoimprint lithography, to produce precisely organized and well defined pattern and functional structures of NPs useful in nanoelectronics, spintronics, sensor, and photovoltaic applications.[52] Self-assembly also represents an important step of simplifying the overall traditional manufacturing procedure by replacing some of the sophisticated multi-step lithography process. Various interactions used in bulk and interface assembly can be applied to the surface as well, such as covalent bonding, electrostatic interactions, hydrogen bonding and host guest interactions, depending on the nature of the NPs and desired structures.

For example, Kim et al. used alkylbromide-functionalized SAMs to couple Co-NPs to a silicon surface through direct nuclecophilic substitution by tethered amine groups.[53] Huskens and Reinhoudt et al. used 3 nm Au-NPs to generate a patterned thiol functionalization on an unpatterned silicon surface.[54] Willner et al. reported the use of electrochemical crosslinking to assemble p-Aminothiophenol-capped cadmium sulfide (CdS) NPs onto p-aminothiophenol functionalized Au electrode surfaces.[55] The dianiline-bridged CdS nanoparticles assembled on the Au electrode exhibited highly efficient photoelectrochemical properties in the presence of triethanolamine as sacrificial electron donor.

Our group described a new approach for binding monolayer of NPs on surfaces via dithiocarbamate (DTC) chemistry.[56] An amine terminated SAM was converted to DTC in the presence of CS2 solution affording the in-situ capturing of Au NPs from the solution. The primary amine was converted to DTC, which can then place exchange with the existing ligands on Au-NPs, effectively binding the NPs to the surface (Figure 1.11). Combined with micro contact printing, a stable patterned NP monolayer was fabricated as well.

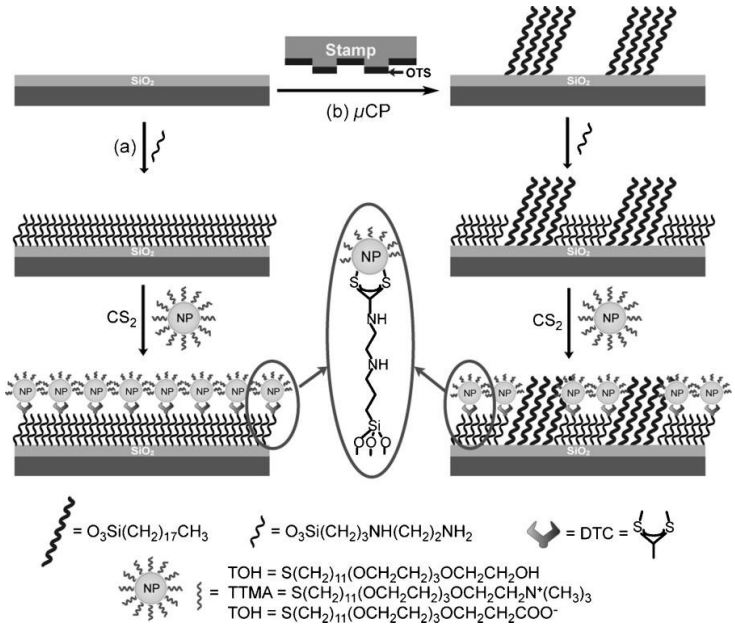

Figure 0.11 DTC-mediated binding of NPs to amine-terminated SAMs on a) unpatterned and b) μCP patterned surfaces. (reproduced form reference 56)

Another interesting approach to create nanostructures on surfaces is layer-by-layer assembly (LbL), which is based on the consecutive adsorption of polyanions and polycations from dilute aqueous solutions onto a charged substrate, as demonstrated first by Decher.[57] Using the LbL approach, numerous optoelectronic and biomaterials have been fabricated including light emitting diodes, single electron charging devices, and drug delivery vectors.[58, 59] Kotov et al. developed this technique for nanoparticle assembly.[60] This is an effective technique for tailoring the thickness of nanoparticles, which can further control the interactions between NPs and functionalized surfaces since polyelectrolytes can be used to adjust interlayer-separation by well-defined distances.[61]

Hydrogen bonding has been extensively employed for assembling nanoparticles onto surfaces. For example, Binder et al. have developed a methodology for NP binding on surfaces using directed, specific molecular interactions.[62] Au nanoparticles were anchored onto the surface as a result of the multiple hydrogen-bonds formed between barbituric acid molecules and surfaces bearing Hamilton-type receptors with binding constant as high as 10^5 M^{-1} (Figure 1.12).

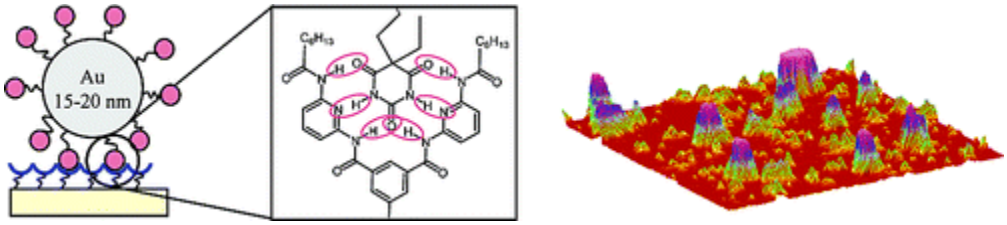

Figure 0.12 Nanoparticle binding mediated by Hamilton-type receptors. (reproduced form reference 62)

Host-guest chemistry involves the complexation of two or more molecules that are held together in a unique structure based on specific interaction including hydrophobic interaction, Van der Waals forces and hydrogen bonding, where the bond between hosts and guests is reversibly formed and broken.[63] Cyclodextrin is a popular host molecule for a variety of organic guest molecules, forming stable and specific inclusion complexes.[64] This type of host-guest molecules

has been used for nanoparticle surface assembly. For example, Huskens and Reinhoudt et al. introduced the concept of 'molecular printboards',[65] in which CD SAMs on gold or silicon oxide surfaces were used as a printboard. The print board can be selectively printed with multivalent guest molecules, and host-functionalized NPs can be further linked to the surface using the guest molecule as "glue".[66]

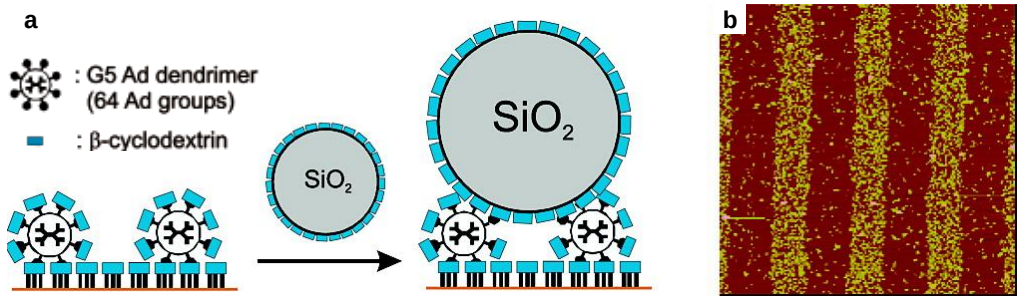

Figure 0.13 a) Assembly of a-Cyclodextrin-Functionalized Silica Nanoparticles on a-Cyclodextrin Molecular Printboards on Silicon Oxide through Multivalent Host-Guest Interactions Employing the G5 Adamantyl-Terminated PPI Dendrimer as a Supramolecular Glue. b) AFM imagine of the patterned gold nanoparticle layer. (reproduced from reference 66)

Top-down lithography methods can be also directly used to fabricate nanoparticle patterns on surface, such as dip-pen lithography. Dip-pen lithography techniques were first invented by Chad Mirkin, which initially used AFM tip as pen and thiol molecules as ink to write on the gold surface and this method has been expanded to various type of functional materials.[67] Directly writing NPs on a surface by AFM tip using NPs as ink has been used by Wang and coworkers to create conductive silver nanoparticle lines.[68]

1.3 Exchange Coupling and Transport in Nanoparticle Assemblies

In molecules, coupling between proximate atoms generates molecular orbitals, and energy levels split into bonding and antibonding states, as described by molecular orbital theory.[69] In the condensed phase, coupling between periodically arranged atoms leads to multi-fold splitting of the energy levels and the formation of an energy continuous band that is formulated by block

function. Depending on the electronic structure and arrangement of atoms, different band structures form in different solids leading to their specific optical and charge transport properties.[70]

As artificial atoms, coupling between NPs has direct similarity to atoms and can be treated following the same methodology as molecular systems. Meanwhile, NPs system has its own unique features that have to be considered in modeling the artificial solids. For example, besides the coupling, charge transport in NPs assemblies is also affected by quantum charging due to their nano-scale size.[71] The coupling is not only limited to electron wavefunciton either, but also exists in localized surface plasmon of noble metal NPs.[72] We focus on electron wave function coupling here only.

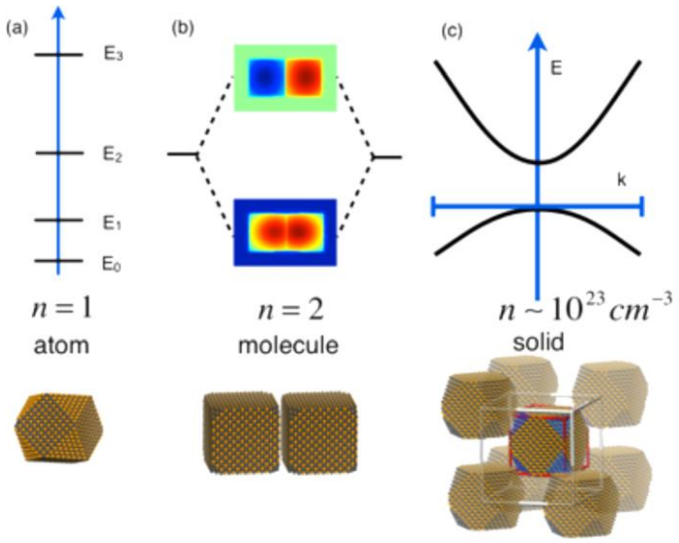

Figure 0.14 Evolution of the electronic structure from (a) discrete energy levels NPs as artificial atoms to (b) hybridized energy levels in artificial molecules and (c) continuous energy bands in NPs artificial solids. (reproduced from reference 28)

1.3.1 Exchange coupling energy

The electronic coupling between NPs can be treated just like atom system. (Fig. 1.14). As the separation between two neighboring NPs is reduced, their envelope wave functions can overlap, leading to quantum mechanically coupled NPs. The simplified two-dot system shown in Fig.

1.14(b) can thus be considered as an artificial molecule. The emerging bonding and antibonding states and their dependence on inter-particle separation have been investigated in GaAs/AlGaAs artificial molecules using photoluminescence (PL) spectroscopy.[73]

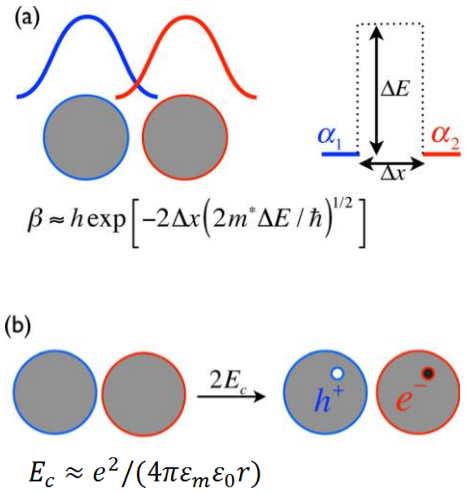

Figure 0.15 Electronic coupling between proximate NPs. (a) Quantum mechanical coupling arises from overlap of the envelope wave functions. The coupling energy depends exponentially on the inter NPs separation and the height of the energy barrier. (b) Electrostatic charging energy (E_c) arises from the Coulombic energy penalty to add or remove a charge from the NPs. (reproduced from reference 28)

The strength of the coupling is represented by the coupling energy and is also related to the electron tunneling rate. Electrons can tunnel between the dots at a rate Γ proportional to the coupling energy β~ h Γ, where h is Planck's constant. The strength of the coupling depends exponentially on the spatial width (Δx) and square root of energy barrier height (ΔE) between the NPs. The tunneling rate can be approximated as:[74]

$$\beta/h \approx \exp\left[-2\Delta x\left(\frac{2m^*\Delta E}{\hbar}\right)^{1/2}\right] \qquad (2)$$

Where m* is the electron effective mass. This equation illustrates that the tunneling rate drops exponentially with increasing separation between the NPs. Control of the interparticle distance

(by, for example, particle ligand length) and energy barrier (by, for example, introducing conjugated molecular linkers) are the key for modulating the strength of electronic coupling between the NPs. [10]

1.3.2 Charging energy

Coulumbic charging energy E_c arises from the energy cost that has to be paid to put an additional electron on the NC.[75, 76] It is also referred to as the self-capacitance of individual NPs. As shown in Figure 1.15b, charging energy is inversely related to the NC radius (r) and static dielectric constant of the surrounding medium (ε_m).

In an array of weakly coupled NCs, the electron transport can occur by sequential tunneling between the neighboring particles and the charging energy creates the Coulomb energy gap (Hubbard gap) $E \approx 2E_c$, which suppresses low-bias conduction in the effect known as the Coulomb blockade (Figure 1.16).[26, 75, 76] The weakly coupled states can exist only if coupling energy is smaller than the charging energy $b < E_c$. This requirement ensures that charges can flow by tunneling and yet are sufficiently localized so that charge states of the junction are well-defined by the energy time uncertainty principle in quantum mechanics.[77] In an array of strongly coupled metallic NCs, the discrete wave functions form a band with width proportional to the exchange coupling energy. As the inter particle distance decreases, the bandwidth increases (as shown in Figure 1.16), until $\beta > E_c$. The Coulomb gap disappears and carriers can move freely throughout the NP solid. This sudden change in behavior is known as the Mott metal–insulator transition (MIT).[78, 79] Above the transition point, the coherent molecular-type orbitals extend over many NPs in analogy to an ordinary crystal.

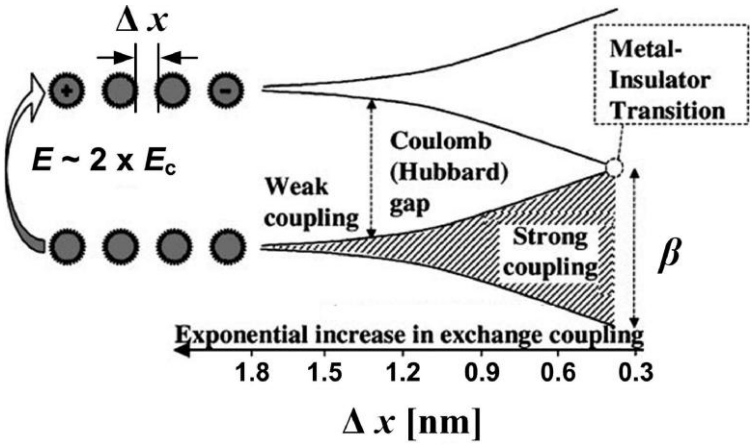

Figure 0.16 Electronic structure and interparticle interactions in a nanocrystal solid. At large interparticle distance Δ*x*, the nanocrystals are electrically isolated, and the nanocrystal solid is an insulator with a Coulomb gap. As the interparticle distance decreases, exchange interactions become significant, and the electronic wave functions of the individual nanocrystals spread out over multiple particles. At the point of metal-insulator transition, the delocalized orbitals extend over the entire nanocrystal solid. (reproduced from reference 26)

Ligand-tailored MIT in metallic NP assemblies has long been an important research subject. Zabet-Khosousi et al. studied the charge transport properties of 5 nm Au NPs films linked by $HS(CH_2)_nSH$ (n = 2-10) and observed MIT at n =5. At the transition point, the conductivity of the NC solid increased by more than 2 orders of magnitude.[80] Liu et al. studied $CH_3(CH_2)_{n-1}SH$ capped 1.7 nm Au NPs as a function of the inter-NP separation (n=6, 9, 12, 15) using valence-band photoemission spectroscopy. For n>9, they observed a low density of states at the NP Fermi level, which was due to the large charging energy of the small NPs. For n< 6, however, they observed an increase in the density of states at the Fermi level, and this was attributed to electron delocalization for sufficiently small inter-NP separation.[81] The transition to delocalized behavior can also be observed optically. As shown by Bawendi, the optical absorption spectra approached that for the bulk CdSe when the separation between the NPs decreased.[26]

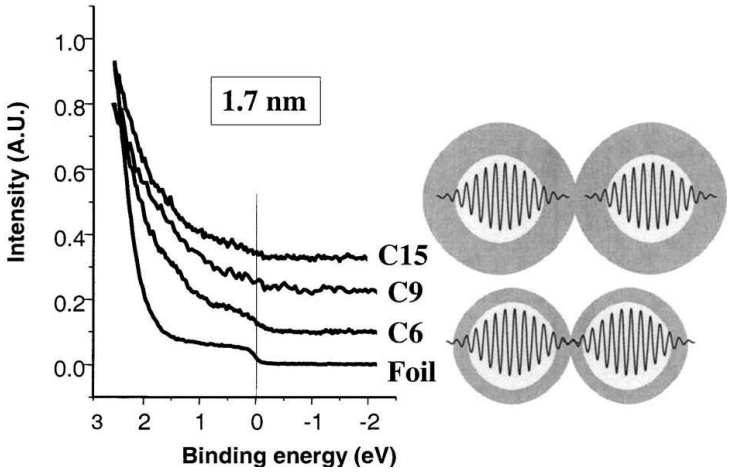

Figure 0.17 Effect of inter-NP separation (as determined by the length of alkyl chains in the NP ligand) on the density of states of $CH_3(CH2)_{n-1}S$-capped 1.7 nm Au NPs. The spectrum of a pure gold foil is shown for comparison. (Reproduced from reference 81)

1.3.3 Role of ligands

From the above discussion, we have seen the critical effects of the ligand. On one hand, they stabilize the particle and define the boundary of the NPs, without which NPs cannot actually exist. On another hand, they determine the electronic coupling across the NPs boundary. Modulating the ligand by molecular engineering thus becomes the critical point to reach a good balance between isolation and coupling of NPs for desired collective properties. The rich variety of readily available linker molecules provides the opportunity for precisely tuning interparticle electronic coupling and there has been significant progress in controlling and understanding the inter-particle coupling in NP aggregates.

The most common ligands described in the literature are based on organic hydrocarbon molecules with anchoring end groups. Such molecular structure offers high chemical flexibility in the organic synthesis point of view. However, most organic ligands act as insulating dielectric barriers between NPs. The wide barrier created by the ligand shell effectively localizes the wave function within individual NPs, resulting in negligible overlap between electronic wave functions across the NPs and hindering charge transport. Numerous research reports the effect of length of

ligand molecules on charge transport in arrays of metallic NCs, most commonly, Au and Ag NPs capped with alkylthiol molecules. Chemical approaches to resolve this challenge rely on the exchange of the insulating ligand with shorter molecules to facilitate inter-particle coupling.

Talapin and Murray showed that hydrazine treatment of PbSe NP films removed the oleic acid ligand and decreased inter-NP surface- to-surface spacing from 1.1 to 0.3 nm. This reduction of the artificial bond length led to higher quantum exchange coupling and increased the conductance through the NP array by ten orders of magnitude.[82]

The use of variable length bifunctional linkers allows for systematic tuning of the inter particle spacing and thus charge transfer dynamics. Choi et al. demonstrated the exponential decay of exciton dynamics as the inter-particle distance increases using a series of n-phenyl dithiol linked semiconductor nanoparticles, as shown in Fig 1.18. Moreover, this work also illustrated that coupling-induced tunneling between neighboring NPs can also split photogenerated excitons in NP films in absence of electrical or chemical potential gradients, which is quite desirable for photovoltaic applications.[83]

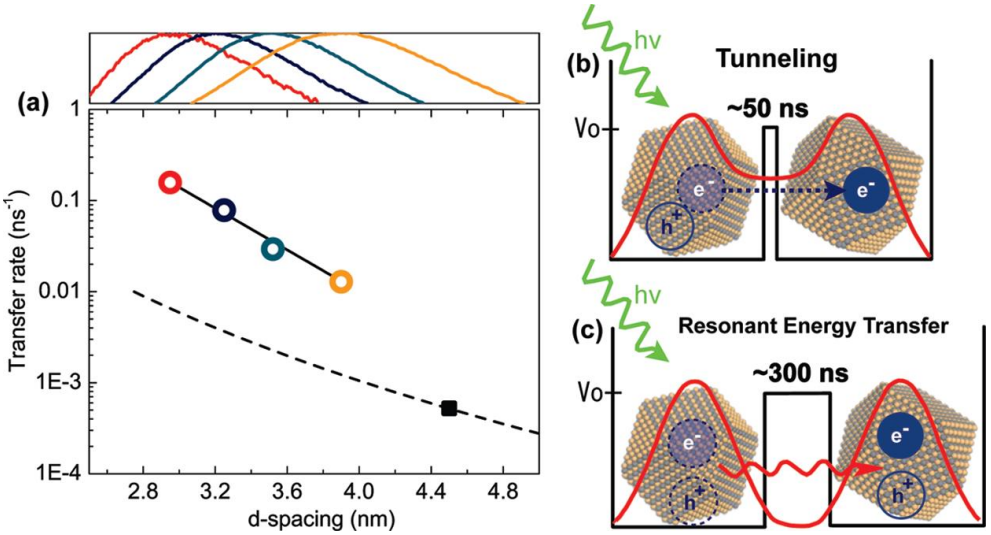

Figure 0.18 Tunable artificial bond length realized through variable length bifunctional linkers. (a) Charge transfer rates as a function of interdot spacing measured with GISAXS. Single exponential decay fit (black solid line) indicates that the charge transfer occurs via tunneling of charge through a potential barrier. Resonant energy transfer is shown in by black rectangle and the calculated energy transfer rates, dotted line, for corresponding interdot spacing This indicates that exciton dissociation via tunneling is the dominant pathway(b), and resonant energy transfer is dominant in low inter- NC coupling regime (c). (reproduced from reference 83)

The chemical nature of the linker molecule itself is also important. The electronic structure of the spacer can be tuned to possess energy levels that are resonant with the quantum-confined energy levels of the NPs, e.g., by choosing either conjugated aromatic or aliphatic spacers with the help of electron donating or withdrawing groups on the spacer. These aspects have been studied in detail in the context of single molecule electronics. Insights from the single-molecule studies provide important guidance for future work in controlling the coupling between NPs.[84] Binding groups of the ligand to the NPs have proved to be another key point for ligand engineering. By replacing thiol group with conjugated dithiocarbomate group, Wessel et al. found that the conductivity of gold NPs increases by several orders of magnitude. [85] Table 1-2 lists several typical ligands used for NP assemblies and their character in NP coupling.

Table 0-2 Different types of surface ligands used in nanoparticles and nanoparticle assemblies (reproduced from reference 10)

Ligand type	Molecular structure	Interparticle spacing	Functions, characteristics, typical examples
Molecules with single head group and a long hydrocarbon chain	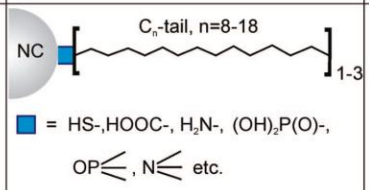	>1.5 nm	• Most common ligands used for NC synthesis • Form stable colloidal solutions • Hydrophobic surface • Form highly insulating NC solids, σ ~10^{-12}-10^{-9} S cm^{-1}
Short-chain molecules with single head group	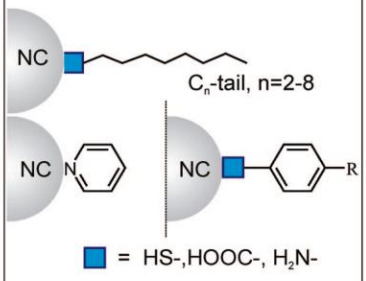	0.3-1 nm	• Treatment of NC solids or ligand-exchange in solutions • Decreased colloidal stability • Improved electronic transport compared to long-chain ligands • Reported detectivity of ~10^{12}-10^{13} Jones in photodetectors on PbS NCs caped with butylamin • Conductivities of up to 10^{-1} S cm^{-1} in arrays of metallic NCs
Cross-linking molecules with two end groups	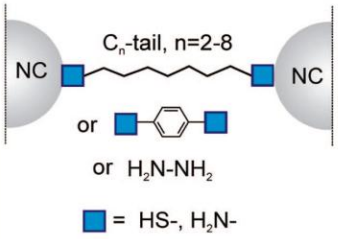	0.3-1 nm	• Mainly prepared by treating NC solids • μ up to 2 cm^2 V^{-1} s^{-1} in arrays of PbSe NCs treated with N_2H_4 • μ~10^{-2} cm^2 V^{-1} s^{-1} in arrays of CdSe NCs treated with 1,4-phenylenediame • Solar cells based on PbS and PbSe NC solids showed power conversion efficiencies of up to 2.1%
Metal chalcogenide complexes	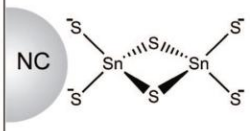	≥ 0.5 nm	• Prepared via solution phase ligand-exchange • Complete removal of original organic ligands • Hydrophilic surface • High conductivities of ~200 S cm^{-1} in Au-$Sn_2S_6^{4-}$NC solids

1.4 Dissertation Overview

As has been explained above, organizing nanoparticles into ordered structures and tuning their coupling are key topics in nanoscience and technology for constructing novel optical and electrical artificial materials. My research integrates the surface chemistry of nanoparticles, interfacial assembly and lithography techniques to construct nanoparticle based functional structures. Assembly of NPs at surface and water-oil interface, modulation of the charge and energy transport in NPs aggregate and compost system were achieved.

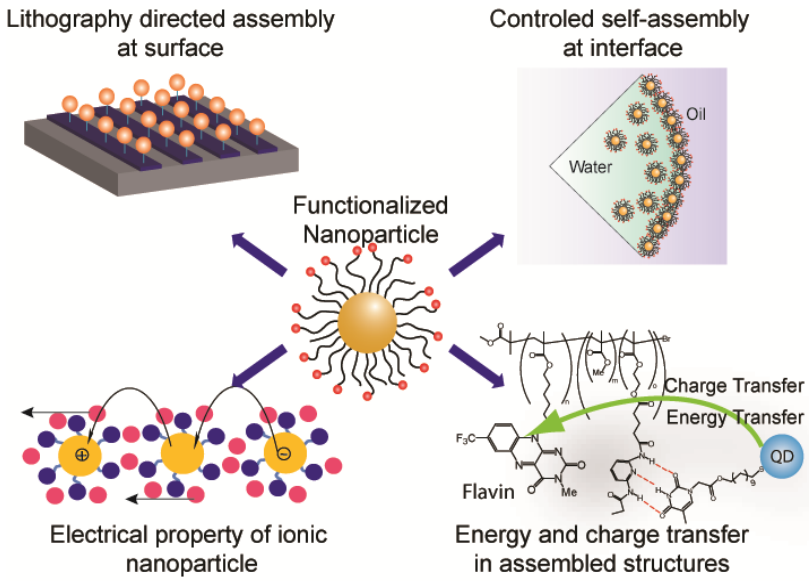

Figure 0.19. Schematic view of nanoparticle assemblies for functional structures.

Multiple hydrogen bonding interaction are known as a specific and selective “lock-key” type of interactions, which is the basis of molecular recognition and has been used widely in the construction of supramolecular materials. In chapter 1, we fabricated supramolecular gel array and nanoparticles are reversibly and selectively incorporated by using complimentary hydrogen bonding interaction. The methodology in this research provides a potentially useful system for integrating material properties of nanoparticles and gels with ‘lock and key’ capabilities offered by molecular recognition.

Nanoimprint lithography (NIL) is an important top-down lithography technique feathering high resolution and high through put. We invented a simple and versatile method to activate and functionalize nanoimprinted polystyrene (PS)-based surfaces that usually is used as innert mask layer. UV irradiation can simultaneously crosslink and photo-oxidate chloromethylstyrene to generate chemically active aldehyde groups. After modifying the pattern using thiol molecule bearing hydrazine via nucleophilic addition reaction between amines and aldehydes, nanoparticles can be readily immobilized onto patterned surfaces. Bioconjugation is also realized by immobilization of active enzymes onto the pattern. Chapter 2 will describe this novel method in detail.

Direct imprinting of nanoparticles is desired as a simple and fast way for nanoparticle patterning. Unfortunately, this is usually impossible as NPs are powder-like solids due to the rigid inorganic core and the crystallinity of the alkane ligands. Chapter 4 introduces a special type of gold nanoparticles with liquid-like processible properties. Stable, high resolution patterns can be created by molding the NP film using NIL technique. Moreover, photo-responsive and patterned conductivity were found for this NP film.

It has been recognized that surface properties of NPs has a significant influence on their dynamic interfacial behavior. However, this idea has not been examined carefully and systematically in experiments because of the difficulty in adjusting the subtle chemistry of the particle surface. Described in chapter 5, we engineer the surface chemistry of the gold nanoparticles by a series of ligand with head groups of different hydrophobicity and explore the assembly dynamics of the these monolayer-protected NPs at the toluene–water interface by dynamic surface tension measurements. The research revealed several very important facts about the NPs interfacial assembly process that were not well recognized before. For example, the assembly dynamics of the NPs at the interface follows an interaction-based mixed kinetic diffusion mechanism where

the adsorption of NPs at the interface played a more critical role than diffusion, and the adsorption is determined by both the surface hydrophobicity and detailed chemistry.

In chapter 6, we functionalize the gold nanoparticles using ionic ligands feathering positive charge immobilized on gold nanoparticle, neutralized by mobile counter ions. The ionic activity of the ligand and electronic activity of the metal nanoparticles are well integrated into one material and the ligand provides a variable dielectric environment to modulate the charge transport properties as well. By using impedance spectroscopy (IS), we observed a modulated ionic and electric conductance of this NP film. We have explored the possibility of this ionic gold nanoparticle as a sensing platform using its impedance behavior in response to different solvent environments.

We also used hydrogen bonding supramolecular interactions to assemble quantum dots and flavin polymers where efficient energy transfer between quantum dot donor and flavin acceptor was found in both solution phase and thin film of the assembly. This is described in chapter 7. To support chapter 7, chapter 8 provides a detailed study of the energy and electron transfer using flavin as acceptor for future possibility of quantum dot–flavin assemblies for photovoltaics.

1.5 References

1 Yin, Y.; Alivisatos, A. P. *Nature* **2005**, *437*, 664.

2 Daniel, M. C.; Astruc, D. *Chem. Rev.* **2004**, *104*, 293.

3 Lu, Z.; Yin, Y. *Chem. Soc. Rev.* **2012**, *41*, 6874.

4 Indira, T.; Lakshmi, P. *Int. J. Phar. Sci. Nanotech.* **2010**, *3*, 1035.

5 Lu, X.; Rycenga, M.; Skrabalak, S. E.; Wiley, B.; Xia, Y. *Ann. Rev. Phys. Chem.* **2009**, *60*, 167.

6 Bera, D.; Qian, L.; Tseng, T.-K.; Holloway, P. H. *Materials* **2010**, *3*, 2260.

7 Hervés, P.; Pérez-Lorenzo, M.; Liz-Marzán, L. M.; Dzubiella, J.; Lu, Y.; Ballauff, M. *Chem. Soc. Rev.* **2012**, *41*, 5577.

8 Luo, X.; Morrin, A.; Killard, A. J.; Smyth, M. R. *Electroanalysis* **2006**, *18*, 319.

9 Saha, K.; Agasti, S. S.; Kim, C.; Li, X.; Rotello, V. M. *Chem. Rev.* **2012**, *112*, 2739.

10 Talapin, D. V.; Lee, J.-S.; Kovalenko, M. V.; Shevchenko, E. V. *Chem. Rev.* **2010**, *110*, 389.

11 Brust, M.; Fink, J.; Bethell, D.; Schiffrin, D. J.; Kiely, C. *J. Chem. Soc. Chem. Commun* **1995**, 1655.

12 Quaroni, L.; Chumanov, G. *J. Am. Chem. Soc.* **1999**, *121*, 10642.

13 (a)Steigerwald, M. L.; Brus, L. E. *Acc. Chem. Res.* **1990**, *23*, 183. (b) Talapin, D. V.; Rogach, A. L.; Kornowski, A.; Haase, M.; Weller, H. *Nano Lett.* **2001**, *1*, 207.

14 Shevchenko, E. V.; Talapin, D. V.; Schnablegger, H.; Kornowski, A.; Festin, O.; Svedlindh, P.; Haase, M.; Weller, H. *J. Am. Chem. Soc.* **2003**, *125*, 9090.

15 Sun, S. *Adv. Mater.* **2006**, *18*, 393.

16 Tao, A. R.; Habas, S.; Yang, P. *Small* **2008**, *4*, 310.

17 Park, J.; Joo, J.; Kwon, S. G.; Jang, Y.; Hyeon, T. *Angew. Chem. Int. Ed.* **2007**, *46*, 4630.

18 Templeton, A. C.; Wuelfing, W. P.; Murray, R. W. *Acc. Chem. Res.* **2000**, *33*, 27.

19 Moores, A.; Goettmann, F. *New J. Chem.* **2006**, *30*, 1121.

20 Soreni-Harari, M.; Yaacobi-Gross, N.; Steiner, D.; Aharoni, A.; Banin, U.; Millo, O.; Tessler, N. *Nano lett.* **2008**, *8*, 678.

21 Yaacobi-Gross, N.; Garphunkin, N. *ACS Nano* **2012**, 3128.

21 Frederick, M. T.; Amin, V. A.; Cass, L. C.; Weiss, E. A. *Nano lett.* **2011**, *11*, 5455.

22 Ghosh, A.; Basak, S.; Wunsch, B. H.; Kumar, R.; Stellacci, F. *Angew. Chem. Int. Ed.* **2011**, *50*, 7900.

23Upadhyayula, V. K. K. *Anal. Chim. Acta.* **2012**, *715*, 1.

24 Jong, W. H. De; Borm, P. J. A. *Inter. J. Nanomed.* **2008**, *3*, 133.

25 De, M.; Ghosh, P. S.; Rotello, V. M. *Adv. Mater.* **2008**, *20*, 4225.

26 Murray, C.; Kagan, C. R.; Bawendi, M. G. *Ann. Rev. Mater.* **2000**, *30*, 545.

27 Choi, C. L.; Alivisatos, a P. *Ann. Rev. Phys. Chem.* **2010**, *61*, 369.

28 Hanrath, T. *J. Vac. Sic. Technol. A* **2012**, *30*, 030802.

29 Taleb, a.; Petit, C.; Pileni, M. P. *J. Phys. Chem. B* **1998**, *102*, 2214.

30 Murray, C.; Kagan, C. R.; Bawendi, M. G. *Ann. Rev. Mater.* **2000**, *30*, 545.

31 Pileni, M. P. *J. Phys. Chem. B* **2001**, *105*, 3358.

32 Grzelczak, M.; Vermant, J.; Furst, E. M.; Liz-Marzán, L. M. *ACS nano* **2010**, *4*, 3591.

33 Kinge, S.; Crego-Calama, M.; Reinhoudt, D. N. *ChemPhysChem* **2008**, *9*, 20.

34 Bishop, K. J. M.; Wilmer, C. E.; Soh, S.; Grzybowski, B. a *Small* **2009**, *5*, 1600.

35 Hermanson, K. D.; Lumsdon, S. O.; Williams, J. P.; Kaler, E. W.; Velev, O. D. *Science* **2001**, *294*, 1082.

36 Erb, R. M.; Son, H. S.; Samanta, B.; Rotello, V. M.; Yellen, B. B. *Nature* **2009**, *457*, 999.

37 Palermo, V.; Samorì, P. *Angew. Chem. Int. Ed.* **2007**, *46*, 4428.

38 Arumugam, P.; Xu, H.; Srivastava, S.; Rotello, V. M. *Polym. Int.* **2007**, *56*, 461.

39 Boal, A. K.; Ilhan, F.; DeRouchey, J. E.; Thurn-Albrecht, T.; Russell, T. P.; Rotello, V. M. *Nature* **2000**, *404*, 746.
40 Srivastava, S.; Samanta, B.; Jordan, B. J.; Hong, R.; Xiao, Q.; Tuominen, M. T.; Rotello, V. M. *J. Am. Chem. Soc.* **2007**, *129*, 11776.
41 Park, S. Y.; Lytton-Jean, A. K. R.; Lee, B.; Weigand, S.; Schatz, G. C.; Mirkin, C. a *Nature* **2008**, *451*, 553.
42 Kalsin, A. M.; Fialkowski, M.; Paszewski, M.; Smoukov, S. K.; Bishop, K. J. M.; Grzybowski, B. *Science* **2006**, *312*, 420.
43 Böker, A.; He, J.; Emrick, T.; Russell, T. P. *Soft Matter* **2007**, *3*, 1231.
44 Duan, H.; Wang, D.; Kurth, D. G.; Möhwald, H. *Angew. Chem. Int. Ed.* **2004**, *43*, 5639.
45 Böker, A.; Lin, Y.; Chiapperini, K.; Horowitz, R.; Thompson, M.; Carreon, V.; Xu, T.; Abetz, C.; Skaff, H.; Dinsmore, a D.; Emrick, T.; Russell, T. P. *Nat. Mater.* **2004**, *3*, 302.
46 Bigioni, T. P.; Lin, X.-M.; Nguyen, T. T.; Corwin, E. I.; Witten, T. a; Jaeger, H. M. *Nat. Mater.* **2006**, *5*, 265.
47 Binks, B. *Curr. Opin. Colloid Interface Sci.* **2002**, *7*, 21.
48 Yang, X.-C.; Samanta, B.; Agasti, S. S.; Jeong, Y.; Zhu, Z.-J.; Rana, S.; Miranda, O. R.; Rotello, V. M. *Angew. Chem. Int. Ed.* **2011**, *50*, 477.
49 Arumugam, P.; Patra, D.; Samanta, B.; Agasti, S. S.; Subramani, C.; Rotello, V. M. *J. Am. Chem. Soc.* **2008**, *130*, 10046.
50 Dinsmore, A. D. *Nat. Mater.* **2007**, *6*, 921.
51 Herzig, E. M.; White, K. A.; Schofield, A. B.; Poon, W. C. K.; Clegg, P. S. *Nat. Mater.* **2007**, *6*, 966.
52 Shipway, A. N.; Katz, E.; Willner, I. *ChemPhysChem* **2000**, *1*, 18.
53 Park, J.-I.; Lee, W.-R.; Bae, S.-S.; Kim, Y. J.; Yoo, K.-H.; Cheon, J.; Kim, S. *J. Phys. Chem. B* **2005**, *109*, 13119.
54 Paraschiv, V.; Zapotoczny, S.; Jong, M. R. de; Vancso, G. J.; Huskens, J.; Reinhoudt, D. N. *Adv. Mater.* **2002**, *14*, 722.
55 Granot, E.; Patolsky, F.; Willner, I. *J. Phys. Chem. B* **2004**, *108*, 5875.
56 Park, M.-H.; Ofir, Y.; Samanta, B.; Arumugam, P.; Miranda, O. R.; Rotello, V. M. *Adv. Mater* **2008**, *20*, 4185.
57 Decher, G. *Science* **1997**, *277*, 1232.
58 Crespilho, F.; Zucolotto, V.; Jr, O. O.; Nart, F. *Int. J. Electrochem. Sci* **2006**, *1*, 194.
59 Hammond, P. T. *Materials Today* **2012**, *15*, 196.
60 Kotov, N. A.; Dekany, I.; Fendler, J. H. *J. Phys. Chem.* **1995**, *99*, 13065.
61 Caruso, F.; Caruso, R. A.; Möhwald, H. *Science* **1998**, *282*, 1111.

62 Zirbs, R.; Kienberger, F.; Hinterdorfer, P.; Binder, W. H. *Langmuir* **2005**, *21*, 8414.

63 Mulder, A.; Huskens, J.; Reinhoudt, D. N. *Org. Biomol. Chem.* **2004**, *2*, 3409.

64 Rekharsky, M. V.; Inoue, Y. *Chem. Rev.* **1998**, *98*, 1875.

65 Huskens, J.; Deij, M. a; Reinhoudt, D. N. *Angew. Chem. Int. Ed.* **2002**, *41*, 4467.

66 Mahalingam, V.; Onclin, S.; Péter, M.; Ravoo, B. J.; Huskens, J.; Reinhoudt, D. N. *Langmuir* **2004**, *20*, 11756.

67 Salaita, K.; Wang, Y.; Mirkin, C. A. *Nat Nano* **2007**, *2*, 145.

68 Wang, H.-T.; Nafday, O. a.; Haaheim, J. R.; Tevaarwerk, E.; Amro, N. a.; Sanedrin, R. G.; Chang, C.-Y.; Ren, F.; Pearton, S. J. *Appl. Phys. Lett.* **2008**, *93*, 143105.

69 Friedman, P. W. A. R. S. *Molecular Quantum Mechanics*; 5th ed.; Oxford University Press: Oxford, 2011; p. 592.

70 Charles Kittel *Introduction to Solid State Physics*; 8th ed.; John Wiley & Sons: Weinheim, 2004; p. 704.

71 Kempen, H. van; Dubois, J. G. A.; Gerritsen, J. W.; Schmid, G. *Phys. B* **1995**, *204*, 51.

72 Halas, N.; Lal, S.; Chang, W.; Link, S.; Nordlander, P. *Chem. Rev.* **2011**, *111*, 3913.

73 Schedelbeck, G. *Science* **1997**, *278*, 1792.

74 Zabet-Khosousi, A.; Dhirani, A.-A. *Chem. Rev.* **2008**, *108*, 4072.

75 Vanmaekelbergh, D.; Liljeroth, P. *Chem. Soc. Rev.* **2005**, *34*, 299.

76 Beloborodov, I.; Lopatin, A.; Vinokur, V.; Efetov, K. *Rev. Mod. Phys.* **2007**, *79*, 469.

77 Kane, J.; Ong, J.; Saraf, R. F. *J. Mater. Chem.* **2011**, *21*, 16846.

78 Imada, M.; Fujimori, A.; Tokura, Y. *Rev. Mod. Phys.* **1998**, *70*, 1039.

79 Mott, N. *Proc. R. Soc. Lond. A* **1982**, *382*, 1.

80 Zabet-Khosousi, A.; Trudeau, P.-E.; Suganuma, Y.; Dhirani, A.-A.; Statt, B. *Phys. Rev. Lett.* **2006**, *96*, 2.

81 Liu, H.; Mun, B.; Thornton, G.; Isaacs, S.; Shon, Y.-S.; Ogletree, D.; Salmeron, M. *Phy. Rev. B* **2005**, *72*, 155430.

82 Talapin, D. V.; Murray, C. B. *Science* **2005**, *310*, 86.

83 Choi, J. J.; Luria, J.; Hyun, B.-R.; Bartnik, A. C.; Sun, L.; Lim, Y.-F.; Marohn, J. a; Wise, F. W.; Hanrath, T. *Nano Lett.* **2010**, *10*, 1805.

84 Tao, N. J. *Nat. Nano.* **2006**, *1*, 173.

85 Wessels, J. M.; Nothofer, H.-G.; Ford, W. E.; Wrochem, F. von; Scholz, F.; Vossmeyer, T.; Schroedter, A.; Weller, H.; Yasuda, A. *J. Am. Chem. Soc.* **2004**, *126*, 3349.

CHAPTER 2

NANOPARTICEL FUNCTONALIZED SUPRAMOLECULAR MICROGEL ARRAY THROUGH COMPLEMENTARY HYDROGEN BONDING INTERACTION

2.1 Introduction

Molecular self-assembly can be described as the thermodynamically controlled association of molecules into structurally well defined, stable aggregates through non-covalent interactions,[1] including van der Waals interaction, π-π stacking, electrostatics, metal coordination, and hydrogen bonding. These supramolecular interactions that define the self-assembly process are responsible for the highly ordered, diverse systems found in nature, and also provide inspiration for the creation of new self-assembled supramolecular materials.[2-11] Supramolecular gels represent a particularly interesting family of self-assembled structures, and are three-dimensional (3D) networks formed by small molecules, oligomers or polymers through non-covalent interaction linkages. These systems feature reversibility, self-healing ability and selectivity compared with traditional polymer gels, and have applications in areas including bio-delivery, controlled membrane and tissue engineering.[12-19]

Specific interactions, such as multiple hydrogen bonding motifs and metal coordination have been widely employed in the construction of supramolecular polymer materials.[4-10, 15-23] For example, we have shown that random copolymers of polystyrene functionalized with complementary diamidopyridine (**PS-DAP**) and thymine (**PS-Thy**) moieties (Figure 2.1A and 1B) form supramolecular assemblies including vesicular complexes in non-competitive solvents.[23, 24] A key feature of these vesicular structures is that they are metastable, forming gels over the course of hours. These gels provide a potentially useful system for integrating material

properties of gels with 'lock and key' capabilities offered by molecular recognition. In this chapter, we demonstrate selective deposition of **PS-DAP**/**PS-Thy** gels onto pre-patterned silicon substrates. These microgel arrays can be crosslinked, and selectively and reversibly functionalized by nanoparticles through complementary hydrogen bonding interactions to provide polymer/nanoparticle composite micro-structure patterns with fluorescent or magnetic properties.

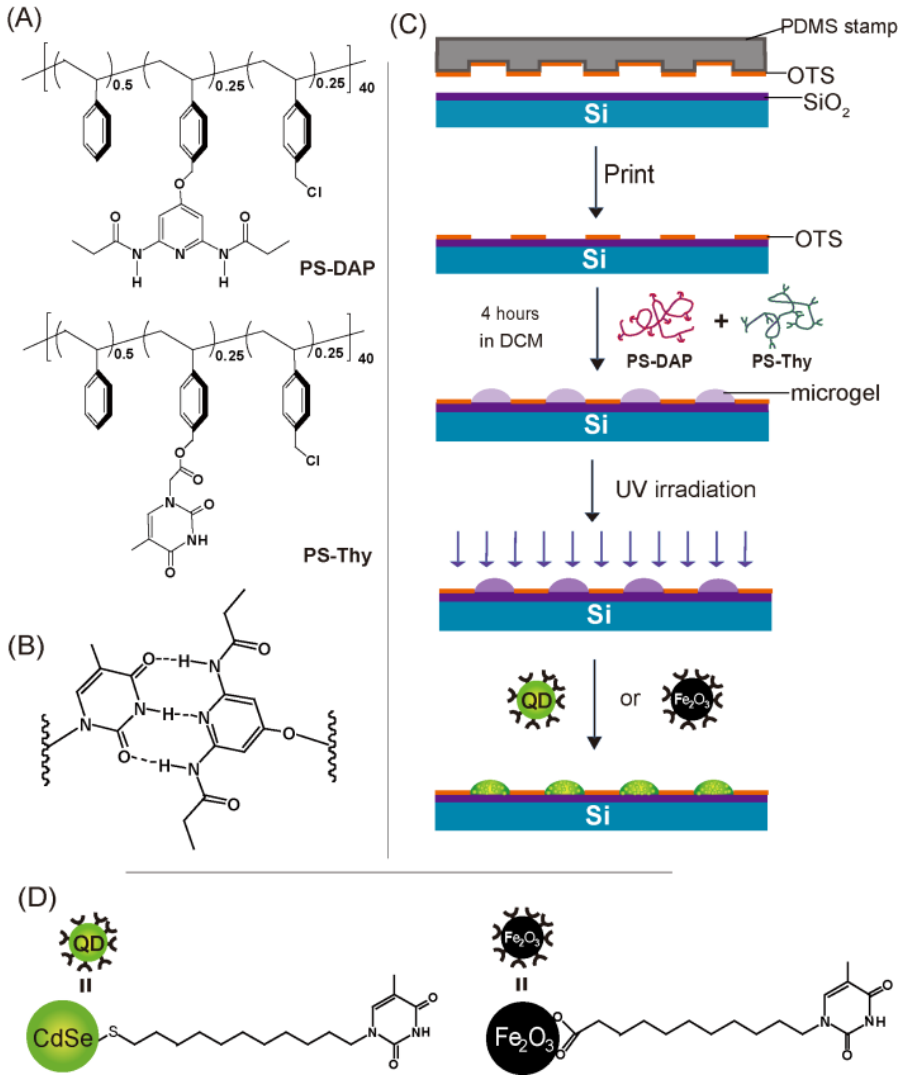

Figure 0.1 A) Molecular structure of **PS-Thy** and **PS-DAP**. B) Multiple hydrogen bonding interaction between Thy and DAP. C) Schematic illustration of the pattern fabrication process. D) Structure of the nanoparticles.

2.2 Results and Discussion

2.2.1 Surface pattering and gel array formation

Patterned substrates were prepared using microcontact printing.[25, 26] Octadecyltrichlorosilane (OTS) was stamped on to clean silicon wafers using PDMS stamp to create hydrophobic (OTS) grids, leaving 5 μm hydrophilic bare Si/SiO_2 squares on the surface (Figure 2.1C). The polymer gel precursor was made by mixing 1:1 ratio of **PS-DAP** and **PS-Thy** solutions (1mg/mL in dichloromethane). The patterned silicon wafers were then immersed into **PS-DAP**/**PS-Thy** solution for 5 hours, followed by gentle rinsing with dichloromethane (DCM). The surface morphology of the wafer was investigated using optical microscopy.

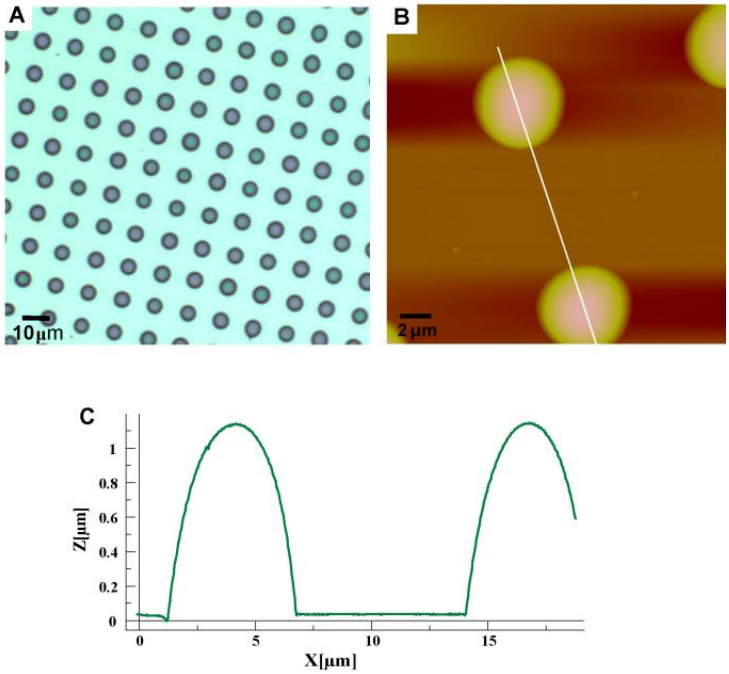

Figure 0.2 A) Optical microscope picture of the polymer complex pattern on silicon surface. B) AFM image of the pattern and C) the section analysis.

As shown in Figure 2.2A, deposition of the gel occurred selectively on the hydrophilic features of the substrates, presumably due to hydrogen bonding between the polymer side chains and the pendant hydroxyl groups of the SiO_2 surface. Interestingly, the gels are circular, in contrast to the

square features of the substrate. Atomic force microscope (AFM) shows that the topology of the gels is hemispherical, with ~1μm height and ~5 μm diameter, which is consistent with the feature size of the stamp (Figure 2.2 B-C). Presumably the circular spots arise from the lower surface energy of the hemispherical shape.

2.2.2 Incorporation of surface modified nanoparticle to microgel

The formation of the gel is mediated by complementary hydrogen bonding, which in turn gives the pattern with attractive properties that are not accessible for traditional polymer patterns.[27, 28] The polymer gel allows further selective functionalization with materials bearing the complementary hydrogen bonding moieties (**Thy** or **DAP**). As an example, CdSe quantum dots (**QD**)[29] bearing **Thy** ligands (**QD-Thy**) provide luminescent gels by dipping the wafer into **QD-Thy** solution for 5 min, followed by solvent washing and Ar flow drying (Figure 2.3A).

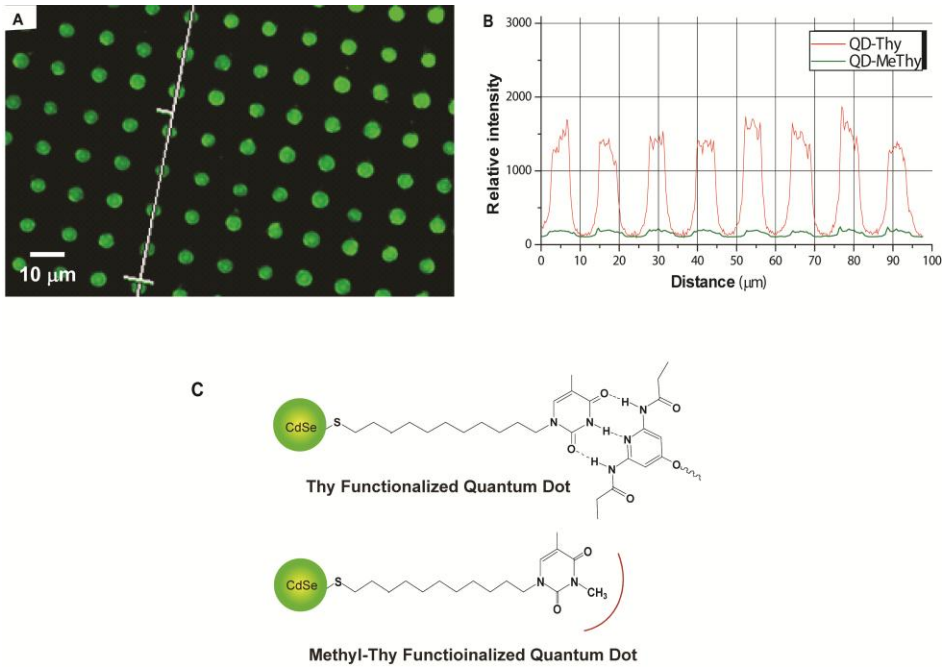

Figure 0.3 A) Fluorescence microscope image of the microgel functionalize by **QD-Thy**. B) Relative light intensity profile across the surface along the white line in A) by **QD-Thy** (red line) and **QD-MeThy** (green line) under the same exposure time. (C) Structure of **QD-Thy** and **QD-MeThy**.

The relative fluorescence intensity profile across the surface (Figure 2.3B) is homogeneous for each spot, indicating a uniform distribution of the **QD**. This functionalization is very specific as little or no uptake was observed with highly analogous N-methylated thymine ligand CdSe **QD** (**QD-MeThy**) incapable of three-point hydrogen bonding (Figure 2.3B).[30]

Magnetic properties were readily incorporated into the gels using thymine functionalized superparamagnetic iron oxide (**Fe_2O_3-Thy)** nanoparticles.[31] Magnetic force microscopy (MFM) was used to characterize the surface after uptake of the magnetic nanoparticles. Based on the large feature size and height of the gels, a lift scan height of 100 nm was selected. Whereas a phase difference (~5 ^{o}) was seen with the gel functionalized with **Fe_2O_3-Thy** (Figure 2.4), no obvious phase difference was observed prior to functionalization (Figure 2.4b). This control study confirms the MFM signal originates from the incorporation of the nanoparticles in the gel but not from the topology-caused artifact. A gradual increase of the MFM signal, from edge to the center of the spot, supports the hemispherical topology of the features, and suggests that the nanoparticles are incorporated throughout the microgel.

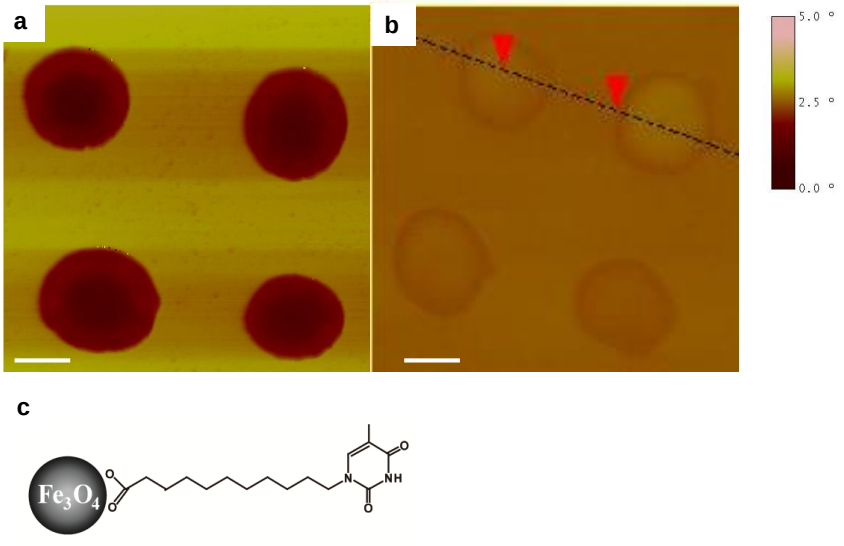

Figure 0.4 MFM phase image of the microgel pattern before (b) and after functionalized with **Fe_2O_3-Thy** nanoparticles (a). c) is the structure of **Fe_2O_3-Thy** nanoparticle.

2.2.3 Reversible incorporation of NP

One of the attractive advantages of using hydrogen bonding interactions is their reversibility. As formed, the **PS-DAP/PS-Thy** gels are unstable towards competitive solvents such as methanol and tetrahydrofuran (THF), which could disrupt hydrogen bonding. To provide a stable material, we crosslinked the microgel patterns using 254 nm UV irradiation for 20 minutes, rendering the gel stable to all common solvents tested, including THF and methanol.[32] No apparent difference in the morphology of the surface was seen before and after the UV irradiation. Moreover, selective uptake of thymine-functionalized materials was retained, as demonstrated using **QD-Thy** and **QD-MeThy** particles above.

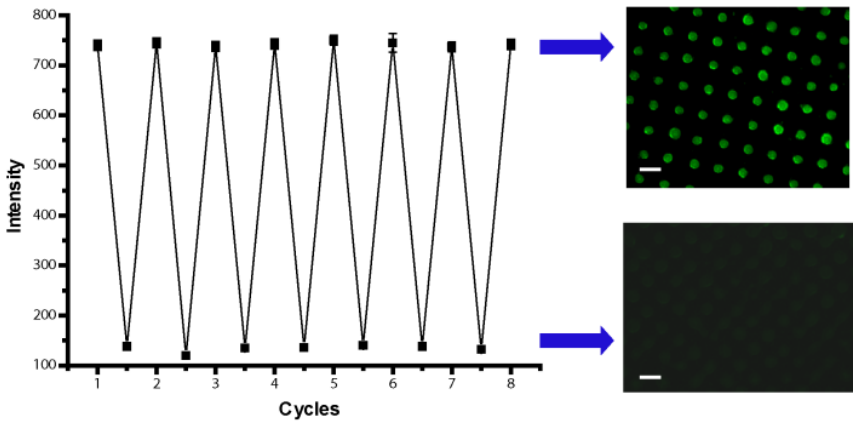

Figure 0.5 Relative fluorescence light intensities of the crosslinked gel pattern in repeating **Thy-QD** load-unload process. Scale bars are 10μm.

After crosslinking, **QD-Thy**, incorporated into the crosslinked gel pattern could be washed out by immersion in THF without disrupting the gel structure. The gels could be reloaded with **QD-Thy**, and the load-unload process was repeated without any decrease of the fluorescence intensity (Figure 2.5). As such, these systems provide a reusable platform for the construction of hybrid material micro-structures.

2.3 Experimental Section

2.3.1 Materials and chemicals

All chemicals and solvents were purchased from Aldrich or Fisher and were used as received without further purification unless otherwise noted. **PS-Thy** and **PS-DAP** were synthesized according to previous reports.[30] PDMS elastomer kits (Sylgard 184) were purchased from Dow Corning Corporation (Midland, MI). The synthesis ***QD-Thy and QD-MeThy*** nanoparticles has been described before.[30] Synthesized nanoparticles were dispersed in a mixed solvent of 10% THF and 90% DCM.

2.3.2 Synthesis of 11-Thymine-undecanoic acid

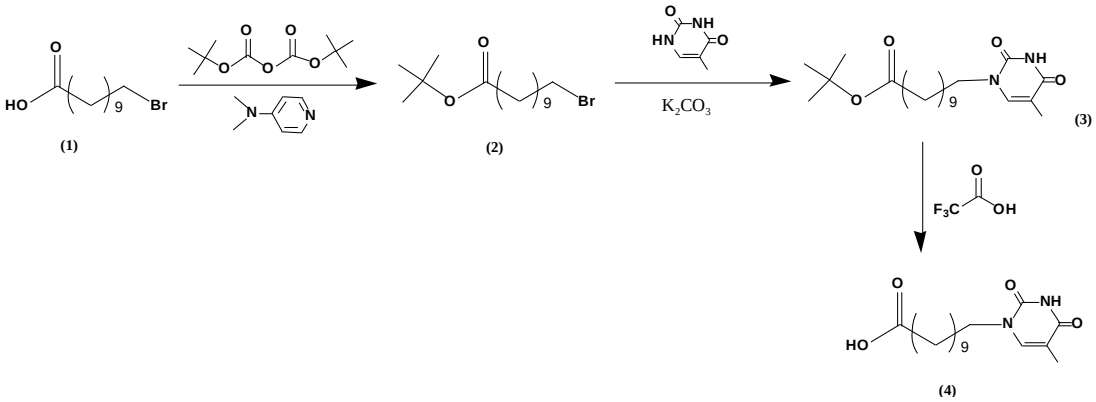

*Synthesis of 11-Bromo-undecanoic acid tert-butyl ester (2):*11-bromo-undecanoic acid (1) (2g, 10.25 mmol) and di-tert-butyldicarbonate (3.35 g, 15.37 mmol) were dissolved in 30 ml of t-butanol. Catalytic amount of N,N-dimethyl pyridine (0.13 g, 0.1mmol) was added to the reaction mixture. The reaction mixture was stirred for 3 h. The solvent was evaporated under reduced pressure to afford reddish oily liquid. This crude product was purified by flash silica column chromatography using mixed solvent system (Hexane : ethyl acetate= 5:1) as an elute, yield reddish colored oily liquid (2.2 g, 85 %).

1HNMR (400 MHz, $CDCl_3$): delta (ppm) 3.4 (t, 2H, -CH2-Br), 2.2 (t, 2H, -CO-CH2-C-), 1.75 (m, 2H, -CH2-C-Br), 1.7-1.1 (m, 23H, CH_2 and O-C$(OCH_3)_3$)

Synthesis of 11-Thymine-undecanoic acid tert-butyl ester (3): Compound 2 (0.321 g, 1 mmol), thymine (0.252 g, 2 mmol) and K_2CO_3 (0.552 g, 4 mmol) were dissolved in 20 ml DMF. The solution was stirred overnight at 60 °C. K_2CO_3 was removed by suction filtration and DMF was evaporated under reduced pressure. The crude product was purified by column chromatography on silica gel using a mixed solvent of hexane and ethyl acetate (v : v = 1 : 1), yielding 2 as a white solid. (0.295 g, 81%).

^{1}H NMR (400 MHz, $CDCl_3$): δ (ppm) 8.24 (s, 1H, NH), 6.97 (s, 1H, C=CH-C), 3.67 (t, 2H, N-CH_2-C), 2.19 (t, 2H, CO-CH_2-C), 1.92 (s, 3H, =C-CH_3), 1.7-1.1 (m, 23H, CH_2 and O-C(OCH_3)$_3$).

Synthesis of 11-Thymine-undecanoic acid (4): Compound 3 (0.366 g, 1 mmol) was dissolved into a mixed solvent of dichloromethane and trifluoroacetic acid (v : v = 1 : 1). The solution was stirred overnight at room temperature. Viscous oil-like crude product was got after the removal of the solvent by rotate evaporation. Add water into the crude product and sonicate the mixture for 10 min to get a white precipitate. After suction filtration to get rid of the liquid and washing by water, white solid product was obtained. (0.290 g, 94%).

^{1}H NMR (400 MHz, CD_3OD): δ (ppm) 7.44 (s, 1H, C=CH-C), 3.72 (t, 2H, N-CH_2-C), 2.29 (t, 2H, CO-CH_2-C), 1.90 (s, 3H, =C-CH_3), 1.68-1.60 (m, 4H, CH_2), 1.40-1.25 (m, 12H, CH_2).

2.3.3 Synthesis of thymine functionalized Fe_2O_3 NP

Fe_2O_3-Thy nanoparticles were synthesized from oleic acid coated 6 nm iron oxide nanoparticles[33] using place-exchange reaction. In typical experiment, 30 mg of the original Fe_2O_3 nanoparticles and 100 mg of Thy-carboxylic acid ligand were dissolved in 5 mL DCM. Reaction mixture was purged with Ar and heated for 2 days at 40 °C in a closed vial. DCM was evaporated and free ligands were removed by washing with ethanol for two times. The resulting black residue was re-dispersed in DCM and methanol mixture (9:1).

2.3.4 Patterning and gel array formation

The microcontact printing of OTS on Si/SiO_2 wafer was performed as described by Jeon et al,[26] and the PDMS stamp was made by standard method as described by Xia and Whitesides.[25]

The polymer gel precursors solution was prepared by mixing together 1 mg/mL solutions of **PS-Thy** and **PS-DAP** in DCM with a 1:1 (v:v) ratio. The pre-patterned silicon wafer was dipped into the precursor solution for 5 hours followed by a gentle rinsing using DCM. Finally the patterned substrate was dried with Ar flow and use for imaging.

Crosslinking of microgel was performed under a Spectroline ENF-240C UV light using 254 nm UV light for 20 minutes.

2.3.5 Incorporation of nanoparticles into microgel

To incorporate the nanoparticles into the polymer complex patterned on the surface, the substrate was dipped into the nanoparticle solution for 5 min, followed by solvent rinsing and drying under Ar flow. The **QD-Thy** was removed from the crosslinked gel pattern by dipping the substrate into THF solvent for 1 hour.

2.3.6 Imagining characterization

Optical and fluorescence microscope images were taken on Olympus BX51 optical microscope system and Olympus IX51 reflected fluorescence systems respectively.

AFM and MFM were performed on a Digital Instruments IIIa scanning probe microscope, and the images were obtained in the tapping mode under ambient conditions. The MFM image was obtained in the tapping and lift mode with a magnetic tip (Veeco MESP with Co/Cr alloy coating on both sides) at a lift scan height of 100 nm.

2.4 Conclusion

In this chapter, we have demonstrated the creation of patterned microgels composed of complementary polystyrene chains functionalized with diamidopyridine and thymine functionality. These gels could be selectively functionalized using nanoparticles bearing complementary hydrogen bonding moieties. Moreover, these gels could be crosslinked, allowing reversible incorporation of nanoparticles. Taken together, the 'lock and key' attributes of these gels make them highly attractive materials for the creation of modular functional materials.

2.5 References

1 Whitesides, G. M.; Mathias, J. P.; Seto, C. T. *Science* **1991**, *254*, 1312.

2 Fyfe, M. C. T.; Stoddart, J. F. *Acc. Chem. Res.* **1997**, *30*, 393.

3 Hof, F.; Craig, S. L.; Nuckolls, C.; Julius Rebek, J. *Angew. Chem. Int. Ed.* **2002**, *41*, 1488.

4 Binder, W. H.; Kluger, C.; Straif, C. J.; Friedbacher, G. *Macromolecules* **2005**, *38*, 9405.

5 South, C. R.; Burd, C.; Weck, M. *Acc. Chem. Res.* **2007**, *40*, 63.

6 Kumar,A. M. S.; Sivakova, S.; Fox, J. D.; Green, J. E.; Marchant, R. E.; Rowan, S. J. *J. Am. Chem. Soc.* **2008**, *130*, 1466.

7 ten Brinke, G.; Ruokolainen, J.; Ikkala, O. in *Hydrogen Bonded Polymers, Vol. 207*, **2007**, pp. 113.

8 Fogleman, E. A.; Yount, W. C.; Xu, J.; Craig, S. L. *Angew. Chem. Int. Ed.* **2002**, *41*, 4026.

9 Serpe, M. J.; Craig, S. L. *Langmuir* **2007**, *23*, 1626.

10 Kushner, A. M.; Gabuchian, V.; Johnson, E. G.; Guan, Z. *J. Am. Chem. Soc.* **2007**, *129*, 14110.

11 Li, M.; Yamato, K.; Ferguson, J. S.; Singarapu, K. K.; Szyperski, T.; Gong, B. *J. Am. Chem. Soc.* **2008**, *130*, 491.

12 Abdallah, D. J.; Weiss, R. G. *Adv. Mater.* **2000**, *12*, 1237.

13 Estroff, L. A.; Hamilton, A. D. *Chem. Rev.* **2004**, *104*, 1201.

14 Sangeetha, N. M.; Maitra, U. *Chem. Soc. Rev.* **2005**, *34*, 821.

15 Binder, W. H.; Petraru, L.; Roth, T.; Groh, P. W.; Pálfi, V. S.; Ivan, K. B. *Adv. Funct. Mater.* **2007**, *17*, 1317.

16 Yount, W. C.; Loveless, D. M.; Craig, S. L.; *J. Am. Chem. Soc.* **2005**, *127*, 14488.

17 Hirst, R.; Smith, D. K.; Feiters, M. C.; Geurts, H. P. M.; Wright, A. C. *J. Am. Chem. Soc.* **2003**, *125*, 9010.

18 Zhang, Y.; Gu, H.; Yang, Z.; Xu, B. *J. Am. Chem. Soc.* **2003**, *125*, 13680.

19 Shi, N. E.; Dong, H.; Yin, G.; Xu, Z.; Li, S. H. *Adv. Funct. Mater.* **2007**, *17*, 1837.

20 Brunsveld, L.; Folmer, B. J. B.; Meijer, E. W.; Sijbesma, R. P.; *Chem. Rev.* **2001**, *101*, 4071.

21 Crespo-Biel, O.; Ravoo, B. J.; Reinhoudt, D. N.; Huskens, J. *J. Mater. Chem.* **2006**, *16*, 3997.

22 Pollino, J. M.; Stubbs, L. P.; Weck, M. *J. Am. Chem. Soc.* **2004**, *126*, 563.

23 Ilhan, F.; Galow, T. H.; Gray, M.; Clavier, G.; Rotello, V. M. *J. Am. Chem. Soc.* **2000**, *122*, 5895.

24 Uzun, O.; Sanyal, A.; Nakade, H.; Thibault, R. J.; Rotello, V. M. *J. Am. Chem. Soc.* **2004**, *126*, 14773.

25 Xia, Y.; Whitesides, G. M. *Angew. Chem. Int. Ed.* **1998**, *37*, 550.

26 Jeon, N. L.; Finnie, K.; Branshaw, K.; Nuzzo, R. G. *Langmuir* **1997**, *13*, 3382.

27 Nie, Z.; Kumacheva, E. *Nat. Mater.* **2008**, *7*, 277.

28 Cheng, J. Y.; Ross, C. A.; Smith, H. I.; Thomas, E. L. *Adv. Mater.* **2006**, *18*, 2505.

29 Trindade, T.; O'Brien, P.; Pickett, N. L. *Chem. Mater.* **2001**, *13*, 3843.

30 Thibault, R. J.; Uzun, O.; Hong, R.; Rotello, V. M. *Adv. Mater.* **2006**, *18*, 2179.

31 Lu, A.-H.; Salabas, E. L.; Schüth, F. *Angew. Chem. Int. Ed.* **2007**, *46*, 1222.

32 Yan, M.; Harnish, B. *Adv. Mater.* **2003**, *15*, 244.

33 Sun, S.; Zeng, H.; Robinson, D. B.; Raoux, S.; Rice, P. M.; Wang, S. X.; Li, G. *J. Am. Chem. Soc.* **2004**, *126*, 273.

CHAPTER 3

FUNCTIONALIZATION OF NANOPATTERNED POLYMER FILMS THROUGH AMINE-ALDEHYDE CHEMISTRY FOR NANOPARTICLE AND ENZYME IMMOBILIZATION

3.1 Introduction

Post-functionalization of polymer surfaces is a critical tool for utilization of polymeric materials.[1, 2] Surface properties, such as chemical reactivity, surface energy, hydrophobicity, hydrophilicity, and bio-compatibility can be modulated through surface functionalization to address application-specific requirements for adhesion,[3] friction, protective coatings,[2, 4] biomaterials,[5, 6] medicine[7] and microelectronic devices.[2] Due to the inert nature of most polymer materials, polymer surfaces must be activated prior to functionalization. Activation can be accomplished by ionized gas treatment,[8] corona discharge,[9] UV irradiation,[10] wet chemistry,[11] or physical adsorption.[12] Carboxylate, amine, unsaturated C-C bond, and peroxide are common active groups generated by these processes. The desired functionalization can then be accomplished by carrying out chemical reactions,[8] or further polymerization,[10] depending on the choice active surface groups.

The use of electrophilic groups for covalent surface modification is complicated by the lability of these moieties to hydrolysis. Aldehyde groups, however, are generally unreactive towards water, but readily undergo nucleophilic addition reactions to generate a variety of products such as imines, cyanohydrins, and acetals. Despite this versatility, aldehydes are seldom used in polymer synthesis, primarily due to difficulties in monomer synthesis, and reactivity of this group during polymerization. Here, we present a simple and versatile method to activate polystyrene-based surfaces with aldehyde groups through simultaneous crosslinking and photooxidation of chloromethylstyrene films patterned via nanoimprint lithography (NIL).[13, 14, 15] Significantly, the

aldehyde moiety was stable to plasma etching, allowing functional polymer nanostructures to be formed in a single step without additional resists.[16, 17] Dyes, nanoparticles, and enzymes can be readily immobilized onto these films via nucleophilic addition reaction of their pendant amines with aldehydes.

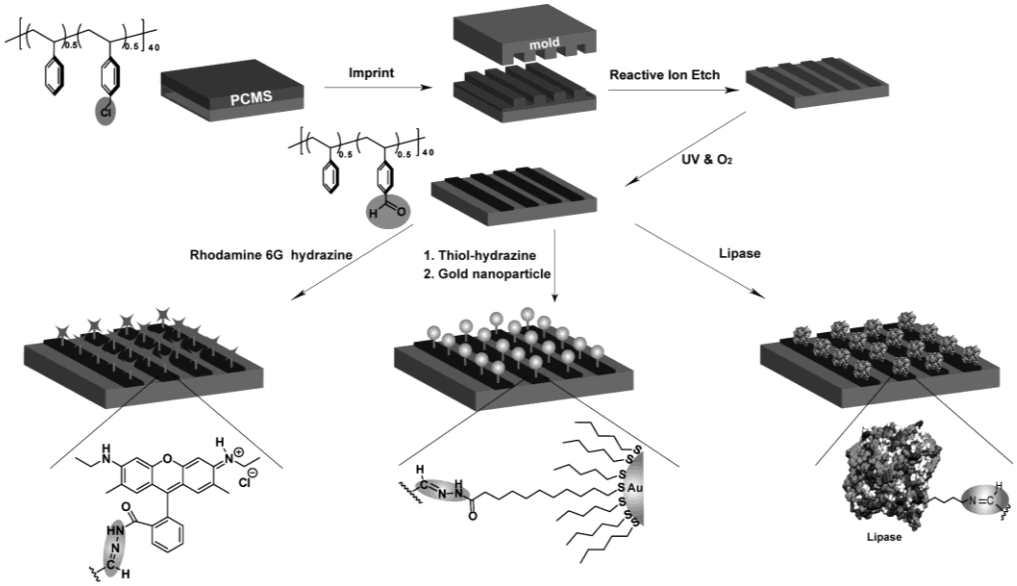

Figure 0.1 Schematic illustration of the nanoimprinting lithography and functionalization process

3.2 Results and Discussion

3.2.1 Nanoimprint lithography of the polymer film and photo-activation

The precursor patterned PCMS polymer films were fabricated through hot molding NIL with a stiff silicon mold (Figure 3.1). The residual layer was then removed through an O_2 RIE etch. The patterned PCMS film was then exposed to a 254nm UV irradiation for 2 hours at ambient conditions. This step had two functions. First, UV irradiation generated aldehyde groups on the polymer film through photooxidation. Second, the polystyrene-based polymer was simultaneously cross-linked by UV irradiation through a photo-generated radical crosslinking reaction, making the film stable to both organic and aqueous solvents.[18]

Attenuated total reflection infrared (ATR-IR) spectroscopy was used to monitor chemical changes during the etching and crosslinking steps. Both pure PS and PCMS film showed little

detectable change in the ATR-IR spectrum after etching step, with the exception of a decrease of the strength of the aromatic peaks between 1600 cm $^{-1}$ and 1400 cm $^{-1}$. Although the presence of the carbonyl groups on the polymer surface after O_2 plasma etching was confirmed by XPS,[19] the number of the groups present might be too low to be detected by ATR-IR. After UV irradiation, however, a strong carbonyl group peak at ~1720 cm^{-1} appeared in the ATR-IR spectrum of PCMS film. Meanwhile, only a low broad peak of hydroxyl group was found between 3600 cm^{-1} and 3200 cm^{-1}, indicating that the carbonyl group absorbance is primarily due to aldehyde and not carboxylic acid functionality.

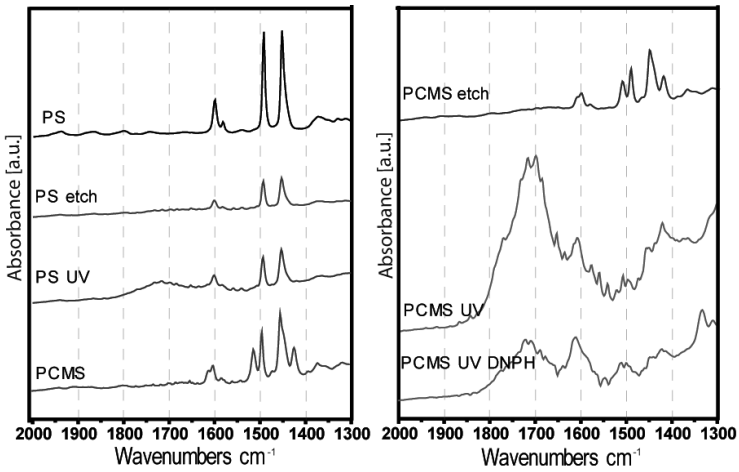

Figure 0.2 ATR-IR spectrum of PS and PCMS at different steps of the fabrication process.

To further confirm the presence of aldehyde groups, 2, 4-dinitrophenylhydrazine (DNPH, Brady's reagent) was reacted with the polymer film. It is well established that DNPH reacts selectively with carbonyl group of aldehydes while leaving carboxylic acid or ester intact. Since the hydrazone products of the reaction between DNPH and aldehyde have no significant absorbance in ~1700cm^{-1} area of IR spectrum, a decrease of the carbonyl peak was expected. A substantial decrease in the carbonyl peak was observed after immersing the UV irradiated PCMS film into DNPH solution for 10 min. (Figure 3.2) As a control experiment, pure PS film shows only very weak carbonyl absorbance after UV exposure. These results clearly demonstrate that an UV

exposure, in ambient environment for two hours, can generate abundant aldehyde groups on an inert PCMS resist film, and that benzylic chloro groups play a key role in this process.

As a proof-of-concept of polymer functionalization using the aldehyde functionality, we reacted the PCMS pattern with modified Rhodamine 6G bearing a reactive hydrazine group (Figure 3.1 and 3.3). After dipping UV irradiated PCMS pattern into a Rhodamine-hydrazine methanol solution at a pH of 4 for 10 minutes, we observed a clear pattern by fluorescence microscopy. This indicated the successful immobilization of the Rhodamine dye upon the polymer surface. A control UV-irradiated PS substrate showed no observable fluorescence under the same conditions.

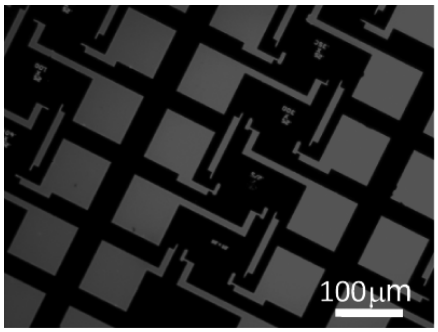

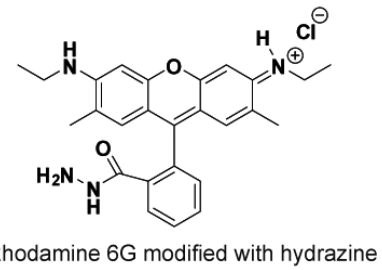

Figure 0.3 Fluorescence microscope image of the PCMS pattern after UV irradiation and Rhodamine-hydrazine modification.

3.2.2 Immobilization of Gold NPs on pattern surface

Nanoparticles are an emerging and versatile assembly unit in material science. The deposition of nanoparticles onto patterned surfaces represents a modular approach to tune the electronic, magnetic, optical, and biological properties of functionalized polymer surfaces.[20, 21] Gold nanoparticles (AuNP) were likewise immobilized onto our activated patterns by simple post functionalization. A heterobifunctional tethering molecule (11-mercaptoundecane hydrazine), was used to immobilize gold nanoparticles onto the activated polymer surface (Figure 3.4 D). The UV irradiated PCMS substrate was placed into the 11-mercaptoundecane-hydrazine methanol solution at pH 4 for 1 hour to generate the thiol functionalized surface. The substrate was then incubated in a pentanethiol-protected gold nanoparticle solution for 8 hours to enable a place exchange reaction of the tethered thiol groups with the pentanethiol ligand on the nanoparticle.

XPS was used to monitor the deposition process (Figure 3.4). After introduction of the tethering molecule, we see the characteristic N 1s and S 2p peaks of the tethering molecule at ~ 399 eV and 165 eV respectively on the substrate. Very strong Au 4f peaks were also found at ~88 and 84 eV after the immobilization step that clearly demonstrate successful functionalization of the pattern by gold nanoparticles. A control PCMS film irradiated by UV, but without the hydrazine thiol present in the place exchange reaction mixture showed only a very weak gold signal, demonstrating that uptake was tether-driven.

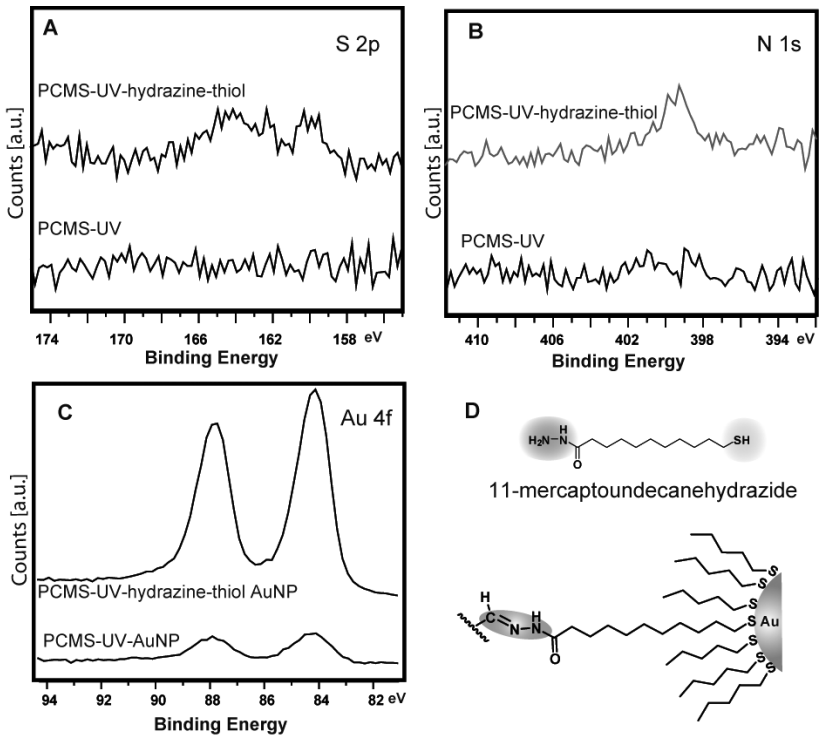

Figure 0.4 XPS of sulfur (A), nitrogen (B) and gold (C) of PCMS film before and after hydrazine-thiol molecule and gold nanoparticle modification. (D) is the structure of tethering molecule and the anchoring chemistry.

3.2.3 Enzyme immobilization and their activity

Immobilization of proteins onto polymer surfaces is central to many analytical tools and techniques in biomedicine and biotechnology [22, 23] Aldehyde groups have been extensively used to covalently immobilize proteins onto such surface through reaction with the amine on exposed lysine residues.[24, 25, 26] To demonstrate this capability with our films, we immobilized a lipase

enzyme from *Candida rugosa* onto patterned polymer surfaces. An UV-irradiated PCMS substrate was incubated in a 22μM lipase solution in PBS at pH 7.4 (48 hours at room temperature). The substrate was then sonicated in PBS for 20 seconds and rinsed thoroughly with PBS and deionized water to remove any physisorbed lipase. XPS measurement of the polymer surface showed a clear N 1s peak after lipase modification, likely due to the abundant nitrogen atoms present in the enzyme. The successful immobilization of the enzyme is further demonstrated using the fluorescent Rhodamine B isothiocyanate labeled lipase. Using fluorescence microscopy, we were able to see a red fluorescent pattern due to the Rhodamine B-labeled lipase. A control PCMS lacking immobilized lipase shows only very weak fluorescence when treated under the same conditions.

The lipase-catalyzed hydrolysis of 4-methylumbelliferyl butyrate was used to quantify the activity of the immobilized enzyme.[27] An increase in fluorescence signal at 460 nm over time was measured (zero-order kinetics for initial product formation was assumed). The reaction solution was stirred rapidly to ensure homogeneity and to eliminate limitations introduced by mass transport processes. Activity was indeed maintained by the lipase while immobilized to the PCMS substrate (Figure 3.5), whereas a UV-irradiated PS film modified by lipase exhibited very low fluorescence at the same wavelength. Using data from the enzymatic reaction, we were able to estimate the density of lipase on the PCMS substrate. First, we prepared a lipase solution that exhibited similar activity to that of the lipase immobilized on PCMS substrate. The concentration of lipase in solution at generating this activity level was then translated into a 2D area density of surface size consistent with the polymer substrate (see experimental section). Using this method, we estimated the equivalent active lipase area density to be in the order of 10^{-14} mol/mm^2. The size of the *candida rugosa* lipase is 10.5x10.67x5.98 nm by X-ray measurement. If we assume a sphere close packing of the lipase on a 2D surface, the calculated area density of the lipase is also around 10^{-14} mol/mm^2. The similarity of these values indicates that the lipases are indeed closely packed upon the polymer surface, and that the majority maintain their activity.

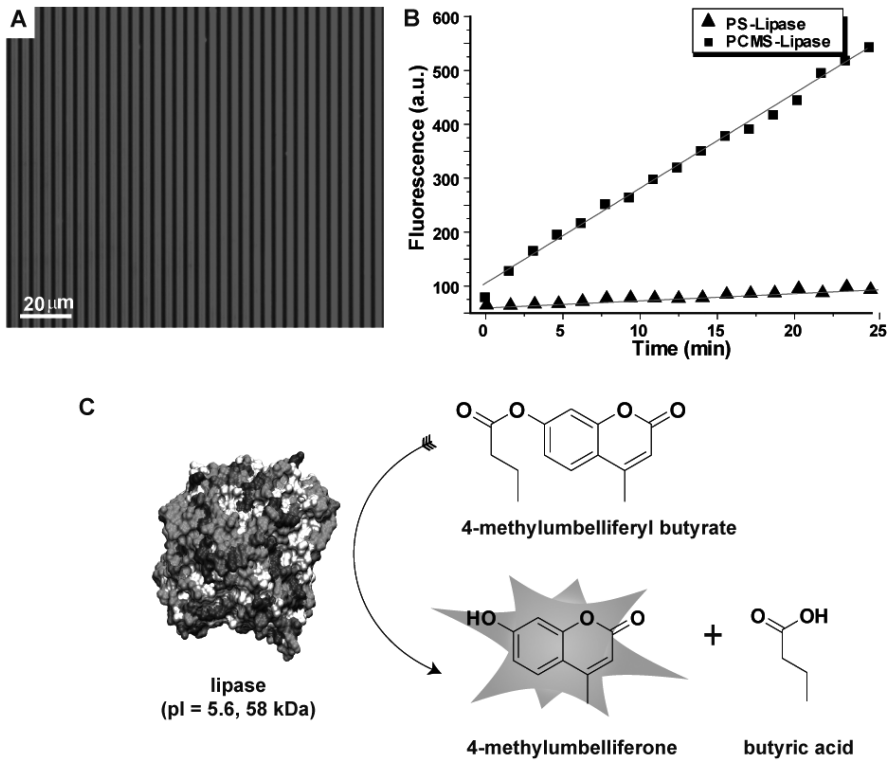

Figure 0.5 (A) Fluorescence microscope image of the Rhodamine B isothiocyanate labeled lipase immobilized on PCMS pattern. (B) Activity of the lipase immobilized on the PCMS film. (C) Hydrolysis reaction of 4-methylumbelliferyl butyrate catalyzed by lipase

3.3 Experimental Section

3.3.1 Materials

Poly (styrene-*p*-(chloromethyl) styrene) (PCMS) was prepared as described in our previous reports.[28] Gold nanoparticle with pentanethiol ligand was fabricated following the procedure described by Brust et al.[29]

The synthesis *Rhodamine 6G hydrazide (Rhodamine-hydrazine):* Rhodamine 6G (0.5 g, 1.04 mmol) and hydrazine hydrate (0.5g, 10 mmol) was mixed in methanol and stir overnight. The precipitate was filtrated by suction filtration and rinsed several times by methanol to afford the product as a white power. ^{1}H NMR (400 MHz, $CDCl_3$, TMS): δ 7.96 (m, 1H, C-CH=C), 7.42 (m, 2H, C-CH=C), 7.06 (d, 1H, C-CH=C), 6.38 (s, 2H, C-CH=C), 6.25(s, 2H, C-CH=C), 3.57 (m, C-NH-NH-C), 3.52 (t, 2H, Ar-NH-C), 3.2 (m, 4H, N-CH_2-C), 1.90 (s, 6H, Ar-CH_3), 1.33 (t, 6H, C-CH_3). ESI-MS, calcd for $C_{26}H_{29}N_4O_2$ ($M+H^+$) 429.2, found 429.1.

The synthesis *11-Mercaptoundecanehydrazide (Hydrazine-Thiol):* A mixture of hydrazine (1.37 g, 43 mmol) and methyl 11-mercaptoundecanoate (1.0 g, 4.30 mmol) were dissolved in methanol (5 mL). After stirring for 3h at 70 °C, the solvent was removed under reduced pressure. The crude product was then poured into a mixture of dichloromethane and distilled water. Organic layer was separated and concentrated at reduced pressure to afford the compound as a white powder. (0.78 g, 78 %) ^{1}H NMR (400 MHz, $CDCl_3$, TMS): δ 6.98 (s, 1H, -NH-), 3.90 (s, 2H, -NH_2), 2.50 (q, J = 7.2 Hz, 2H, HS-CH_2-), 2.50 (q, J = 7.3 Hz, 2H, -CH_2-CO-), 1.55 (m, 2H, −CH_2−), 1.25 (m, 14H, −CH_2−). ^{13}C NMR (100.64 MHz, $CDCl_3$, TMS) δ 174.05, 34.57, 34.01, 29.42, 29.36, 29.25, 29.02, 28.33, 25.49, 24.65.

Lipase labeling by Rhodamine B isothiocyanate: Rhodamine B isothiocyanate (2 mg) was dissolved 0.5 mL dimethyl sulfoxide and Lipase *candida rugosa* (6 mg) was dissolved in 2 mL 0.1M sodium bicarbonate solution. The two solutions were mixed and stirred in ice-water bath for 12 hours. The solution filtrated by filter with pore size of 0.45 μm to remove precipitates and then purified by centrifugal filters using phosphate buffered saline as washing solution.

3.3.2 Nanoimprint lithography and surface activation

Nanoimprinting of the polystyrene (PS) and PCMS was performed using a Nanonex NX-2000 nanoimprinter with a patterned silicon mold that contained test patterns of various feature sizes. Imprinting was performed at 150 °C and a pressure of 400 PSI for 2 minutes. The residual layer from the imprinting process was etched by reactive ion etching (RIE) under the following conditions: pressure 250 mTorr, inductive coupled plasma 150 W, reactive ion etching 30 W, Oxygen 50 SCCM, for 90 s. The UV irradiation was performed under a Stratagene 1800 UV stratalinker for 2 hours in an ambient condition.

3.3.3 Gold Nanoparticle immobilization

The UV irradiated PCMS substrate was placed into the 11-mercaptoundecane-hydrazine methanol solution at pH 4 for 1 hour. Then it was incubated in a pentanethiol-protected gold

nanoparticle toluene solution for 8 hours to enable a place exchange reaction of the tethered thiol groups with the pentanethiol ligand on the nanoparticle. The substrate was rinsed thoroughly with toluene and dried by air flow.

3.3.4 Lipase immobilization and activity estimation

The *candida rugosa* lipase was purchased from Aldrich and the solution concentration of the lipase was calibrated by the absorbance at 256nm using UV-Vis spectroscopy. The UV irradiated PCMS substrate was incubated in a 22 M lipase solution in phosphate buffer (**PBS**) at pH 7.4 for 48 hours in room temperature. After this, the substrate was sonicated in PBS for 20 seconds and then rinsed thoroughly by PBS and DI-water to remove all physisorbed lipase.

The lipase-catalyzed hydrolysis of 4-methylumbelliferyl butyrate (MUBB, Aldrich) was used as a test reaction to assess the activity of immobilized enzyme. 5 mg MUBB was dissolved into 10 ml PBS solution. MUBB cannot completely be dissolved. The 100 μl saturated MUBB solution was diluted into 20 ml using PBS. The concentration of MUBB was not well estimated, but was kept the same for all the measurements. The fluorescence measurement was conducted on PTI QM-3 Luminescence Spectrofluorometer. The fluorescence increase at 460 nm over time was measured by fluorometer, assuming zero-order kinetics for initial product formation. The test reaction was done in a 3 ml glass cuvette. The PCMS substrate with lipase immobilized was laid on the bottom of the cuvette and the solution was stirred rapidly to ensure homogeneity and the absence of mass transport limitations.

3.3.5 Calculation of the area density of the lipase on the PCMS surface

The activity of the lipase immobilized on a 5×5 mm^2 PCMS was monitored by fluorometer using the procedure as described above. A similar activity was found using a ~0.6 nM lipase solution as shown in the figure below. We multiply the concentration of the lipase solution with the volume used in the experiment (3 ml) and then divided by 25 mm^2 to get the active lipase area density on PCMS surface. The density obtained by this calculation is around $4\times10^{10}/mm^2$.

The X-Ray crystal determined size of the lipase is 10.5×10.67×5.98 nm. Assuming a sphere close packing with diameter of 6 nm on the surface, the density is $3.2\times10^{10}/mm^2$. The two similar values imply that most of the lipase on PCMS surface is still active. The higher experimental value might originate from the roughness of the PCMS surface.

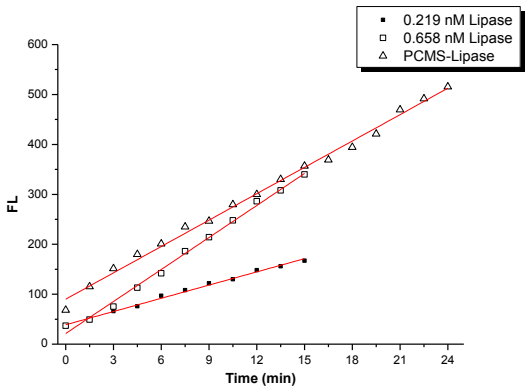

Figure 0.6 Estimation of the amount of lipase immobilized on PCMS film. Similar activity as the Lipase on film was obtained in the lipase solution of concentration of ~0.6 nM.

3.4 Conclusion

In summary, we have put forward a simple method to activate the inert polymer resist pattern from NIL using chloromethyl styrene copolymer and UV irradiation. The activated polymer resist pattern can be easily functionalized by dye, nanoparticle and enzyme using amine aldehyde chemistry. Given the veratility shown in the report, this methodology is expected to become a general method for polymer surface functionalization and for nanoparticle and protein immobilization and patterning.

3.5 References

1 Garbassi, F.; Morra, M.; Occhiello, E. *Polymer Surfaces from Physics to Technology*, Wiley, Chichester, England **1994**.

2 Bergbreiter, D. E.; Sprinivas, B.; Xu, G.-f.; Aguilar, G. ; Ponder, B. C.; Gray, H. N.; Bandella, A. in *Symposium on Polymer Surfaces and Interfaces: Characterization, Modification and Application* (Eds.: K. L. Mittal, K.-W. Lee), Utrecht, Netherlands, Boston, MA, **1997**, pp. 3.

3 Lee, K. W.; Kowalczyk, S. P.; Shaw, J. M.; *Macromolecules* **1990**, *23*, 2097.

4 Nuzzo, R. G.; Smolinsky, G.; *Macromolecules* **1984**, *17*, 1013.

5 Goddard, J. M.; Hotchkiss, J. H. *Prog. Polym. Sci.* **2007**, *32*, 698.

6 Chen, H.; Yuan, L.; Song, W.; Wu, Z.; Li, D. *Prog. Polym. Sci.* **2008**, *33*, 1059.

7 Braybrook, J. H.; Hall, L. D. *Prog. Polym. Sci.* **1990**, *15*, 715.

8 Schönherr, H.; Hruska, Z.; Vancso, G. J. *Macromolecules* **1998**, *31*, 3679.

9 Song, J.; Gunst, U.; Arlinghaus, H. F.; Vancso, G. J. *Appl. Surf. Sci.* **2007**, *253*, 9489.

10 Deng, J.; Wang, L.; Liu, L.; Yang, W. *Prog. Polym. Sci.* **2009**, *34*, 156.

11 Silva, R.; Muniz, E. C.; Rubira, A. F. *Langmuir* **2009**, *25*, 873.

12 Bergbreiter, D. E.; Chance, B. S. *Macromolecules* **2007**, *40*, 5337.

13 Huang, C.; Dong, B.; Lu, N.; Yang, B.; Gao, L.; Tian, L.; Qi, D.; Wu, Q.; Chi, L. *Small* **2009**, *5*, 583.

14 Subramani, C.; Ofir, Y.; Patra, D.; Jordan, B. J.; Moran, I. W.; Park, M.-H.; Carter, K. R.; Rotello, V. M. *Adv. Funct. Mater.* **2009**, *19*, 2937.

15 Mele, E.; Di Benedetto, F.; Persano, L.; Cingolani, R.; Pisignano, D. *Nano Lett.* **2005**, *5*, 1915.

16 Guo, L. J. *Adv. Mater.* **2007**, *19*, 495.

17 McAlpine, M. C.; Friedman, R. S.; Lieber, C. M. *Nano Lett.* **2003**, *3*, 443.

18 Yan, M.; Harnish, B. *Adv. Mater.* **2003**, *15*, 244.

19 Greenwood, O. D.; Boyd, R. D.; Hopkins, J.; Badyal, J. P. S. in *International Symposium on Polymer Surface Modification: Relevance to Adhesion* (Ed.: K. L. Mittal), Utrecht, Netherlands : VSP, 1996, Las Vegas, Nevada, **1993**, pp. 17.

20 Kinge, S.; Crego-Calama, M.; Reinhoudt, D. N.; *Chemphyschem* **2008**, *9*, 20.

21 Andrew, N. S.; Eugenii, K.; Itamar, W. *Chemphyschem* **2000**, *1*, 18.

22 Phizicky, E.; Bastiaens, P. I. H.; Zhu, H.; Snyder, M. ; Fields, S. *Nature* **2003**, *422*, 208.

23 Wilson, D. S.; Nock, S. *Angew. Chem. Inter. Ed.* **2003**, *42*, 494.

24 MacBeath, G.; Schreiber, S. L. *Science* **2000**, *289*, 1760.

25 Jones, R. B.; Gordus, A.; Krall, J. A.; MacBeath, G. *Nature* **2006**, *439*, 168.

26 Rozkiewicz, D. I.; Kraan, Y.; Werten, M. W. T.; Wolf, F. A. d.; Subramaniam, V.; Ravoo, B. J.; Reinhoudt, D. N. *Chem. Eur. J.* **2006**, *12*, 6290.

27 Roberts, I. *Lipids* **1985**, *20*, 243.

28 Ilhan, F.; Gray, M.; Blanchette, K.; Rotello, V. M. *Macromolecules* **1999**, *32*, 6159.

29 Brust, M.; Walker, M.; Bethell, D.; Schiffrin, D. J.; Whyman, R. *J. Chem. Soc., Chem. Commun.* **1994**, 801.

CHAPTER 4

CONTROL OF SURFACE TENSION AT LIQUID-LIQUID INTERFACE USING NANOPARTICLES AND NANOPARTICLE-PROTEIN COMPLEXES

4.1 Introduction

Emulsions stabilized by nanoparticles, novel surface-active materials and emulsion stabilizers,[1] have applications in diverse areas including catalysis,[2,3] drug delivery,[4] and food science.[5] In these systems, nanoparticles (NPs) stabilize the liquid-liquid interface through the minimization of interfacial energy of the system.[6] In addition to stabilization of the interface, the dynamic nature of the NP assembly at liquid-liquid interfaces can be used to generate defect-free organized nanostructures.[7] Assembly of nanocrystals into 2D constructs using these emulsion platforms provides a strategy for the creation of novel multiscale materials with unique electronic, magnetic and optical properties.[8] Recently, assembly of bionanoparticles, such as proteins, virus particles, and other supramolecular protein assemblies, have shown promise for creating highly organized biomolecular systems utilizing their monodisperse sizes, biocompatibility, and ease of functionalization at the interface.[9]

Interparticle interaction at liquid-liquid interfaces is one of the key determinants for emulsion stabilization.[10] Prior approaches to the creation of nanoparticle-stabilized emulsions have focused on chemical cross-linking of NPs assembled at the oil-water interface.[11] Recently, supramolecular interactions have been used for fabricating robust microcapsules.[12] In particular, charge-mediated assembly of NPs and proteins has been used to provide lateral stabilization of the emulsions.[3] Key requirements of this approach are the amphiphilic nature of the resulting supramolecular assemblies and their instantaneous migration to the interface; the synergistic interaction of NP-

protein complex at the interface and the dynamics of interfacial adsorption are crucial factors governing the stability of liquid-liquid emulsions.[13]

Surface tension is a fundamental quantity that relates to the properties of the assembly and segregation dynamics of surface active materials at phase interfaces, plays a crucial role in the process of emulsion formation and stabilization.[14,15] In this article, we report the dynamic interfacial behaviour of monolayer-protected gold NPs and NP-protein conjugates at toluene-water interface using dynamic surface tension measurements. It was found that the dynamics of the assembly of the monolayer protected NPs follows an interaction based mixed kinetic-diffusion mechanism, where the adsorption of NPs at the interface is the rate-controlling step rather than diffusion. These studies indicate that both the hydrophobicity and detailed structure of the NP monolayer play a critical role in the interfacial assembly with the particle alone and with the particle-protein assemblies.

4.2. Results and Discussions

4.2.1 Structure of nanoparticles

We synthesized five structurally related cationic gold NPs (Figure 4.1a) featuring 2 nm cores to isolate the role of NP surface hydrophobicity on interfacial assembly. These gold NPs provide multivalent binding with anionic proteins, forming complexes through electrostatic and hydrophobic interactions.[16] Additionally, these bio-inspired NPs feature a tetra(ethylene glycol) spacer in the ligand shell to both isolate the effects of the headgroup[17] and minimize denaturation of the bound protein.[18] We used acid phosphatase (PhosA) as a model anionic protein due to its relatively large size (Mw = 110 kDa, dimension = 12.6 nm × 20.7 nm × 7.3 nm) and negative charge at neutral pH (pI = 5.2).

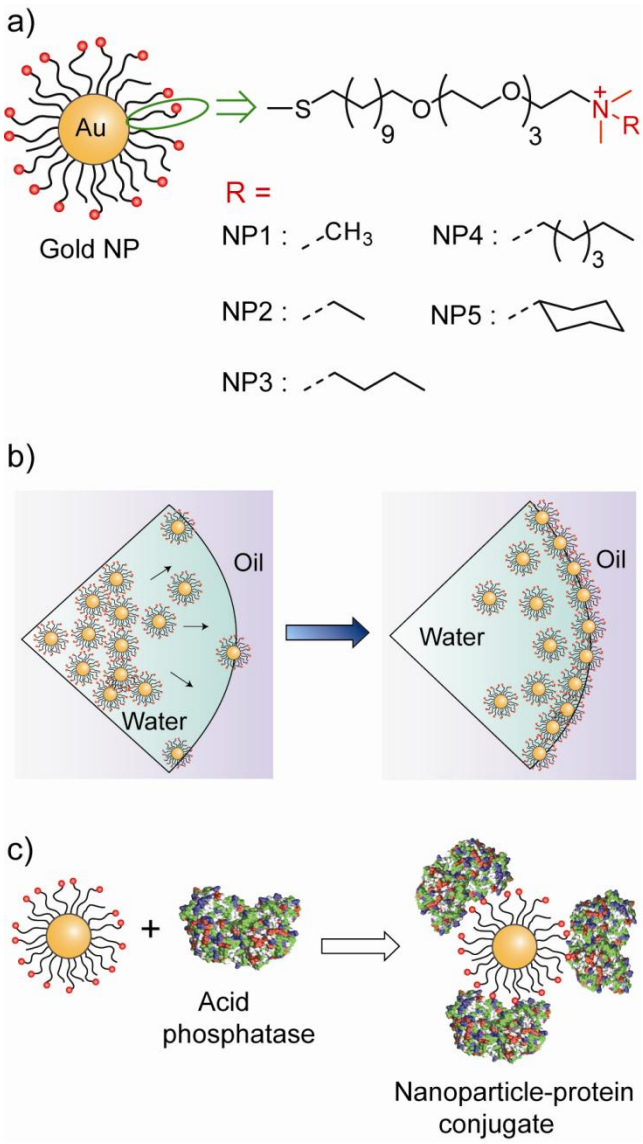

Figure 0.1(a) Structure of the NPs and their monolayer ligand shells. (b) Schematic of the assembly of particle at the oil-water interface. Initially the surface coverage is very low, and then rapidly covers the interface. At the steady state, complete monolayer coverage is observed when packing rearrangement and conformational changes occur. (c) Schematic of NP-protein complex formation.

4.2.2 Assembly dynamics of nanoparticle at interface

We first studied time dependent pendant drop tensiometer measurements at the water-toluene interface for the particles (NP1 – NP5) at 1 μM in 5 mM sodium phosphate (PBS) buffer at pH 7.4. Figure 4.2 presents the dynamic surface tension (γ_t) plots for NP1 to NP5, where the

interfacial tension decreases with time approaching an equilibrium value. In the early stage, interfacial tension drops rapidly due to instantaneous self-assembly of the NPs at the interface. Once the droplet is mostly covered by NPs, the decrease in interfacial tension reaches a dynamic equilibrium where the rate of adsorption of NPs at the interface equals the rate of desorption (Figure 4.1b).[25] It can be observed that the experimental meso-equilibrium γ (γ_{eq}) value decreases significantly with increasing hydrophobicity of the particles (Figure 4.2). NP4 and NP5 having ligand headgroups of same alkyl chain length, and hence similar hydrophobicity, attain similar γ_{eq}, but exhibit a different kinetic behaviour (*vide infra*).

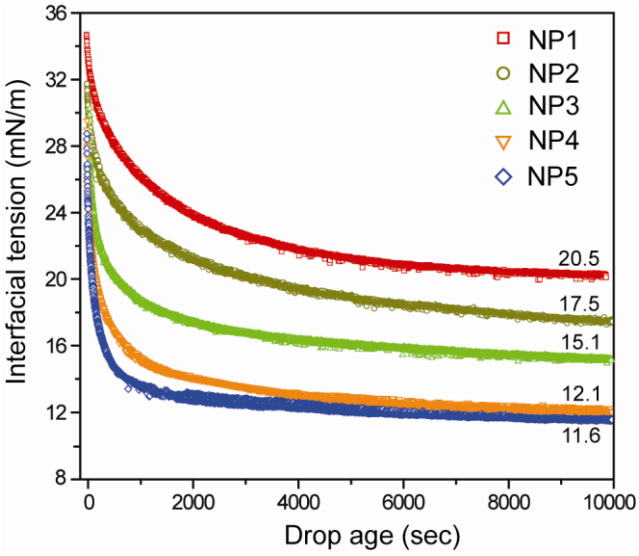

Figure 0.2 Time dependence of the interfacial tension for gold NPs of different monolayer structures at the same bulk concentration of 1 μM at the toluene-water interface. The numbers near each plot indicate γ_{eq} value at 10000 sec.

The variation in interfacial tension with different NPs can be explained by the effect of their surface functionality on assembly at the oil-water interface. Hydrophobic NP4 and NP5 behave as amphiphilic surfactants at the water-toluene interface, resulting in the maximum reduction in equilibrium interfacial tension. More hydrophilic NP2 and NP3 behave as moderately weak amphiphiles and intermediate γ_{eq} values are observed, while hydrophilic NP1 provides the

smallest amount of effective interfacial tension reduction. In addition to providing enhanced surface activity, increasing hydrophobicity of the nanoparticle accelerates the emulsification process.

The kinetic behavior of the surface tension of the NP stabilized water-in-oil emulsions was obtained using γ_t vs time plots fitted to the empirical Hua and Rosen equation[19] that has been widely employed for interpreting dynamic surface tension behaviors. One form of the equation is given by Equation 1:

$$\gamma_t = \gamma_m + (\gamma_0 - \gamma_m)/[1 + (t/t^*)^n] \qquad (1)$$

where, γ_t is the surface tension at any time t, γ_0 is the surface tension of the pure solvent, γ_m is the surface tension at meso-equilibrium, t^* is the half-time for reaching γ_m, and n is a dimensionless exponent. Assuming that the value of γ_0 is held constant at value for the pure buffer surface tension, there are three adjustable parameters: γ_m, t^*, n. These parameters were estimated by computer fitting of the measured dynamic surface tension data. By differentiating Equation 2 with respect to t and substituting t for t^*, the maximum surface tension decay rate, ν_{max}, of γ is obtained as follows:

$$\nu_{max} = n(\gamma_0 - \gamma_m)/4t^* = -(d\gamma_t/dt)_{t^*} \qquad (2)$$

All the γ_t vs time plots were fitted nicely with correlation coefficients being ≥0.99 and the results are presented in Table 1. It can be observed that γ_m decreases from NP1 to NP4 as the hydrophobicity increases. Also, NP4 and NP5 with similar hydrophobicity show a similar γ_m value. We next investigated the quantitative relationship between hydrophobicity of the ligand headgroup with surface tension at the meso-equilibrium. We determined the computed octanol-water partition coefficient (P_{oct}) of the NP headgroups, which can be used as a measure of hydrophobicity.[20] We observed a linear decrease in γ_m with increasing hydrophobicity of the

ligand headgroups as shown in Figure 4.3. The data set was fitted well by Equation 3 with a correlation of 0.965:

$$\gamma_m = 18.66 - 2.204\log_{10} P_{oct} \qquad (3)$$

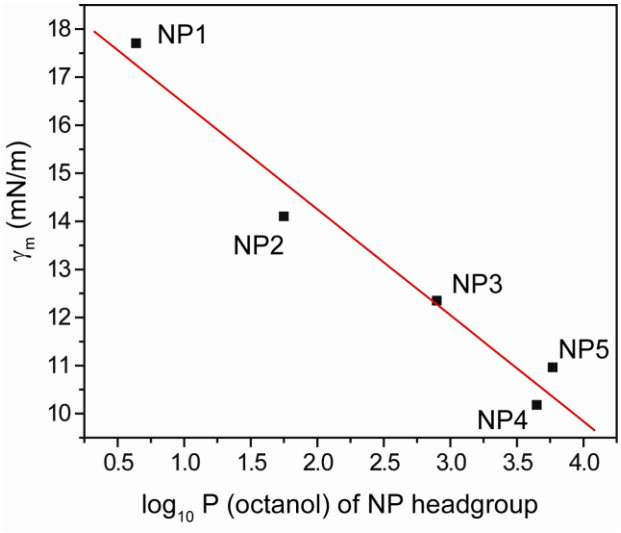

Figure 0.3 Plot of γ_m vs partition coefficient of the headgroups on the particle monolayer.

Effect of NP monolayer on their dynamics at the toluene-water interface, isolated from the Hua-Rosen parameters t^* and γ_{max}, provides a mechanistic insight of particle segregation at the interface. It can be observed that with increasing hydrophobicity from NP1 to NP5 the values of t^* decreases gradually, while the γ_{max} increases. Since the hydrodynamic size of the NPs increases from NP1 to NP5 (Table 4.1), diffusion-controlled mechanism alone cannot explain the observed trend of dynamics. Presumably, it is the adsorption rate at the interface that determines the kinetic parameters of the system. NPs with increased lipophilicity tend to possess higher adsorption rate towards the interface, and hence a faster dynamics is expected. However, NP5 exhibit a 2.3-fold faster decay rate of γ_t than NP4, even though their hydrophobicities are quite similar. Structural attribute, such as constrained cyclic conformation of NP5 compared to flexible open chain of NP4, possibly helps further in attaining higher decay rate for NP5 relative to NP4.

Table 0-1 Hydrodynamic diameter data obtained from DLS measurements

NPs	Hydrodynamic diameter (nm)
NP1	9.87±2.3
NP2	12.5±2.8
NP3	14.9±3.2
NP4	16.7±5.0
NP5	17.3±5.3

The values of γ_{max} and *t** reflect a major role of intermolecular interactions at the liquid-liquid interface[21] that influences the adsorption energetic barrier induced by the nanoparticle film at the interface. Although, *t** decreases along the series of NPs, a drastic change is observed for NP3 – NP5 compared to NP1 and NP2. It suggests that the increase in alkyl chain length poses an adsorption energetic barrier leading to faster attainment of meso-equilibrium. Again, the time required to reach equilibrium is much higher for NP4 than NP5 reflecting a higher energy barrier for the former particle. This is further supported by the parameter *n*, which is related to the difference between adsorption and desorption energies of the surface active moieties.[22] Since, the decrease in *n* value suggests a decrease in the adsorption rate relative to that of desorption, a higher adsorption barrier is expected by the adsorbed molecules for NP4, with an open hydrocarbon chain, compared to NP5 having a cyclic chain. Taken together, the interfacial behaviours of the monolayer protected NPs indicate the presence of an interaction based mixed kinetic-diffusion mechanism.

Table 0-2 Dynamic surface tension parameters calculated from γ_t vs. time plots at the toluene-water interface

NPs	γ_m (mN/m)	t^* (sec)	n	γ_{max} (mN/m-sec)
NP1	17.7	1100	0.807	2.7×10^{-3}
NP2	14.1	907	0.596	3.0×10^{-3}
NP3	12.35	158	0.442	14.1×10^{-3}
NP4	10.18	102	0.517	28.2×10^{-3}
NP5	10.96	53	0.641	64.5×10^{-3}

4.2.3 Assembly dynamics of nanoparticle-protein complex at interface

We next explored the role of NP hydrophobicity on the stabilization of liquid-liquid interfaces using protein-particle assemblies. We prepared NP-protein complex by mixing positively charged NPs and negatively charged PhosA in PBS buffer with consequent incubation to facilitate complexation. From our previous studies, we found that NP-protein conjugates with reduced charge successfully stabilized oil-water interface.[3,4] To obtain neutral conjugate, we performed zeta potential (ζ) titration of NPs with varying PhosA concentration (Figure 4.4a). Depending on the functional headgroups, each NP exhibits drastically different binding stoichiometry with PhosA (Figure 4.4b). At the obtained ratios, different NP-protein assembly structure could be envisaged[23] (Figure 4.1c), contributing to the interfacial tension modulation. The optimal charge neutralization ratio was used for further interfacial tension measurements.

a)

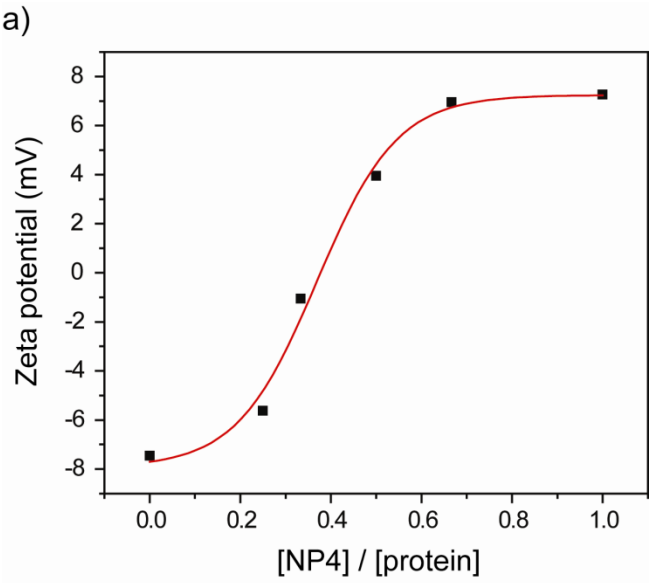

b)

NPs	[NP]/[protein] at neutralization	Zeta potential (mV)
NP1	1.25	-1.2
NP2	1.00	-1.12
NP3	0.50	+1.03
NP4	0.34	-1.05
NP5	0.28	+1.72

Figure 0.4 (a) Representative ζ-potential measurements of PhosA-nanoparticle 4 conjugate prepared by varying molar ratios of nanoparticles to PhosA. The red line represents the best fitting through sigmoidal equation. (b) NP-protein ratios at ζ ~0.

The interfacial behavior of NPs-PhosA complex is shown in Figure 4.5a. It is evident that all five NP-PhosA complexes show lower interfacial tension value at equilibrium (quasi) and a faster dynamics compared to NPs alone. The NP1-PhosA complexes show highest interfacial tension (γ ~13.6 mN/m) whereas NP5-PhosA complexes show minimum (γ ~7.9 mN/m) indicating maximum stabilization at the oil-water interface. However, the Hua-Rosen model fails for the NP-PhosA complexes and the data could not be fitted, presumably due to other processes such as particle-NP assembly. Significantly, the ratio of the equilibrium surface tension values of NP alone and NP-protein are nearly constant value regardless of the particle, suggesting that the interfacial energy can be predictably tuned with these systems.

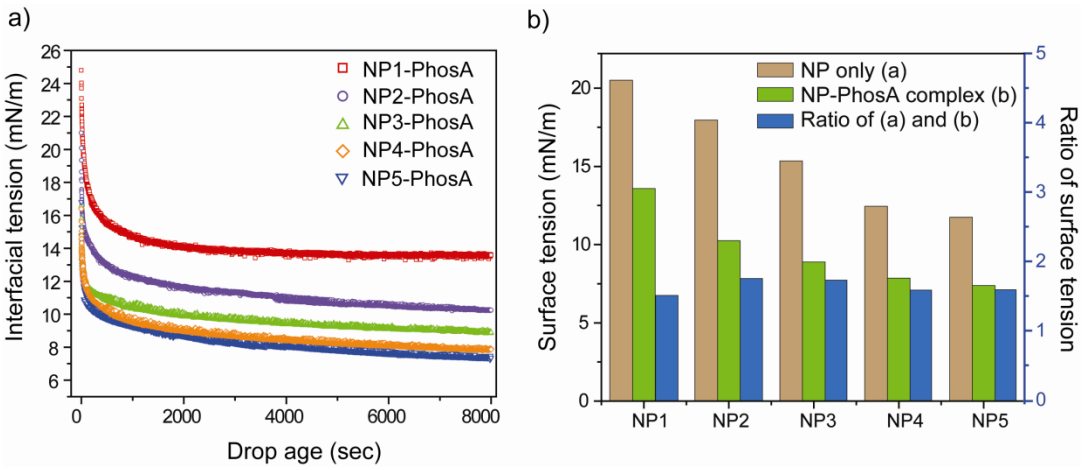

Figure 0.5 (a) Interfacial tension vs time plot for NP-protein conjugates at the charge neutralization ratio. (b) Comparison of the surface tension values of the NPs and the corresponding NP-PhosA conjugates at 8000 sec and their ratio.

4.3 Experimental Section

4.3.1 Materials.

All materials were purchased from Sigma-Aldrich and used without further purification. For all measurements, NPs and protein were dispersed in 5 mM Phosphate buffered (PBS) at pH 7.4.

4.3.2 Nanoparticle synthesis

Nanoparticles were synthesized according to the literature reported procedures.[24] In short, 1-pentanethiol coated gold NPs (C_5-NP) were fabricated using $NaBH_4$ reduction of $HAuCl_4$ salt. The ligands with varying hydrophobic chains were then synthesized and place-exchanged onto 2 nm core C_5-NPs. All the five NPs in the study were prepared from the same C_5-NP core so that the NPs differ only in terms of the desired surface functionalities.

4.3.3 Tensiometer measurements

The dynamic surface tension of the NPs and NP-protein conjugates at the toluene/water interface was measured using the pendant drop method (OCA20, Dataphysics, Stuttgart). The setup of the pendant drop apparatus is shown elsewhere.[25] A Syringe filled with solution of NPs or NP-protein complexes connected to a needle was fixed vertically with the needle immersed in toluene phase.

A small amount of solution was injected from the syringe to form a drop. The variation of drop shape with time was captured by automated camera at particular time interval and the interfacial tension (γ) was estimated by data fitting using the Laplace–Young equation:

$$\gamma = \Delta\rho g d_e / H \qquad (4)$$

Where $\Delta\rho$ is the density difference between the liquid drop and its surrounding medium, g is the gravitational acceleration, d_e the largest horizontal diameter of the drop, H is a function of S_n ($=d_n/d_e$), in which d_n is the horizontal diameter at a distance equal to d_e (n/10) from the bottom of the drop. All experiments were performed at room temperature (23±1°C).

4.3.4 DLS and Zeta potential measurements

Hydrodynamic radius and zeta potential of NPs and NP-protein complexes were measured by dynamic light scattering (DLS) in 5 mM phosphate buffer (pH=7.4) using a Malvern ZetasizerNano ZS instrument. All the NP-protein complexes were incubated for 30 mins prior to measurements. Solutions of NPs and NP-protein complexes at different ratios were placed in a cuvette and average of 3 measurements were considered.

4.3.5 Curve fitting and partition coefficient calculation

Both the linear and non-linear curve fitting was performed using Origin 7 software following iterative method.

The $Log_{10}P$ values were estimated for the headgroup of each ligand (starting from the quaternary nitrogen, e.g. $(CH_3)_2NCH_3$ for NP1; $(CH_3)_2NCH_2CH_3$ for NP2 etc.) using a molecular mechanics methodology. The force field employed was a MMFF under a TNCG methodology using octanol and water as the first and second solvents respectively. The calculations were continued until gradient convergence, using MacroModel 8.0 under Maestro 9.5 interface.

4. 4 Conclusions

We have studied the assembly behavior of NPs and NP-protein complexes at a liquid-liquid interface. These studies demonstrate that subtle monolayer structure of the NPs play an important role in stabilizing the liquid-liquid interface. As hydrophobicity of the ligand in the monolayer increases, NPs tend to create more stable interface with a linear decrease in meso-equillibrium surface tension is observed. Notably, the dynamic interfacial behaviors follow a mixed kinetic-diffusion mechanism, where the rate-controlling adsorption step are governed by hydrophobicity as well as the structure of the NP layer at interface which set the energy barrier for their adsorption. Constrained hydrophobic head group was found to be helpful for faster assembly. These studies also demonstrate that further modulation occurs after complexation of the NPs with an electrostatically complementary protein. Given the importance of the assembly behaviour of NPs in affecting the size and stability of the droplet in emulsion process,[15] these studies provide useful guidelines for designing appropriate NPs for emulsion and interfacial stabilization.

4.5 References

1. Binks, B. P. *Phys. Chem. Chem. Phys.* **2007**, *9*, 6298.

2. Crossley, S.; Faria, J.; Shen, M.; Resasco, D. E. *Science* **2010**, *327*, 68.

3. Samanta, B.; Yang, X.-C.; Ofir, Y.; Park, M.-H.; Patra, D.; Agasti, S. S.; Miranda, O. R.; Mo, Z.-H.; Rotello, V. M. *Angew. Chem. Int. Ed.* **2009**, *48*, 5341.

4. Yang, X.-C.; Samanta, B.; Agasti, S. S.; Jeong, Y.; Zhu, Z.-J.; Rana, S.; Miranda, O. R.; Rotello, V. M. *Angew. Chem. Int. Ed.* **2011**, *50*, 477.

5. Dickinson, E. *Curr. Opin. Colloid Interface Sci.* **2010**, *15*, 40.

6. (a) Pieranski, P. *Phys. Rev. Lett.* **1980**, *45*, 569. (b) Binks, B. P.; Lumsdon, S. O. *Langmuir* **2000**, *16*, 8622. (c) Dinsmore, A. D.; Hsu, M. F.; Nikolaides, M. G.; Marquez, M.; Bausch, A. R.; Weitz, D. A. *Science* **2002**, *298*, 1006.

7. (a) Boeker, A.; He, J.; Emrick, T.; Russell, T. P. *Soft Matter* **2007**, *3*, 1231. (b) Patra, D.; Sanyal, A.; Rotello, V. M. *Chem. Asian J.* **2010**, *5*, 2442. (c) Binks, B. P.; Horozov, T. S. In *Colloidal Particles at Liquid Interfaces*; Cambridge University Press, **2006**. (d) Kim, J.-W.; Lee, D.; Shum, H. C.; Weitz, D. A. *Adv. Mater.* **2008**, *20*, 3239. (e) Binks, B. P.; Clint, J. H.; Fletcher, P. D. I.; Lees, T. J. G.; Taylor, P. *Langmuir* **2006**, *22*, 4100.

8. (a) Lin, Y.; Skaff, H.; Boker, A.; Dinsmore, A. D.; Emrick, T.; Russell, T. P. *J. Am. Chem. Soc.* **2003**, *125*, 12690. (b) Patra, D.; Malvankar, N.; Chin, E.; Tuominen, M.; Gu, Z.; Rotello, V. M. *Small* **2010**, *6*, 1402. (c) Duan, H. W.; Wang, D. Y.; Sobal, N. S.; Giersig, M.; Kurth, D. G.; Mohwald, H. *Nano Lett.* **2005**, *5*, 949.

9. (a) Lee, L. A.; Wang, Q. *Nanomedicine* **2006,** *2*, 137. (b) Fujii, S.; Aichi, A.; Muraoka, M.; Kishimoto, N.; Iwahori, K.; Nakamura, Y.; Yamashita, I. *J. Colloid Interface Sci.* **2009,** *338*, 222. (c) He, J.; Niu, Z.; Tangirala, R.; Wan, J.-Y.; Wei, X.; Kaur, G.; Wang, Q.; Jutz, G.; Boeker, A.; Lee, B.; Pingali, S. V.; Thiyagarajan, P.; Emrick, T.; Russell, T. P. *Langmuir* **2009,** *25*, 4979. (d) Kaur, G.; He, J.; Xu, J.; Pingali, S. V.; Jutz, G.; Boeker, A.; Niu, Z.; Li, T.; Rawlinson, D.; Emrick, T.; Lee, B.; Thiyagarajan, P.; Russell, T. P.; Wang, Q. *Langmuir* **2009,** *25*, 5168. (e) Hermanson, K. D.; Huemmerich, D.; Scheibel, T.; Bausch, A. R. *Adv. Mater.* **2007,** *19*, 1810.

10. Bresme, F.; Oettel, M. *J. Phys. Condens. Mat.* **2007**, *19*, 413101.

11. (a) Patra, D.; Pagliuca, C.; Subramani, C.; Samanta, B.; Agasti, S. S.; Zainalabdeen, N.; Caldwell, S. T.; Cooke, G.; Rotello, V. M. *Chem. Commun.* **2009**, 4248. (b) Skaff, H.; Lin, Y.; Tangirala, R.; Breitenkamp, K.; Boker, A.; Russell, T. P.; Emrick, T. *Adv. Mater.* **2005**, *17*, 2082. (c) Arumugam, P.; Patra, D.; Samanta, B.; Agasti, S. S.; Subramani, C.; Rotello, V. M. *J. Am. Chem. Soc.* **2008**, *130*, 10046.

12. (a) Patra, D.; Ozdemir, F.; Miranda, O. R.; Samanta, B.; Sanyal, A.; Rotello, V. M. *Langmuir* **2009**, *25*, 13852. (b) B Wang, B.; Wang, M.; Zhang, H.; Sobal, N. S.; Tong, W.; Gao, C.; Wang, Y.; Giersig, M.; Wang, D.; Moehwald, H. *Phys. Chem. Chem. Phys.* **2007**, *9*, 6313.

13. Miller, R.; Fainerman, V. B.; Makievski, A. V.; Kragel, J.; Grigoriev, D. O.; Kazakov, V. N.; Sinyachenko, O. V. *Adv. Colloid Interface Sci.* **2000**, *86*, 39.

14. Rosen, M. J. *Surfactants and Interfacial Phenomena*, 3rd ed.; Wiley-Interscience, **2004**.

15. (a) Butt, H.-J.; Graf, K.; Kappl, M. *Physics and Chemistry of Interfaces*, 2nd ed.; Wiley-VCH, **2006**. (b) Cardenas-valera, A. E.; Bailey, A. I. *Colloids Surf., A* **1995**, *97*, 1. (c) Wollenweber, C.; Makievski, A. V.; Miller, R.; Daniels, R. *Colloids Surf., A* **2000**, *172*, 91.

16. De, M.; You, C.-C.; Srivastava, S.; Rotello, V. M. *J. Am. Chem. Soc.* **2007**, *129*, 10747.

17. Moyano, D. F.; Rotello, V. M. *Langmuir* **2011**, *27*, 10376.

18. (a) Love, J. C.; Estroff, L. A.; Kriebel, J. K.; Nuzzo, R. G.; Whitesides, G. M. *Chem. Rev.* **2005**, *105*, 1103-1169. (b) Nikolic, M. S.; Krack, M.; Aleksandrovic, V.; Kornowski, A.; Foerster, S.; Weller, H. *Angew. Chem. Int. Ed.* **2006**, *45*, 6577.

19. Hua, X. Y.; Rosen, M. J. *J. Colloid Interface Sci.* **1988**, *124*, 652.

20. Ghose, A. K.; Crippen, G. M. *J. Comput. Chem.* **1986**, *7*, 565.

21. Du, K.; Glogowski, E.; Emrick, T.; Russell, T. P.; Dinsmore, A. D. *Langmuir* **2010**, *26*, 12518.

22. Gao, T.; Rosen, M. J. *J. Colloid Interface Sci*. **1995**, *172*, 242.

23. De, M.; Miranda, O. R.; Rana, S.; Rotello, V. M. *Chem. Comm.* **2009**, 2157.

24. You, C.-C.; Miranda, O. R.; Gider, B.; Ghosh, P. S.; Kim, I.-B.; Erdogan, B.; Krovi, S. A.; Bunz, U. H. F.; Rotello, V. M. *Nat. Nanotechnol.* **2007**, *2*, 318.

25. Kutuzov, S.; He, J.; Tangirala, R.; Emrick, T.; Russell, T. P.; Boker, A. *Phys. Chem. Chem. Phys.* **2007**, *9*, 6351.

CHAPTER 5

DIRECT PATTERNING OF ENGINEERED IONIC GOLD NANOPARTICLES VIA NANOIMPRINT LITHOGRAPHY

5.1 Introduction

Micro/nano-patterning of nanoparticles (NPs) provides access to nanomaterial based microelectronics,[1] photonics,[2] biosensors, and biochips.[3] A wide range of techniques have been used to pattern NPs, including photolithography,[4] scanning probe lithography,[5] electron beam lithography,[6] dip-pen nanolithography,[7] inkjet,[8] microcontact printing,[9] and nanoimprint lithography (NIL).[10] Of these methods, NIL provides a particularly promising patterning tool, with the capability for generating two- and three- dimensional nanostructures with features <50 nm.[11] Polymer imprinting using NIL is a scalable and versatile technique that has been employed in a wide range of applications such as organic electronics,[12] photonics,[13] magnetic devices,[14] and biological applications.[15]

Direct imprinting of nanoparticles would provide expedient access to nanopatterned NP-based materials and devices. However, NPs generally form powder-like solids[16] due to their rigid inorganic core and the crystallinity of the alkane ligands[17, 18] making them difficult to process or imprint. While solvent-based methods have been used to imprint NPs, this approach faces challenges such as shrinkage of the features after solvent removal and delamination of the NPs from the substrate when dry.[19, 20] These issues limit the use imprinting as a strategy for patterning NP films, in particular in high throughput roll-to-roll device fabrication strategies where fluidity is a prerequisite for effective processing.

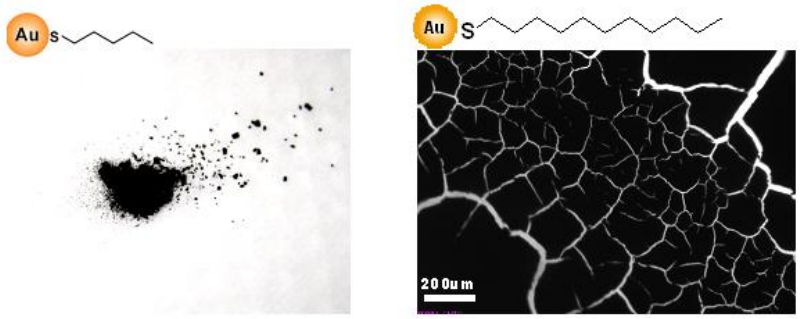

Figure 0.1 Gold NPs with alkane ligands are powder-like (left) and the film is brittle, easy to crack and delamination.

Recently, Giannelis *et al.* have fabricated NPs that flowed freely in the absence of solvent using organic ligands possessing "soft" segments such as poly(ethylene glycol) and an asymmetric ammonium ion (ionic liquid ligand).[21] Similarly, Chen *et al.* synthesized liquid ZnO nanoparticles using an asymmetric ammonium ligand with trifluoromethane sulfonate as the counter ion.[22] The fluid and amorphous nature of these particles[23] suggests that organic ionic liquid ligands could provide an effective strategy for imprint-driven fabrication processes. Effective imprinting, however, would require particles that flow under an external force yet still generate highly stable nanostructures.

In this chapter, we demonstrate that ionically functionalized gold nanoparticles (**AuNP-IL**) can be thermally imprinted to form stable shapes and surface patterns using a polydimethylsiloxane (PDMS) mold (**Figure 5.1**). These particle films are amorphous, providing enhanced processability and imprintability. Stable high resolution nanopatterns were created by imprinting of AuNP-IL films. These films retain the electronic properties of the precursors, allowing direct fabrication of a prototype light modulated device.[16]

5.2 Result and Discusion

5.2.1 AuNP-IL synthesis

The **AuNP-IL** particle used in this study was engineered to provide imprintability. The particles feature a 2.5 nm diameter Au core,[23, 24] a thiol group as the bonding group for the gold nanoparticles, an alkyl chain to stabilize the ligand shell, and a tetra(ethylene glycol) segment with a bulky cyclohexyl ammonium terminus to suppress crystallization (Figure 5.2). Ligands lacking either the tetra(ethylene glycol) segment or the cyclohexyl head group produced either brittle films or demonstrated poor imprintability, indicating that both the chain and headgroup moieties are necessary for imprinting. In contrast, after complete removal of the solvent, **AuNP-IL** films exhibit wrinkles similar to those observed when drying viscous liquids,[25] (Figure 5.2B) indicating flexibility is retained in the thin films.

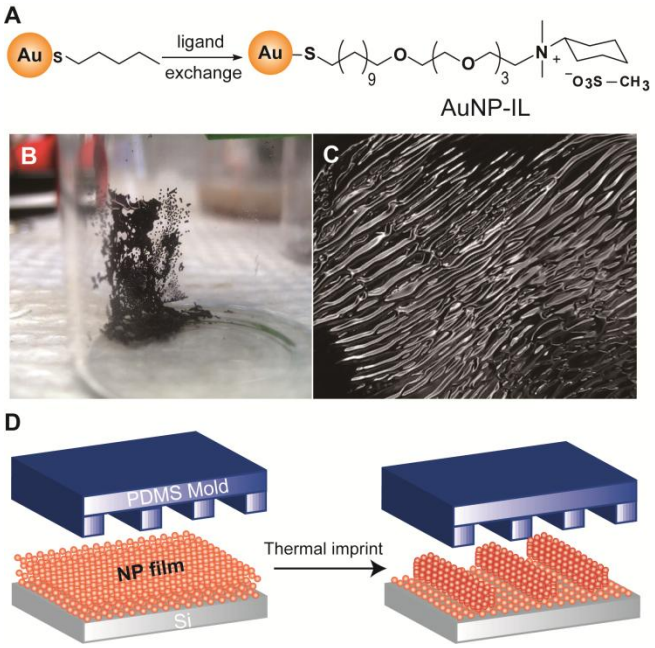

Figure 0.2 (A) Fabrication of the imprintable nanoparticle **AuNP-IL**. (B and C) The physical state of the particles after drying with an air stream. (D) Scheme for the direct imprinting of the **AuNPs-IL**.

5.2.2 Solid state structure characterization

Our initial studies focused on characterization of the composite structures of the **AuNP-IL** films. **AuNP-IL** is highly soluble in solvents such as methanol and ethanol, allowing facile film formation through spincasting concentrated solutions of NP (~600 mg/ml) in methanol. The resulting films were quite homogeneous with no grains or cracks. We used small angle X-ray scattering (SAXS) to characterize the nanocomposite structure of the particle film. As shown in **Figure 5.3a**, only one broad peak appeared in the SAXS scattering curve, corresponding to a center-to-center nanoparticle distance of 4.98 nm. This spacing is consistent with the combined diameter of the core and ligand of **AuNP-IL**. No other peaks were found in the SAXS spectrum, indicating an amorphous liquid-like structure of the nanoparticle aggregate.

Differential scanning calorimetry (DSC) was used to characterize the thermal behavior of **AuNP-IL**. As showed in **Figure 5.3b**, there was only one glass transition state for the ligands on the nanoparticle at -27 °C, with no melting or crystallization observed. This behavior contrasts strongly with nanoparticles functionalized with long chain alkanethiol ligands, where the monolayer generally exhibits melting and crystallization processes at ~40 °C.[18] This lack of phase change indicates that the ligands in the **AuNP-IL** films are in an amorphous state at room temperature, which plays a critical role in the processability of the **AuNP-IL**. The Tg of the ligand in **AuNP-IL** assemblies was higher than that of the ligands themselves (Tg -42°C), a result that may be attributed to the confinement effect of the ligand on the nanoparticle surface.

Atomic force microscopy (AFM) was used to characterize the mechanical properties of the **AuNP-IL** films. As can be seen in **Figure 5.3C**, the compression-retraction curves have a shape typical of deformable materials. Upon compression, we found that the elastic modulus is ~5.8 MPa, which is significantly higher than prior reported nanoparticle liquid by ~2 orders of magnitude[21]. This value is consistent with the moduli of elastomers that have a Tg far below room temperature. Upon tip retraction, a large hysteresis was observed due to the combination of

film adhesion to the silicon tip and the dissipative properties of the **AuNP-IL** film. These dissipative properties are likely associated with the ability of the weakly associated NPs to rearrange and permanently deform, attributes that are crucial for NIL patterning applications. These unique particles find balance between fluid-like properties that aid with imprintability and solid-like properties that allow stable patterns to be created.

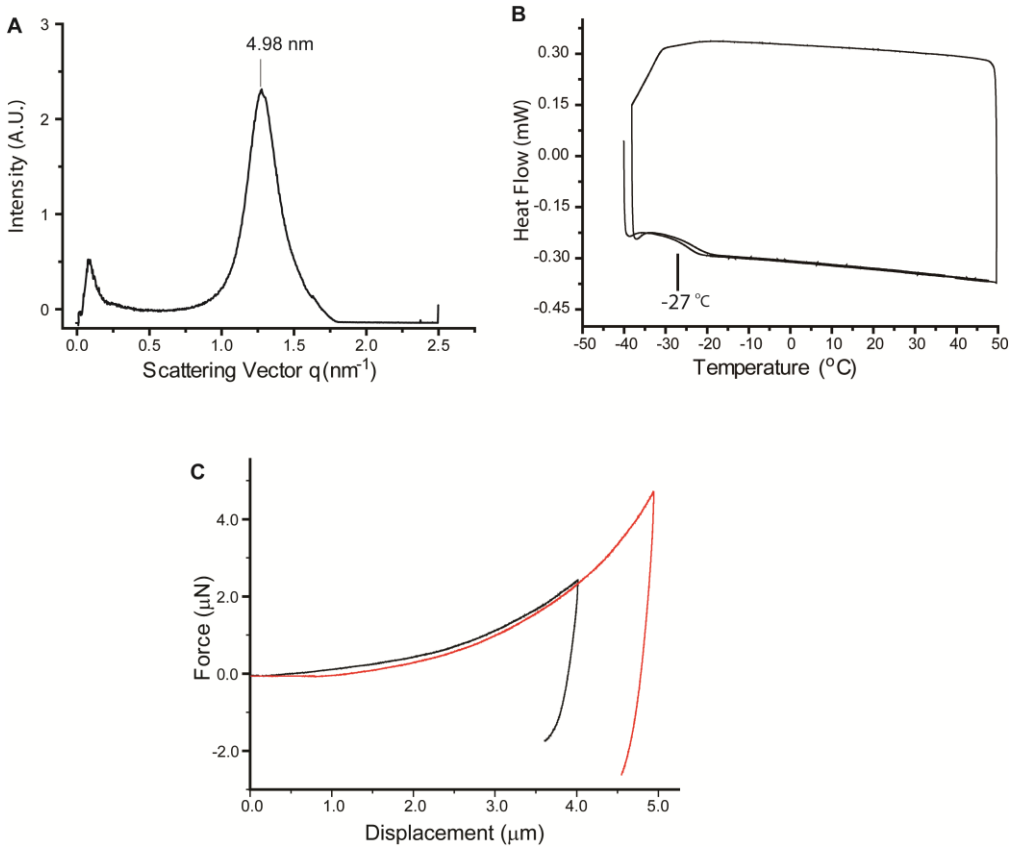

Figure 0.3 a) SAXS spectrum of the nanoparticle aggregate. The peak corresponds to the center-to-center distance of the nanoparticles. No higher level order can be found at a lower scattering vector region. b) DSC trace of the nanoparticle. A glass transition at -27°C can be identified with a heating/cooling rate of 4°C/min. c) Force-displacement curves with different voltage setpoints of 0.5 and 1.0V on the same **AuNP-IL** film showing deformation of the weakly associated NPs.

5.2.3 Nanoimprint lithography of the AuNP-IL

Patterning of **AuNP-IL** was performed at ambient temperature by nanoimprint lithography using a non-adhesive PDMS mold.[11a, 26] No particle transfer from the silica substrate to the PDMS mold

occurred, crucial for successful imprinting. As shown in **Figure 5.4**, the nanoparticle film could be molded into a range of patterns and feature sizes. The ability to pattern positive and negative features via NIL shows that **AuNPs-IL** possess excellent processability, as shown in the AFM images (Figure 5.4d, e). Moreover, these **AuNPs-IL** can be utilized to generate small (400 nm) features (Figure 5.4f). Unlike previous nanoparticle imprinting strategies,[19, 27] no assisting solvents or polymer additives are necessary in this patterning process. It should be noted that the nanoparticle films contain 53% gold by weight (as determined by thermogravimetric analysis, **Figure 5.5**), yet are still processable.

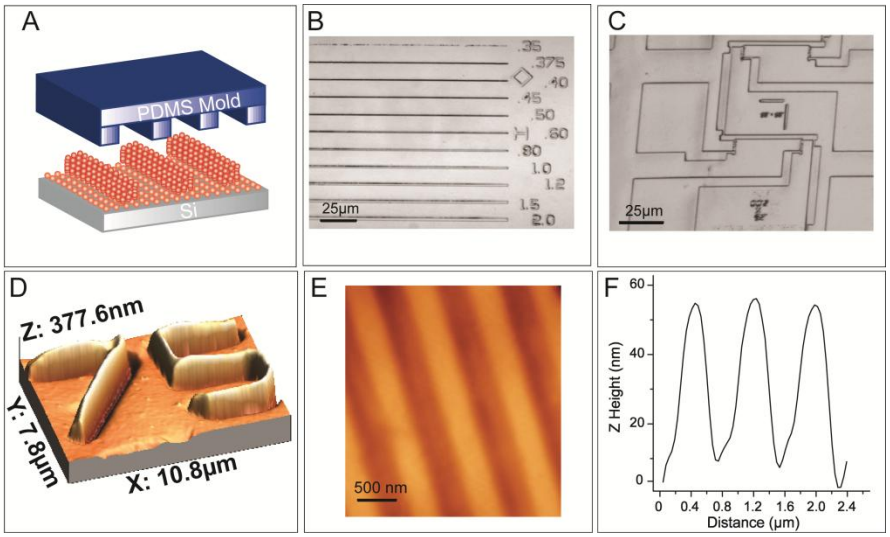

Figure 0.4 AuNP-IL patterns molded by a PDMS stamp. a) Nanomolding process. b and c) Optical microscopy images of the lines and circuit produced by imprinting. d-f) 3D atomic force microscopy images of the imprinted structures.

Stability of imprinted structures is an important requirement for device and materials fabrication. After imprinting, we found no pattern deformation after several months under normal storage conditions. Furthermore, the pattern was also stable at elevated temperatures (140°C for 8 hours) without degradation, indicating that reorganization is slow in the absence of mechanical forces, which we believe is due to the large mass of the nanoparticle and strong inter-particle interactions.

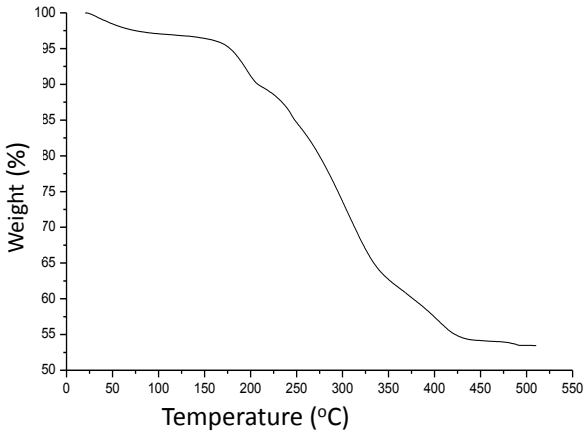

Figure 0.5 Thermogravimetric analysis of the **AuNP-IL**

5.2.4 Conducting properties of the AuNP-IL

Previous nanoparticle imprinting strategies have focused on creation of "bare" metallic features through ligand removal after the printing process.[3a, 27, 28] However, retention of the ligand shell can impart useful functional properties to materials.[29] To this end, we characterized the conductivity at different locations of the patterned gold particle film. The patterns were imprinted on a conductive gold substrate and measured through the film by conductive AFM. As illustrated in **Figure 5.6A**, the current-voltage behaviors of the film are quite similar at different position, with a blocking region below 1V, and a fast increase after that. We attribute the blocking region to contact resistance between the AFM tip and the ionic liquid-coated particles. The conductivity varied with film thickness: the two "peak" positions (1 and 2) of the pattern display a lower conductivity while the "valley" positions (3 and 4) show a higher conductance due to the change in film thickness.

Building on the conductive properties of the **AuNP-IL** films, we next explored photo-controlled conductivity,[2] a key characteristic for photodetectors,[16] sensors,[30] and photoswitches.[2b, 31] To demonstrate the potential of our particles for photomodulation,[32, 33] the **AuNP-IL** films were tested for conductivity under a DC bias. As shown in **Figure 5.6B**, upon the irradiation by a green laser an obvious increase in current was observed. **Figure 5.6C** presents the time

dependence of the photomodulation of the conductance, showing that the photo-modulation is a switchable process, with a relative amplitude of current increase nearly ~43% when the light on in all the cycles. As a control experiment, pure ligand without gold nanoparticles did not show any change in the presence of the light, indicating that the gold nanoparticles are the key to the photomodulated conductance (Figure 5.6D).

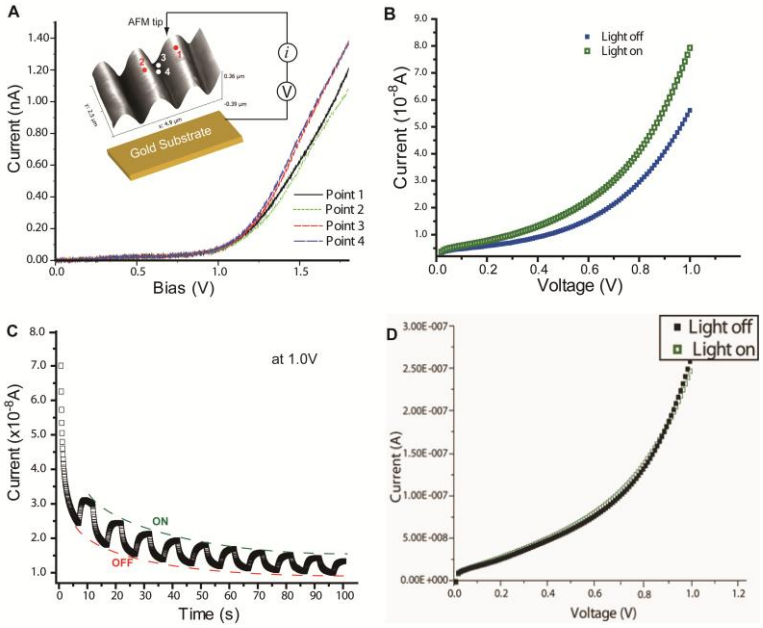

Figure 0.6 A) Current-voltage curves of the patterned nanoparticle film characterized by conductive AFM at different positions with variations in film thickness. B) Current-voltage curve of the nanoparticle at dark and green laser on conditions. C) Current-time curve alternating the laser on and off. D) Current-voltage curve of the ionic liquid ligand at dark and green laser on conditions.

We believe that both ion and electron transport contribute to the conducting property of our **AuNP-IL** considering the ion mobility of the ligand and electron activity of the gold nanoparticles. This can be seen from **figure 5.6C**, where the fast decay at earlier time under DC bias is the charging current by ion and the finite non-decaying current at later time is due to electron transport. The interesting conducting properties of the **AuNP-IL** combing ionic and

electronic properties of ligand and gold core will be further characterized in detail using techniques such as impedance spectroscopy in Chapter 6.

5.3 Experimental Section

5.3.1 AuNP-IL synthesis

The ligands were synthesized according to previous reports [34]. Subsequent place-exchange reaction with pentanethiol-coated gold nanoparticles ($d \approx 2$ nm) resulted in NPs in high yields. ^{1}H NMR spectroscopic investigation revealed that the place-exchange reaction proceeds almost quantitatively and the coverage of cationic ligands on the nanoparticles is near complete [35].

5.3.2 Solid state characterization

SAXS measurements were performed using a three pinhole collimation system and an Osmic MaxFlux X-ray source (Cu K_α, 0.154 nm). The data was collected by a two-dimensional multiwire proportional detector and integrated to yield plots of intensity as a function of the magnitude of the scattering vector, $q = (4\pi/\lambda)\sin(\square)$, where 2θ is the total scattering angle.

Glass-transition temperatures were obtained by DSC using a TA Instruments Dupont DSC Q200. Samples were analyzed at a heating rate of 4 °C min^{-1} from -40 °C to 50 °C under a He flow (25 ml min^{-1}).

TGA was carried out using a TA Instruments TGA 2950 thermogravimetric analyzer with a heating rate of 10 °C min^{-1} from room temperature to 520 °C under nitrogen.

5.3.3 Nanoimprint lithography and characterizatoin

Nanoimprinting of the gold nanoparticles was performed using a Nanonex NX-2000 nanoimprinter with a patterned PDMS mold that contained test patterns with various feature sizes. Imprinting was performed at room temperature at a pressure of 400 PSI for 2 min.

Optical images were taken on an Olympus BX51 optical microscope system. AFM imaging was performed on a Digital Instruments IIIa scanning probe microscope, and the images were

obtained in the tapping mode under ambient conditions. AFM mechanical property characterization was conducted on a Research Asylum MFP-3D atomic force microscope. Veeco model RTESP probes (Phosphorous n-doped Si, nominal tip radius <10nm, cantilever stiffness 20-80N/m) were used. Films for mechanical measurements were fabricated by casting and were ~5-6 micrometers in thickness determined by optical profilometry through the use of a Zygo NewView 7300 profilometer with MetroPro 8.3.2 software for analysis. Force measurements were performed at a rate of 300nm/s at room temperature with set point voltages ranging from 0.5-1.5V. The cantilever stiffness was calibrated before each test by testing a cleaned glass slide.

5.3.4 Photo-responsible and pattern conductivity characterization

Photo-response conductance experiments were performed using a DC power supply in series with a current amplifier (Keithley Model 6487, Picoammeter/Voltage Source). The sample was applied on a self-made glass substrate with two parallel platinum electrodes. A bias voltage of 1V was applied between the two electrodes and the current I through the device was measured. The light modulation experiment was done by irradiating the sample using a green laser with a wavelength of 532nm and at a maximum power of 30 mM.

Conductive AFM measurements were obtained with a Research Asylum MFP-3D atomic force microscope equipped with an Orca module and platinum coated AFM tips purchased from AppNano. After a tapping mode image was obtained, the tip was put into contact mode and measured at various locations.

5.4 Conclusion

We have created engineered nanoparticles that integrate the electronic properties of inorganic nanomaterials with the processibility of organic materials. Films made using this strategy are imprintable, providing stable patterns. These patterned films possess distinctive properties arising from both the core and ligand, providing scalable routes to a range of new devices and materials.

5.5 References

1 a) Kim, W.J.; Kim, S. J.; Lee, K-S.; Samoc, M.; Cartwright, A. N.; Prasad, P. N.; *Nano Lett.* **2008**, *8*, 3262; b) Tans, S. J.; Dekker, C.; *Nature* **2000**, *404*, 834; c) Tricoli, A.; Pratsinis, S. E. *Nature Nanotech*. **2010**, *5*, 54; d) Murray, R. W. *Chem. Rev.* **2008**, *108*, 2688; e) Li, X. L.; Jia, Y.; Cao, A. Y. *ACS Nano* **2010**, *4*, 506; f) Wei, D.; Baral, J. K.; Osterbacka, R.; Ivaska, A. *J. Mater. Chem.* **2008**, *18*, 1853.

2 a) L. Eurenius, C. Haggland, E. Olsson, B. Kasemo, D. Chakarov, *Nat. Photon.* **2008**, *2*, 360; b) H.Nakanishi, K.J.M. Bishop, B.Kowalczyk, A.Nitzan, E.A. Weiss, K.V. Tretiakov, M.M . Apodaca, R. Klajn, J.F. Stoddart, B.A. Grzybowski, *Nature* **2009**, *460*, 371.

3 a) Lee, K.-B.; Kim, E.-Y.; Mirkin, C. A.; Wolinsky, S. M.; *Nano Lett.* **2004**, *4*, 1869. b) Prabhakar A.; Mukherji, S. *Lab Chip* **2010**, *10*, 3422; c) Luo, W.; Chan, E. W.; Yousaf, M. N. *J. Am. Chem. Soc.* **2010**, *132***,** 2614; d) Csucs, D.; Falconnet, G.; Grandin, H. M.; Textor, M.; *Biomaterials* **2006**, *27*, 3044.

4 a) Lu, N.; Gleiche, M.; Zheng, J.; Lenhert, S.; Xu, B.; Chi, L.; Fuchs, H.; *Adv. Mater.* **2002**, *14*, 1812; b) E. Foster, G. Kearns, S. Goto, J. E. Hutchison, *Adv. Mater.* **2005**, *17*, 1542; c) D. Xia, S. R. J. Brueck, *Nano Lett.* **2004**, *4*, 1295.

5 a) Eigler, D. M.; Schweizer, E. K.; *Nature* **1990**, *344*, 524; b) Liu, S.; Schmid, G.; Maoz, R.; Sagiv, J. *Nano Lett.* **2002**, *2*, 1055; c) Chowdhury, D.; Maoz, R.; Sagiv, J. *Nano Lett.* **2007**, *7*, 1770; d) Zheng, H.; Lee, I.; Rubner, M. F.; Hammond, P. T. *Adv. Mater.* **2002**, *14*, 569.

6 a) Subramani, C.; Dickert, S.; Yeh, Y.-C.; Tuominen, M. T.; Rotello, V. M. *Langmuir* **2011,** *27*, 1543; b) Werts,M. H. V.; Lambert, M.; Bourgoin, J.-P.; Brust, M. *Nano Lett.* **2002**, *2*, 43.

7 Liu, X.; Fu, L.; Hong, S.; Dravid, V. P.; Mirkin, C. A.; *Adv. Mater.* **2002**, *14*, 231.

8 a) Sankhe, A.Y.; Booth, B. D.; Wiker, N. J.; Kilbey, S. M. *Langmuir* **2005**, *21*, 5332; b) B. Creran, B. Yan, D. F. Moyano, M. M. Gilbert, R. W. Vachet, V. M. Rotello, *Chem. Commun.* **2012**, *48*, 4543.

9 a) Xia, Y. N.; Whitesides, G. M.; *J. Am. Chem. Soc.* **1995**, *117*, 3274; b) Rozkiewicz, D.I.; Jańczewski, D.; Verboom, W.; Ravoo, B. J.; Reinhoudt, D. N. *Angew. Chem., Int. Ed.* **2006**, *45*, 5292.

10 Chou, S. Y.; Krauss, P. R.; Renstrom, P. J. *Science* **1996**, *272*, 85.

11 a) Ofir, Y.; Moran, I. W.; Subramani, C.; Carter, K. R. V. M. Rotello, *Adv. Mater.* **2010**, *22*, 3608; b) Subramani, C.; Ofir, Y.; Patra, D.; Jordan, B. J.; Moran, I. W.; Park, M.-H.; Carter, K. R.; Rotello, V. M.; *Adv. Funct. Mater.* **2009**, *19*, 2937.

12 a) McAlpine, M. C.; Friedman, R. S.; Lieber, D. M.; *Nano Lett.* **2003**, *3*, 443; b) Cedeno, C. C.; Seekamp, J.; Kam, A. P.; Hoffmann, T.; Zankovych, S.; Torres, C. M. S.; Menozzi, C.; Cavallini, M.; Murgia, M.; Ruani, G.; Biscarini, F.; Behl, M.; Zentel, R.; Ahopelto, J. *Microelectron. Eng.* **2002**, *61*, 25.

13 a) Pisignano, D.; Persano, L.; Mele, E.; Visconti, P.; Anni, M.; Gigli, G.; Cingolani, R.; Favaretto, L.; Barbarella, G.; *Synth. Met.* **2005**, *153*, 237; b) Pisignano, D.; Persano, L.; Raganato, M. F.; Visconti, P.; Cingolani, R.; Barbarella, G.; Favaretto, L.; Gigli, G.; *Adv. Mater.* **2004**, *16*, 525; c) Guo, L. J.; Cheng, X.; Chao, C. Y. *J. Mod. Opt.* **2002**, *49*, 663; d) Cheng, X.; Hong, Y. T.; Kanicki, J.; Guo, L. J. *J. Vac. Sci. Technol. B* **2002**, *20*, 2877; e) Kao, P. C.; Chu, S. Y.; Chen, T. Y.; Zhan, C. Y.; Hong, F. C.; Chang, C. Y.; Hsu, L. C.; Liao, W. C.; Hon, M. H. *IEEE Trans. Electron Devices* **2005**, *52*, 1722.

14 a) Chou, S. Y. *Proc. IEEE* **1997**, *85*, 652; b) Wu, W.; Cui, B.; Sun, X. Y.; Zhang, W.; Zhuang, L.; Kong, L. S.; Chou, S. Y. *J. Vac. Sci. Technol. B* **1998**, *16*, 3825; c) Martin, J. I.; Nogues, J.; Liu, K.; Vicent, J. L.; Schuller, I. K. *J. Magn.Magn. Mater.* **2003**, *256*, 449; d) Glinsner, T.; Hangweier, P.; Luesebrink, H.; Dorsey, P.; Homola, A.; Wachenschwanz, D. *Solid State Technol.* **2005**, *48*, 51; e) McClelland, G. M.; Hart, M. W.; Rettner, C. T.; Best, M. E.; Carter, K. R.; Terris, B. D. *Appl. Phys. Lett.* **2002**, *81*, 1483.

15 a) Cao, H.; Yu, Z. N.; Wang, J.; Tegenfeldt, J. O.; Austin, R. H.; Chen, E.; Wu, W.; Chou, S. Y. *Appl. Phys. Lett.* **2002**, *81*, 174; b) Guo, L. J.; Cheng, X. ; Chou, C. F.; *Nano Lett.* **2004**, *4*, 69; c) Hoff, J. D.; Cheng, L. J.; Meyhofer, E.; Guo, L. J.; Hunt, A. J. *Nano Lett.* **2004**, *4*, 853; d) Falconnet, D. ; Pasqui, D.; Park, S. ; Eckert, R.; Schift, H. ; Gobrecht, J.; Barbucci, R. ; Textor, M. ; *Nano Lett.* **2004**, *4*, 1909.

16 Talapin, D.V.; Lee, J.-S.; Kovalenko, M. V.; Shevchenko, E.V. *Chem. Rev.* **2010**, *110*, 389.

17 Badia, A.; Cuccia, L.; Demers, L.; Morin, F.; Lennox, R.B. *J. Am. Chem. Soc.* **1997**, *119*, 2682.

18 Terrill, R. H.; Postlethwaite, T. A.; Chen, C.-H; Poon, C.-D.; Terzis, A.; Chen, A.; Hutchison, J. E.; Clark, M. R.; Wignall, G. *J. Am. Chem. Soc.* **1995**, *117*, 12537.

19Ko, S.H.; Park, I.; Pan, H.; Grigoropoulos, C.P.; Pisano, A.P.; Luscombe, C.K.; Frechet, J. M. J. *Nano Lett.* **2007**, *7*, 1869.

20 Arango, A.C.; Oertel, D.C.; Xu, Y.; Bawendi, M.G.; Bulović, V. *Nano Lett.* **2009**, *9*, 860.

21 a) Bourlinos, A.B.; Herrera, R.; Chalkias, N.; Jiang, D.D.; Zhang, Q.; Archer, L.A.; Giannelis, E. P. *Adv. Mater.* **2005**, *17*, 234; b) Bourlinos, A.B.; Ray Chowdhury, S.; Herrera, R.; Jiang, D. D.; Zhang, Q.; Archer, L.A.; Giannelis, E. P. *Adv. Funct. Mater.* **2005**, *15*, 1285; c) Warren, S.C.; Banholzer, M. J.; Slaughter, L. S.; Giannelis, E. P.; DiSalvo, F. J.; Wiesner, U. B. *J. Am. Chem. Soc.* **2006**, *128*, 12074; d) Rodriguez, R.; Herrera, R.; Archer, L.A.; Giannelis, E.P. *Adv. Mater.* **2008**, *20*, 4353; e) Jespersen, M. L.; Mirau, P. A.; von Meerwall, E.; Vaia, R.A.; Rodriguez, R.; Giannelis, E.P. *ACS Nano* **2010,** *4*, 3735.

22 Liu, D.-P.; Li, G.-D.; Su, Y.; Chen, J.-S. *Angew. Chem., Int. Ed.* **2006**, *45*, 7370.

23 Brust, M. D.; Schiffrin, J.; Whyman, R.; *J. Chem. Soc., Chem. Commun.* **1994**, 801.

24 Templeton, A. C.; Wuelfing, M. P.; Murray, R. W. *Acc. Chem. Res.* **2000**, *33*, 27.

25 Dealy, J.M.; Larson, R.G. Structure and Rheology Of Molten Polymers - From Structure To Flow Behavior and Back Again, Hanser Publishers **2006**

26 Guo, L.J. *Adv. Mater.* **2007**, *19*, 495.

27 Sivaramakrishnan, S.; Chia, P.-J.; Yeo, Y.-C.; Chua, L.-L.; Ho, P. K. H. *Nat Mater.* **2007**, *6*, 149.

28 Klajn, R.; Bishop, K.J.M.; Fialkowski, M.; Paszewski, M.; Campbell, C.J.; Gray, T.P.; Grzybowski, B.A. *Science* **2007**, *316*, 261.

29 a) Yin, J.; Hu, P.; Luo, J.; Wang, L.; Cohen, M. F.; Zhong, C.-J. *ACS Nano* **2011**, *5*, 6516; b) G. R.Wang, L.Wang, Q. Rendeng, J. Wang, J. Luo, C.-J. Zhong, *J. Mater. Chem.* **2007**, *17*, 457; c) S. I. Lim, C.-J. Zhong, *Acc. Chem. Res.* **2009**, *42*, 798.

30 Sargent, E. H. *Adv. Mater.* **2008**, *20*, 3958.

31 Leatherdale, C.; Kagan, C.; Morgan, N.; Empedocles, S.; Kastner, M.; Bawendi, M. *Phy. Rev. B* **2000**, *62*, 2669.

32 Link, S.; El-Sayed, M. A. *Annu. Rev. Phy. Chem.* **2003**, *54*, 331.

33 a) Hu, M.-S.; Chen, H.-L.; Shen, C.-H.; Hong, L.-S.; Huang, B.-R.; Chen, K.-H.; Chen, L.-C.; *Nat. Mater.* **2006**, *5*, 102; b) Jin, Y.; Friedman, N. *J. Am. Chem. Soc.* **2005**, *127*, 11902; c) Berthold, K.; Hopfel, R.A.; Gornik, E. *Appl. Phys. Lett.* **1985**, *46*, 626.

34 You, C. C.; Miranda, O. R.; Gider, B.; Ghosh, P. S.; Kim, I. B.; Erdogan, B.; Krovi, S. A.; Bunz, U. H. F.; Rotello, V. M.; *Nat. Nanotechnol*. **2007,** 2, 318.

35 Miranda, O.R.; Chen, H. T.; You, C. C.; Mortenson, D. E.; Yang, X. C.; Bunz, U. H. F.; Rotello, V. M.; *J. Am. Chem. Soc.* **2010,** 132, 5285.

CHAPTER 6

MODULATING THE CHARGE TRANSPORT PROPERTIES OF GOLD NANOPARTICLES USING IONIC LIGAND AND ITS APPLICATION FOR GAS SENSING

6.1 Introduction

The assemblies of metal NPs can be regarded as artificial solid with unique optical and electrical properties that are distinct from their respective bulk properties.[1, 2] Intense research interests have been focused on the electronic conductivity properties of films of transition-metal nanoparticles (e.g., Au, Pd, and Ag) that are passivated by an organic monolayer.[3, 4] With such a core-shell inorganic-organic composite nanostructure, the charge transport properties can be tailored by the coupled effects of the electroactive inorganic cores and the insulating organic shells. The cores dictate the Coulomb blockade characteristics by self-capacitance, while the organic ligand shells serve as the insulating barrier, controlling the charge transport properties by determining a series of key parameters, such as particle-particle distance, electronic coupling between particles, and dielectric environment etc.

For nanoparticles that are modified with electrical inactive ligand, such as alkane, electron is the only charge carrier. The electron transport in these gold nanoparticles is generally described using an Arrhenius-type activated tunneling model (eq. 1)[1, 5]

$$\sigma_{EL}(\delta,T) = \sigma_0(e^{-\beta\delta})e^{-E_A/k_BT} \qquad (1)$$

The first exponential term describes the electron tunneling between the particles through the organic matrix, where β is the electron tunneling coefficient in units of $Å^{-1}$ determined by the chemical nature of the ligand, δ the average interparticle distance set up by the length of the ligand.

The second exponential term in eq. 1 describes the activation energy for charge transport by self-capacitance of the nanoparticle, and E_A corresponds to

$$E_{A,GM} = \frac{e^2}{8\pi\epsilon\epsilon_0}\left(\frac{1}{r} - \frac{1}{r+\delta}\right) \qquad (2)$$

where r is the radius of the particles, δ the interparticle distance, and ε the dielectric constant of the surrounding matrix by the ligand.

Engineering the chemistry of the ligand is, therefore, a versatile way of modulating the conducting properties of nanoparticle assemblies and has been widely exploited.[6, 7] For example, Wessels et al showed that fully conjugated ligand (benzene core with dithiocarbomate) can increase conductance significantly relative to the none-conjugated ligand (cyclohexane with thiol) because of lower charge transfer energy barrier (lower β value).[8] Thoms et al revealed a substitution effect of the gold nanoparticles modified by arylthiol ligand, where electron withdrawing substituents markedly increase conductivity which is believed to be due to increased delocalization area for electrons in the transition state.[9]

Most of the ligand engineering for NPs conductance modulation focuses on electrons as the only charge carrier that can be described by equation (1), using ligand such as alkane or conjugated molecules. Ligand with charges and mobile counter ions were exploited recently as new type of ligand for NPs electrical property modulation. For example, Nakanishi et al showed an inverse photoconductivity of silver NP with positive charged ammonium ending group.[10] In another research, they demonstrated the combined electronic and ionic conductance NPs with the same positive charge ligand and mobile counter ions and the resultant dynamic internal gradient is further used to guide the electron flow.[11]

In this chapter, we demonstrated both the ionic and electronic charge transport properties of NPs modulated by ligand engineering. Depending on the chemical structure of the ligand, gold NPs showed electronic, mixed electronic and ionic conductance and a reversible switch between

electron and mixed conductance. We characterized these properties extensively by impedance spectroscopy, where the electronic and ionic conductance of the particle film are obtained simultaneously. The responsive electronic and ionic conductance of the NP in different solvent environments was further explored for possible VOC sensing application.

Impedance spectroscopy (IS) has proved to be a powerful tool to study the localized conduction taking place at electrode, interfacial and bulk using different impedance related complex functions.[12] It has been widely used for solid electrolyte, ceramics and nanostructured solids or nanodispersions. [12, 13, 14] For example, Heath et al ever demonstrated a reversible insulator-to-metal transition in metal nanoparticle monolayer by the change from capacitance to inductance character of the impedance spectroscopy.[15]

6.2 Results and Discussion

6.2.1 Nanoparticle structures and impedance spectroscopy measurement

The particles we used are shown in Figure 6.1, with gold core diameter around 2.5nm obtained by Brust and Schriffin method,[16] and various ligands by the ligand exchange. Three types of ligands are chosen, including the regular alkane thiol and two positively charged ones. The IS measurement setup is shown in Figure 6.1b, where the sample is sandwiched between two gold coated electrodes with thickness and area defined by Kapton film and was laid in vacuum chamber for overnight till stable results reproduced. The typical frequency range of the IS measure is between 3MHz to 0.1Hz with stimulating voltage 100mV.

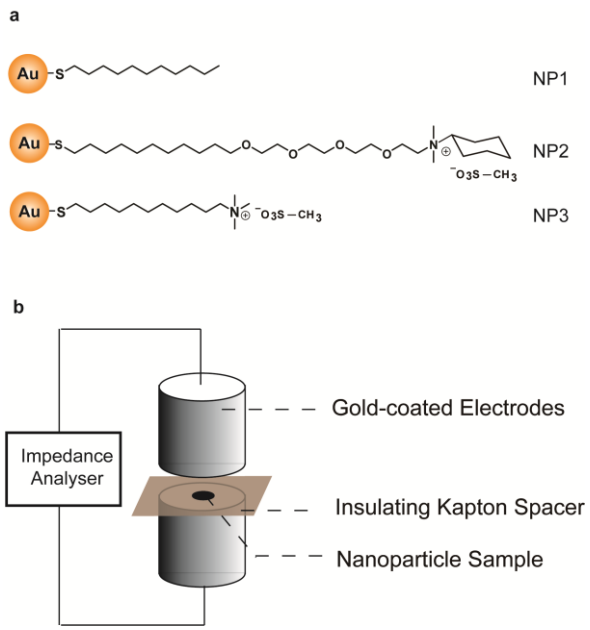

Figure 0.1 a) gold nanoparticles with undecanthiol (NP1), ionic liquid (NP2) and ionic (NP3) ligands used in this research. b) set-up of the impedance spectroscopy.

6.2.2 Impedance behavior of undecanethiol ligand gold NP

The electrical properties of gold nanoparticles with the alkane thiol ligand have been studied extensively in previous years. It is believed to work as inert insulating dielectric layer with quite big energy barrier for electron transfer. As a result, nanoparticles with alkane thiol electronically coupled with each other weakly at long separation space. Electron transfer between particles by tunneling, where the MOs of the alkane molecules assist the charge transport following super exchange mechanism,[17, 18] and the electrons are more localized on nanoparticles. In this situation, the NP aggregate can be modeled by a parallel combination of capacitance and resistance using the "orthodox" theory.[19, 20] This property can be clearly observed by impedance spectroscopy. As shown in Figure 6.2, gold NP film with undecane thiol ligand showed a perfect semicircle in the Nyquist plot, which is a typical result of (RC) parallel circuit, where R represents the electron resistance and C is the cell capacitance, with τ=RC the dielectric relaxation time around 1.8 ms.[21,

[22] We can also conclude from the un-distorted semicircle that there is only one dielectric relaxation time, indicating a homogeneous aggregation state.

The corresponding Bode plots were shown in Figure 6.2 b, where the phase angle and magnitude of the impedance are plotted as a function of frequency. In accordance with the Nyquist plot, we see the phase angle reach around 45° at frequency around 10^3 Hz. At frequency higher than 10^4, the NPs films behave more as an capacitor, with phase angle near -90°, and more as a resister in frequencies lower than 100 Hz. The amplitude of impedance vs frequency plot, in Figure 6.2b on right Y axis, showed only one plateau, a sign of only one charge transfer dynamics in the NP film. This also agreed with the Nyquist plot.

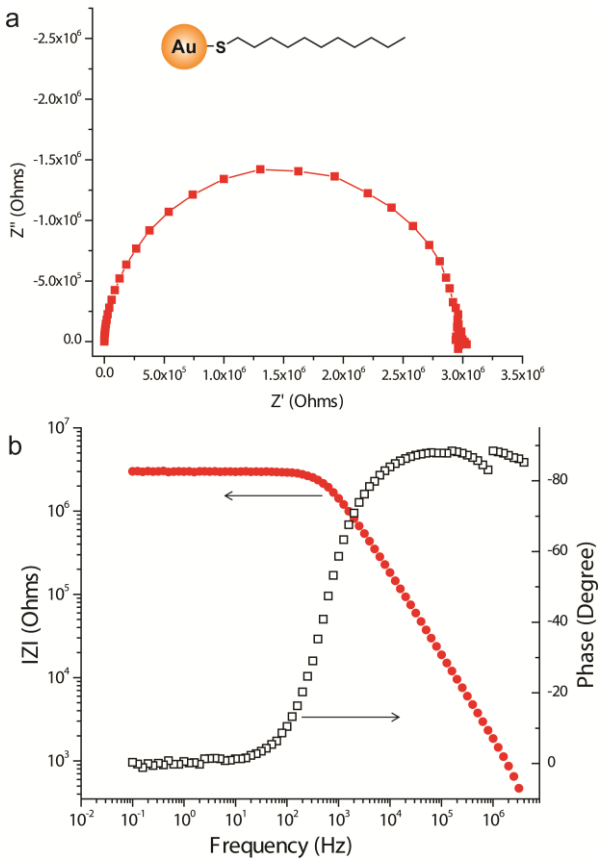

Figure 0.2 a) Nyquist plot of the IS of NP1. A perfect semicircle arc can be seen, indicating a parallel RC circuit with only one dielectric relaxation time. Weak coupling and homogeneous aggregation of the NP can be told from the IS result. b) Bode plots of the IS of NP1, indicating the high frequency capacitance and low frequency conductance properties of the NP1.

6.2.3 Impedance behavior of ionic liquid ligand gold NP

Ligands for NP2 featured a tetra(ethylene glycol) segment with a bulky cyclohexyl ammonium beside the alkyl chain. We have ever demonstrated in our previous research that this ligand is a type of ionic liquid and NP2 with this ligand exhibits liquid-like behavior with fluidity with which direct nano-imprint NP2 into various nano-scale patterns is realized.[23] The charge transport properties of this liquid-like NP with ionic liquid ligand are demonstrated here. The impedance spectroscopy of NP2 is shown in Figure 6.3. In the Nyquist plot, we can see, quite different from NP1, a high frequency semicircle arc followed by an inclined line in the low frequency region. This is a quite typical pattern for ionic conductor, where the arc is assigned to ion conduction and the line arises from the electrode polarization due to the ions accumulated at the blocking electrodes. [24] The ionic conduction is further exploited by the temperature dependent measurement. As shown in Figure 6.3b, the arc shrink as temperature increase, indicating an increased ionic conductance. When the conductance, obtained by fitting the arc at different temperature, was plotted in logarithm as inverse of temperature, a straight line was obtained (Figure 6.3c). This Arrhenius behavior, implying that charge transport is a thermo activated process, is in accordance with ionic conductance, and the activation energy is calculated to be ~39kJ/mol, a reasonable value for intermolecular electrostatic interaction. These results show that the ionic conductance of the ionic liquid ligand is preserved in the NP2 film, agreeing with our previously observed liquid-like behavior of NP2. Since the positive ammonium cation is bonded to gold NPs, we believe the counter ion CH_3-SO_3^- is the mobile charge carrier.

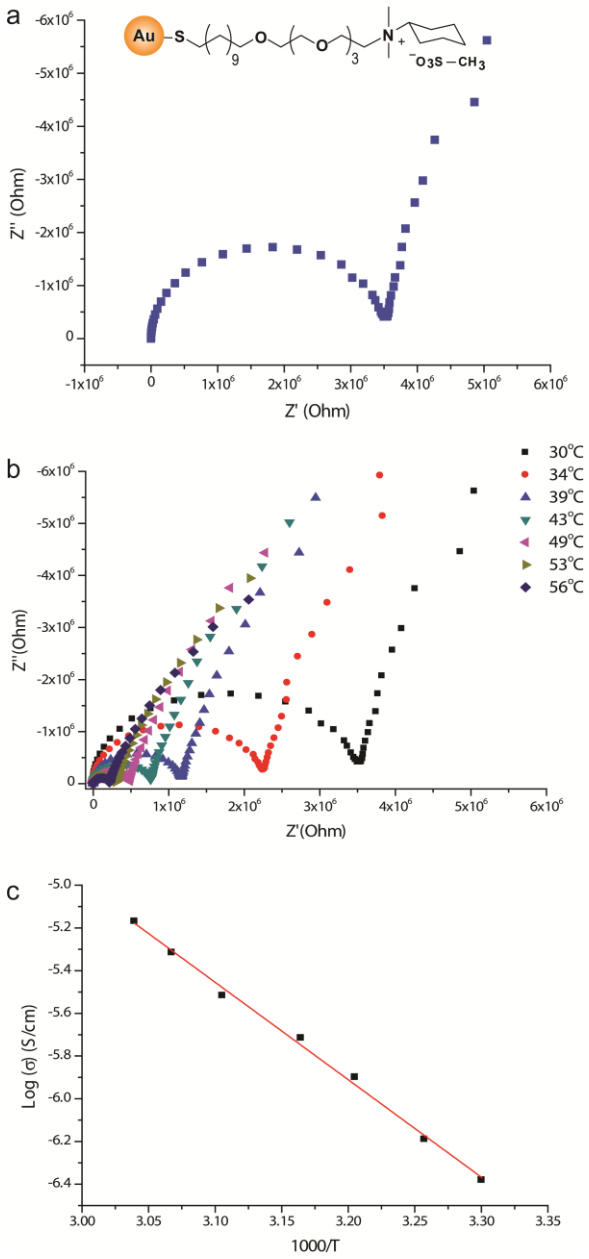

Figure 0.3 ionic conductance of NP2. a) Nyquist plot of the NP2 IS. The semicircle arc indicated ionic conductance, while the inclined line arose from the electrode polarization. b) temperature dependent IS of NP2. As temperature increase, the semicircle arc shrink, indicating ionic conductance increase. c) logarithm of the conductance versus inverse of temperature, Arrhenius type straight line is obtained, which tells that charge transport is a thermo activated process.

The electronic conductance of NP2 cannot be identified in the high frequency region of IS. Further insight into the transport properties were obtained by extension of the IS measurement

into a lower-frequency range. It have ever been demonstrated that impedance spectroscopy over a sufficiently wide frequency range can be used to identify ionic and electronic transport components in nanoparticle composite material and intercalation materials. [25, 26] The IS of the NP2 at extended frequency are shown in Figure 6.4. As can be seen, in the Nyquist plot of Figure 6.4a, the semicircle in the high frequency region is a very small arc at the left bottom corner. Instead of an inclined line going straightly up as seen in Figure 6.3a, the complex impedance actually curved back to the real axis at low frequency, forming another arc. This arc can be assigned as electronic conductance. Since the gold electrodes used in the IS measurement are blocking electrodes for ions, a pure ionic conductor will work like a capacitor at low frequency, where the Nyquist plot should go further away from real axis. However, for an electronic conductor, at low frequency, electrons can keep flowing in and out of the electrode, resulting in a resistor behavior, and this is what was observed in Figure 6.3a.

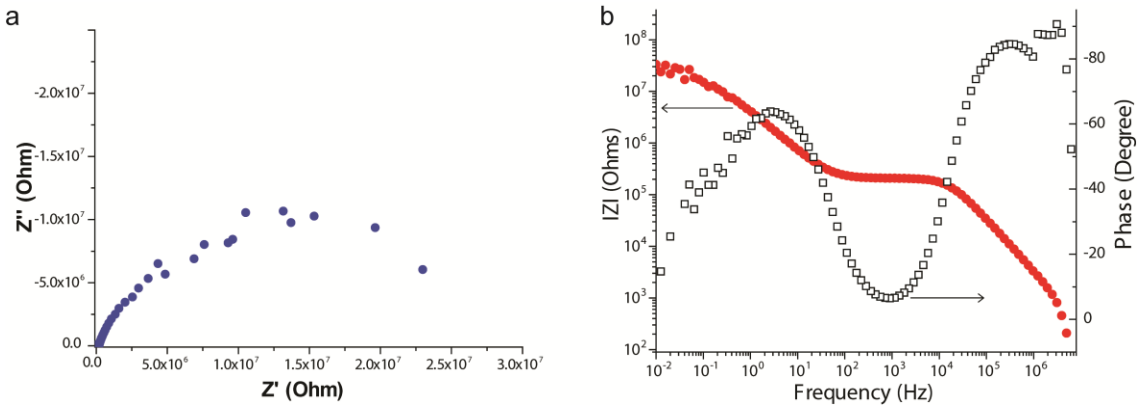

Figure 0.4 IS of NP2 at extended frequency range down to 0.01Hz. a) Nyquist plot of the NP2 IS when going to very low frequency. The semicircle shown in Figure 6.3 is at the left bottom corner of the plot. The inclined line seen in Figure 6.3 returned to the real axis at low frequency, showing electronic conductance. b) corresponding Bode plot of the IS.

The coexistence of ionic and electronic conductance of NP2 can be further confirmed in Bode plots as shown in Figure 6.4b. The magnitude has two plateaus, one at frequency range between 10^2 to 10^4 Hz and another at frequency lower than 10^{-1}Hz, indicating two types of conductance

with different dielectric relaxation times. The corresponding phase diagram is shown in the right Y axis of Figure 6.4b. The two high-to-low phase angle transitions also imply two charge transfer dynamics.

We can clearly see that combing ionic liquid ligands, gold NP film can exhibit combined ionic and electronic conducting properties. The two conductances have very different transport dynamics, with ionic conductance working at higher frequency and electronic conductance at low frequency. This property makes NP2 a special electrical material with selective conducting property at different frequencies with different charge carriers, implying a potential material for functional device applications. For example, Grzybowski and coworkers have utilized the mixed ionic and electronic conductance of ionic ligand gold NPs to control and direct electric current flow. [11, 27]

6.2.4 Impedance behavior of ionic ligand gold NP

The ionic conductance of NP2 depended on the mobile ions and it is believed that the counter ion of the ligand works as a charge carrier. However, as we know, not all ionic compounds can work as an ionic conductor. Ionic liquids are a special case where the ions can move by overcoming the relatively small energy barriers in the fluid environment at room temperature.[28] Ligand of NP3 did not possess flexible ethylene glycol segment and bulky cyclohexyl group on ammonium and is not liquid at room temperature. As shown Figure 6.5a, the Nyquist plot of the NP3 showed only one semicircle arc; no electrode polarization or second arc was observed at frequency as low as 0.1 Hz, which means that ions in NP3 are not mobile and electrons are the only responsible charge carrier for the observed conductivity. This result reveals the importance of the liquid state by the ethylene glycol segment and bulky cyclohexyl group on the ammonium ion for the mobility of the counter ion and the mixed ionic and electronic properties of the gold NPs.

Meanwhile, we found in the presence of small amount of solvents, such as the residual methanol from sample preparation process, NP3 showed similar IS behavior as NP2, as shown in Figure

6.5b. The residual solvent can assist the ion movement and pure electronic conductance changed into mixed electronic and ionic conductance. This unique reversible transition between two conducting states in response to the solvent environment makes this NP an attractive material for sensing applications.

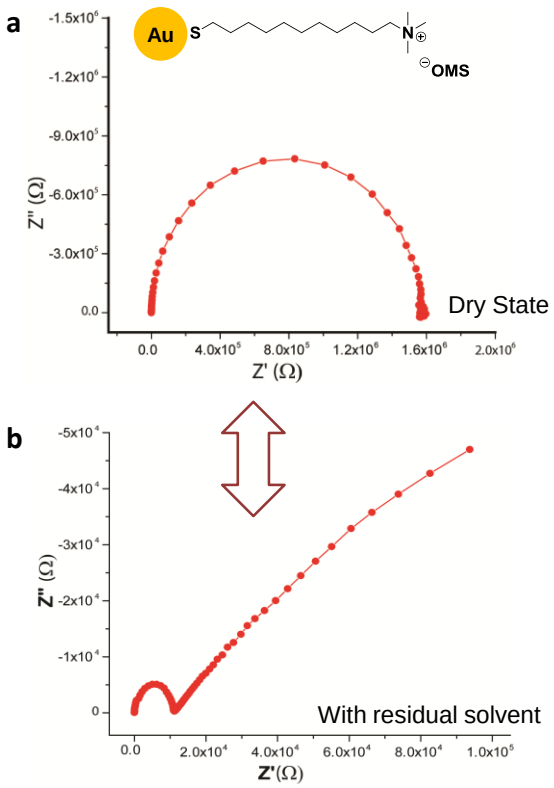

Figure 0.5 Reversible transition between electronic and mixed conductance of the NP3 at dry (a) and with residual solvent state (b).

6.2.5 Sensing based on ionic ligand nanoparticle using IS

Sensing based on the conducting properties of metal nanoparticle films has been explored in recent years.[1, 29] The most widely studied transduction is chemiresistance, based on resistance change of NP film in the presence of analyte, which is indicated by the DC current change when analyte gas, such as volatile organic solvents, flow through the film. Non-ionic ligands, such as alkyl thiol of different chain length and ending groups[30, 31] or different structure, such as dendrimer,[32] are generally used. Here, electrons are the only charge carrier, and analyte absorbed

by the NP film will alter the dielectric electron transfer barrier, inter distance of the NPs, and the corresponding parameters like β, δ and E_A in equation 1. The main disadvantage of this type of sensing is the single signal read-out i.e. the DC current change in presence of analyte, despite the multifold change of the NP film, β, δ and E_A. As a result, the selectivity of chemiresitivity based on a single type of particle is usually poor, because no characteristic signals can be obtained. NP with ionic conductive matrix has also been exploited as a chemiresistive sensor,[33] while, since it was still based on DC measurement, a lot of useful information that can be used as sensing signal is hidden.

We noticed that in the presence of different solvents, our NP3 exhibited different electronic and ionic conductance that can be read out by IS measurement. We thus developed a sensing technique based on ionic ligand gold NPs and IS for volatile organic compounds (VOC).[34] The setup is shown in Figure 6.6a. Gold NPs are drop casted onto the thin film gold electrodes pre-patterned on insulting glass substrate. The gold NP we used is slightly different from NP3 with shorter alkane chain for a better electron conductance in the open parallel electrodes geometry. The chip is placed in a sealed chamber and connected to an impedance analyzer. The VOC gas is carried into the chamber by N_2 gas by flowing through a bubbler containing the VOC liquid. In different VOC environments, the IS measurement was engaged and the spectrum is fitted using the circuit shown in Figure 6.6b, where R_{ion} and R_e are ionic and electronic resistance respectively. For each VOC sample, both R_{ion} and R_e can be read out and used as characteristic signal of the sample. We have tested several common organic solvents, including ethanol, acetone, hexane and dichloromethane (DCM), and results are shown in Figure 6.6c. We can see the ionic and electronic resistances of the NP are quite different; they varied several magnitudes in different VOC environment. Besides the values of the R_{ion} and R_e, the relative magnitude of the two can also be used to distinguish VOCs. For example, out of the four solvents, only in DCM environment, R_{ion} is bigger than R_e.

The change of electronic and ionic conductance in different VOCs depends on many factors, such as the equilibrium between absorbed and free VOC molecules, the ion mobility provided by the VOC, the interparticle distance and dielectric environment change upon VOC adsorption. The interplay between ion and electron transport is another key for the measured responsive electrical properties of NP film. Many questions such as how the movement of the ions changes the tunneling barriers of electron transport and how electron transport alters the micro electrochemical potential environment for ion movement, need to be addressed to get a better understanding of this point.

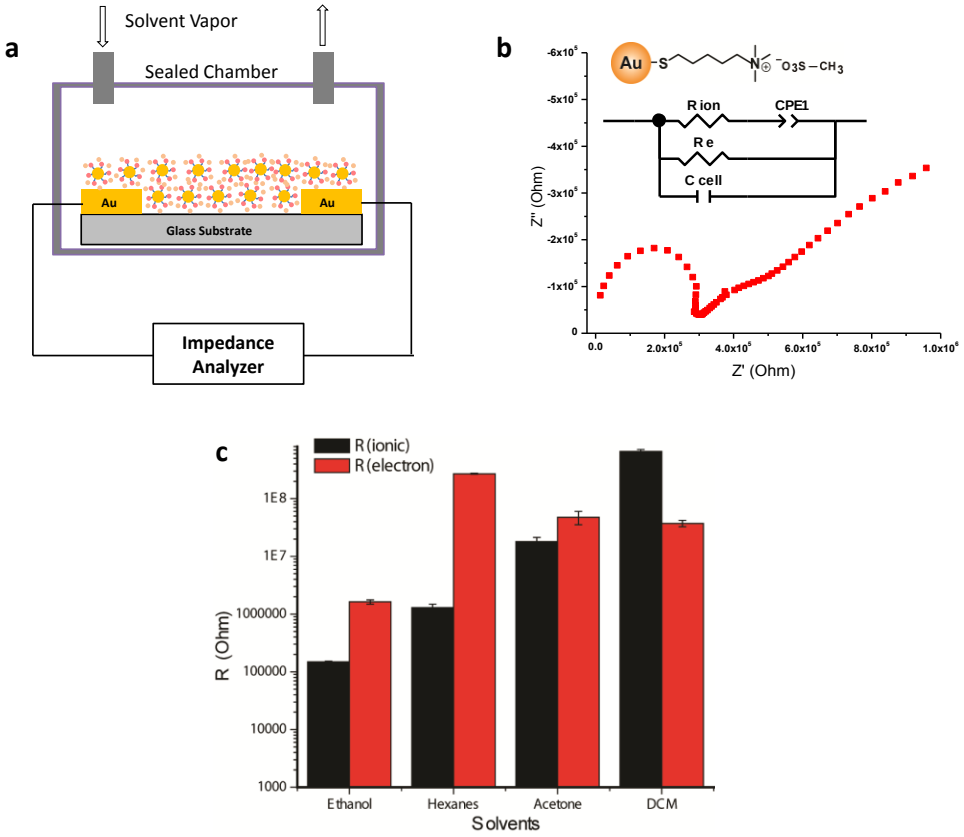

Figure 0.6 a) Setup of the ionic ligand NP sensing using IS. b) Representative Nyquist plot of the NP used for sensing in ethanol environment. The circuit used to fit the IS is also shown, where R_{ion} and R_e are ionic and electronic resistance respectively, C_{cell} is the cell capacitance and CPE is the constant phase element. c) Column diagram of the R_{ion} and R_e in different solvent environment.

6.3 Experimental Section

6.3.1 Nanoparticle synthesis

The ligands were synthesized according to previous reports [35]. Subsequent place-exchange reaction with pentanethiol-coated gold nanoparticles ($d \approx 2$ nm) resulted in NPs in high yields. ^{1}H NMR spectroscopic investigation revealed that the place-exchange reaction proceeds almost quantitatively and the coverage of cationic ligands on the nanoparticles is near complete [36].

6.3.2 Impedance spectrscopy

Impedance spectroscopy was performed using a Solartron 1287 potentiostat and 1252A frequency response analyser in the range 0.1 Hz to 300 kHz and extended to 0.01 H_Z when necessary. Measurements were conducted under vacuum at various temperatures with a sinusoidal excitation root-mean-square voltage of 0.1 V. The sample thickness and contact surface area were controlled by a 125 μm thick Kapton tape with a 0.3175 cm diameter hole. The data are analyzed by ZView with proper choice of circuit model.

6.3.3 VOC sensing

Film gold electrodes patterned on insulting glass substrate were made by photo lithography followed by sputter coating and removal of photo-resist. The gold NP was drop-casted onto the electrode substrate and the chip is placed in a sealed glass chamber and connected to the impedance analyzer. The VOC gas is carried into the chamber by N_2 gas by flowing through a bubbler containing the organic solvent liquid.

6.4 Conclusion

We have investigated in detail the complex electrical properties of gold NPs with alkane or ionic ligands by using impedance spectroscopy. Electronic, mixed ionic & electronic, and responsive conductance were found, which was determined by the ligands of the NPs. Different conducting properties, capacitance or resistance, by either ions or electrons, at different frequency ranges

were also confirmed by IS measurement. Based on the responsive ionic and electronic conductance of the ionic ligand gold NP, we invented a novel method of sensing. Unlike the traditional chemiresistive sensing based on single DC current signal, characteristic ionic and electronic conductance in different environments were used to distinguish volatile organic solvents with a much better selectivity.

6.5 References

1 Zabet-Khosousi, A.; Dhirani, A.-A. *Chem. Rev.* **2008**, *108*, 4072.

2 Halas, N.; Lal, S.; Chang, W.; Link, S.; Nordlander, P. *Chem. Rev.* **2011**, *111*, 3913.

3 Simon, U. *Adv. Mater.* **1998**, *10*, 1487.

4 Schmid, G.; Simon, U. *Chem. Comm.* **2005**, 697.

5 Neugebauer, C. a.; Webb, M. B. *J. Appl. Phy.. Phy.* **1962**, *33*, 74.

6 Terrill, R.; Postlethwaite, T. *J. Am. Chem. Soc.* **1995**, *117*, 12537.

7 Wang, G. R.; Wang, L.; Rendeng, Q.; Wang, J.; Luo, J.; Zhong, C.-J. *J. Mater. Chem.* **2007**, *17*, 457.

8 Wessels, J. M.; Nothofer, H.-G.; Ford, W. E.; Wrochem, F. von; Scholz, F.; Vossmeyer, T.; Schroedter, A.; Weller, H.; Yasuda, A. *J. Am. Chem. Soc.* **2004**, *126*, 3349.

9 Stansfield, G. L.; Thomas, P. J. *J. Am. Chem. Soc.* **2012**, *134*, 11888.

10 Nakanishi, H.; Bishop, K. J. M.; Kowalczyk, B.; Nitzan, A.; Weiss, E. A.; Tretiakov, K. V.; Apodaca, M. M.; Klajn, R.; Stoddart, J. F.; Grzybowski, B. A. *Nature* **2009**, *460*, 371.

11 Nakanishi, H.; Walker, D. a; Bishop, K. J. M.; Wesson, P. J.; Yan, Y.; Soh, S.; Swaminathan, S.; Grzybowski, B. a *Nat. Nano.* **2011**, *6*, 740.

12 Macdonald, J. R. *Impedance Spectroscopy*; Wiley: New York, NY, 1987.

13 Schön, G.; Simon, U. *Colloid Polym. Sci.* **1995**, *273*, 101.

14 Schön, G.; Simon, U. *Colloid Polym. Sci.* **1995**, *273*, 202.

15 Markovich, G.; Collier, C.; Heath, J. *Phys. Rev. Lett.* **1998**, *80*, 3807.

16 Brust, M.; Fink, J.; Bethell, D.; Schiffrin, D. J.; Kiely, C. *J. Chem. Soc. Chem. Commun* **1995**, 1655.

17 Adams, D. M.; Brus, L.; Chidsey, C. E. D.; Creager, S.; Creutz, C.; Kagan, C. R.; Kamat, P. V.; Lieberman, M.; Lindsay, S.; Marcus, R. A.; Metzger, R. M.; Michel-Beyerle, M. E.; Miller, J. R.; Newton, M. D.; Rolison, D. R.; Sankey, O.; Schanze, K. S.; Yardley, J.; Zhu, X. *J. Phys. Chem. B* **2003**, *107*, 6668.

18 Nitzan, A. *Annu. Rev. Phy. Chem.* **2001**, *52*, 681.

19 Hanna, A.; Tinkham, M. *Phy. Rev. B* **1991**, *44*, 5919.

20 Amman, M.; Wilkins, R.; Ben-Jacob, E. *Phy. Rev. B* **1991**, *43*, 1146.

21 Markovich, G.; Collier, C.; Heath, J. *Phys. Rev. Lett.* **1998**, *80*, 3807.

22 Gerhardt, R. *J. Phy. Chem. Solids* **1994**, *55*, 1491.

23 Yu, X.; Pham, J. T.; Subramani, C.; Creran, B.; Yeh, Y.-C.; Du, K.; Patra, D.; Miranda, O. R.; Crosby, A. J.; Rotello, V. M. *Adv. Mater* **2012**, ASAP.

24 Frömling, T.; Kunze, M.; Schönhoff, M.; Sundermeyer, J.; Roling, B. *J. Phys. Chem. B* **2008**, *112*, 12985.

25 Lee, S.; Cummins, M. D.; Willing, G. A.; Firestone, M. A. *J. Mater. Chem.* **2009**, *19*, 8092.

26 Nobili, F.; Tossici, R.; Marassi, R.; Croce, F.; Scrosati, B. *J. Phys. Chem. B* **2002**, *106*, 3909.

27 Yu, X.; Rotello, V. M. *Nat. Nano.* **2011**, *6*, 693.

28 Castner, E. W.; Margulis, C. J.; Maroncelli, M.; Wishart, J. F. *Ann. Rev. Phys. Chem.* **2011**, *62*, 85.

29 Ibañez, F. J.; Zamborini, F. P. *Small* **2011**, 174.

30 Zamborini, F. P.; Leopold, M. C.; Hicks, J. F.; Kulesza, P. J.; Malik, M. a; Murray, R. W. *J. Am. Chem. Soc.* **2002**, *124*, 8958.

31 Peng, G.; Tisch, U.; Adams, O.; Hakim, M.; Shehada, N.; Broza, Y. Y.; Billan, S.; Abdah-Bortnyak, R.; Kuten, A.; Haick, H. *Nat. Nano.* **2009**, *4*, 669.

32 Krasteva, N.; Besnard, I.; Guse, B.; Bauer, R. *Nano Lett.* **2002**, *2*, 551.

33 Gold, S.; Ibañez, F. J.; Zamborini, F. P. *ACS nano* **2008**, *2*, 1543.

34 Han, L.; Shi, X.; Wu, W.; Kirk, F. L.; Luo, J.; Wang, L.; Mott, D.; Cousineau, L.; Lim, S. I.-I.; Lu, S.; Zhong, C.-J. *Sensor Actuat. B Chem.* **2005**, *106*, 431.

35 You, C. C.; Miranda, O. R.; Gider, B.; Ghosh, P. S.; Kim, I. B.; Erdogan, B.; Krovi, S. A.; Bunz, U. H. F.; Rotello, V. M.; *Nat. Nanotechnol*. **2007,** 2, 318.

36 Miranda, O.R.; Chen, H. T.; You, C. C.; Mortenson, D. E.; Yang, X. C.; Bunz, U. H. F.; Rotello, V. M.; *J. Am. Chem. Soc.* **2010,** 132, 5285.

CHAPTER 7

FLUORESCENCE RESONANCE ENERGY TRANSFER IN RECOGNITION-MEDIATED POLYMER-QUANTUM DOT ASSEMBLIES

7.1 Introduction

Organization of the nanoparticles (NPs) into morphologically controlled and organised structures is of great scientific interest for bottom-up fabrication of functional devices in optoelectronics, sensing, catalysis and medicine.[1,2] Directed host-guest assembly of NPs into polymer matrices[3,4] is an effective route to form structured NP assemblies with advantageous optical,[5] electronic,[6] magnetic,[7] and mechanical properties.[8] Polymer mediated self-assembly of NPs yields stable nanocomposites and their properties can be tuned by varying the size and shape of the NPs as well as by altering their surface monolayer.[9] Furthermore, the functionality and structure of the polymer can be modified, lending an additional element of control to the entire assembly process.[10]

In the past, we have demonstrated recognition mediated assembly of NPs into polymer matrices using the "plug and play" polymers.[3] These "plug and play" polymers feature recognition elements designed to interact with specific guest molecules via non-covalent interactions,[11] hence allowing multiple systems to be assembled using a single backbone. In previous studies using gold and magnetic NPs, we have shown that polymer mediated self-assembly of NPs provides structures with increased ordering, controlled inter-particle spacing and tunable physical properties[12] and optical properties.[13]

In this chapter, I will describe the recognition mediated assembly of ZnSe QDs with a chromophore-functionalized polymer, facilitating fluorescence resonance energy transfer

(FRET) from QDs to the chromophore. We have designed and synthesized a polyfunctional copolymer (poly(MMA-*co*-DAP-*co*-Fl)) featuring a solubilising methyl methacrylate (MMA) element, a diamidopyridine (DAP) recognition element and flavin (Fl) chromophore. Thymine functionalized ZnSe QDs (Thy-QDs) were used as guest in the assembly. The choice of the flavin as a chromophore was based on the spectral overlap of flavin absorption with ZnSe QDs emission. The self-assembly was driven by the multivalent DAP-thymine three-point hydrogen bonding complementary interactions[14] that also brought the flavin and QDs into proximity (Scheme 1). Due to the spectral overlap and the close proximity, FRET was observed from ZnSe QDs to flavin both in solution and solid state, as confirmed by steady-state and time resolved photoluminescence measurements. The energy transfer efficiencies were tuned by controlling the molar ratio between QDs and flavin-containing polymer. A control system that cannot participate in hydrogen bonding, N(3)-methyl thymine functionalized ZnSe QDs (MeThy-QDs) was also prepared (Scheme 1).

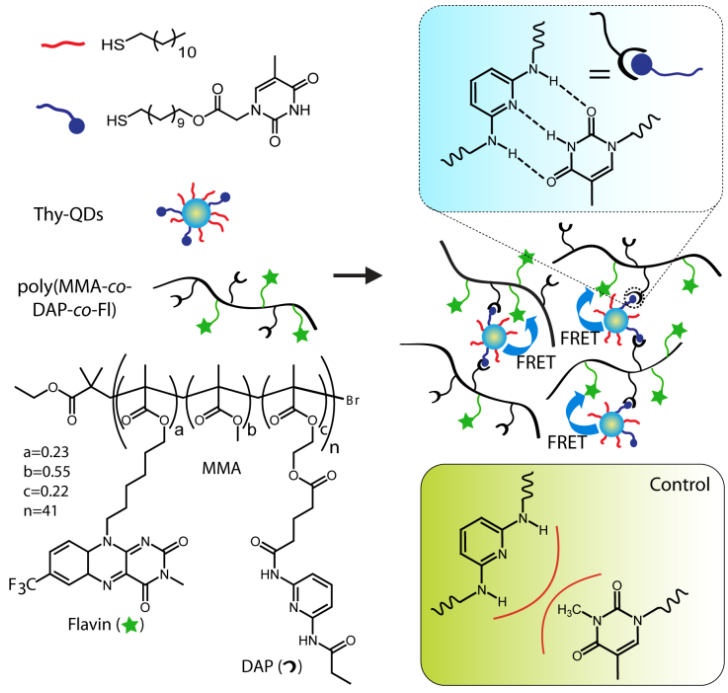

Scheme 0-1 Recognition mediated assembly of Thy-QDs and poly(MMA-*co*-DAP-*co*-Fl).

7.2 Results and Discussion

7.2.1 Flavin polymer synthesis

The random copolymers incorporating a DAP moieties and flavin chromophores were synthesized by atom transfer radical polymerization (ATRP). The polymers were synthesized from their corresponding methacrylate monomer moiety. Methyl methacrylate was incorporated into the copolymer backbone to promote solubility in non-polar solvents while maintaining a small sidechain profile thus reducing the possibility of steric interference towards binding.

7.2.2 Flavin polymer and quantum dots assembly

Addition of the poly(MMA-*co*-DAP-*co*-Fl) to Thy-QDs in non-competitive solvents such as dichloromethane (DCM) and chloroform resulted in the formation of QDs/polymer nanocomposite. Insight into nanocomposite formation was investigated by transmission electron microscopy (TEM) and small angle X-ray spectroscopy (SAXS). TEM images of Thy-QDs (Figure 7.1a and c) show the typical appearance of nanocrystals deposited on a TEM grid from DCM solution. These particles were essentially monodisperse with a 3.5 nm diameter.[15] Significantly, no aggregation was observed as shown in the magnified image (Figure 7.1c). In contrast, structured aggregates of Thy-QDs were formed in presence of the poly(MMA-*co*-DAP-*co*-Fl) (Figure 7.1b). The high magnification image of the nanocomposite reveals close- packed assemblies of Thy-QDs in the polymer matrix (Figure 7.1d). In contrast to Thy-QDs, no such assemblies were observed upon addition of the poly(MMA-*co*-DAP-*co*-Fl) to the MeThy-QDs (Figure 7.2). The magnified image of the control sample showed the light contrast in the background from the polymer, suggesting a clear phase separation between the QDs and the polymer. It demonstrates that the assemblies observed upon addition of poly(MMA-*co*-DAP-*co*-Fl) to Thy-QDs were the result of the specific thymine-DAP hydrogen-bonding interactions.

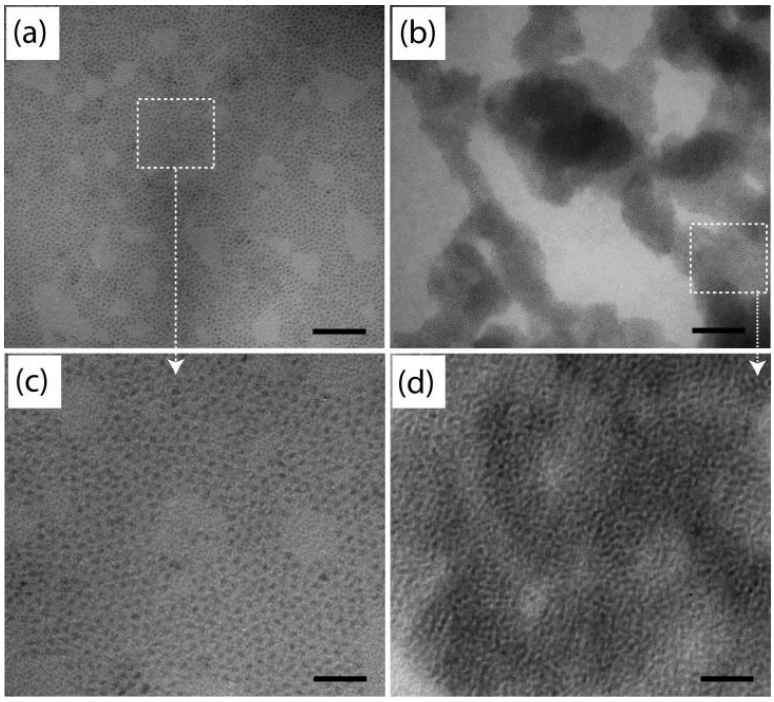

Figure 0.1 TEM image of Thy-QDs in absence (a,c) and presence (b,d) of poly(MMA-*co*-DAP-*co*-Fl). Scale bar in (a) and (b) is 50 nm. Scale bar in (c) and (d) is 20 nm.

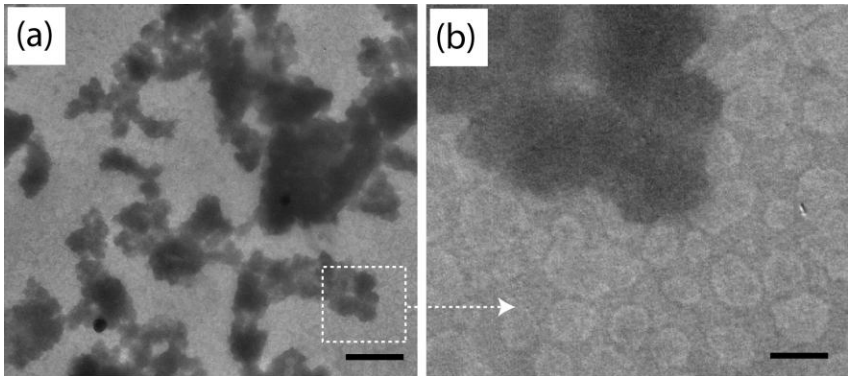

Figure 0.2 TEM images of MeThy-QDs in presence of poly(MMA-*co*-DAP-*co*-Fl). The scale bar in (a) and (b) are 100 nm and 20 nm, respectively.

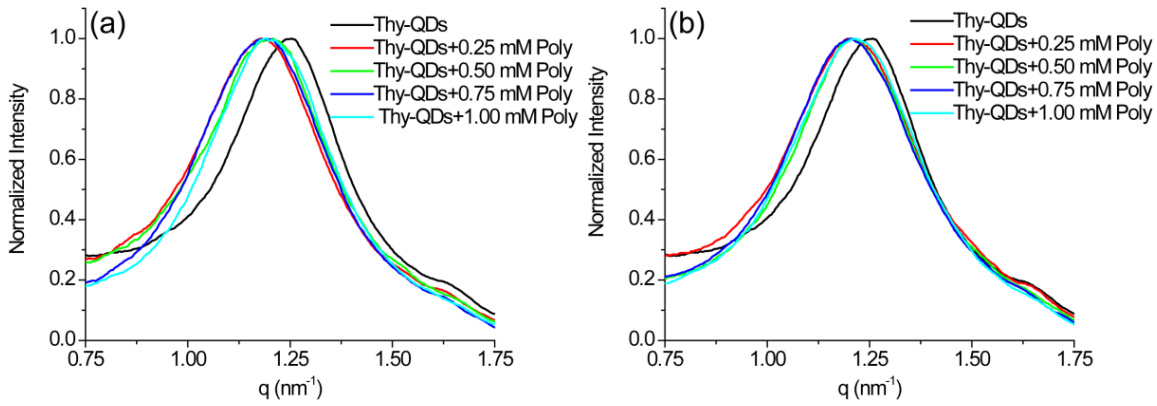

Figure 0.3 Small angle X-ray spectra of Thy-QDs alone and in presence of poly(MMA-*co*-DAP-*co*-Fl) (a) before and (b) after annealing.

Table 0-1 Peak scattering factor (q) and inter-particle distance (d) values of Thy-QDs alone and in presence of poly(MMA-*co*-DAP-*co*-Fl) before and after annealing.

	before annealing		**after annealing**	
	q (nm^{-1})	d (nm)	q (nm^{-1})	d (nm)
Thy-QDs	1.25	5.0	1.25	5.0
Thy-QDs+0.25 mM Poly	1.20	5.2	1.20	5.2
Thy-QDs+0.50 mM Poly	1.21	5.2	1.21	5.2
Thy-QDs+0.75 mM Poly	1.19	5.3	1.20	5.2
Thy-QDs+1.00 mM Poly	1.19	5.3	1.21	5.2

SAXS was used to analyze the structural characteristics of Thy-QDs assemblies in the polymer matrix (Figure 7.3a). SAXS provides quantitative information of inter-particle spacing (d) in the nanoparticles assemblies using $d=2\pi/q$ where q is a wave vector where scattering intensity is maximum. With Thy-QDs drop cast from dichloromethane, a center-to-center particle spacing of 4.99 nm was observed. When 0.25 mM poly(MMA-*co*-DAP-*co*-Fl) was mixed to assemble Thy-QDs, the inter-particle spacing increased to 5.23 nm (Table 7.1). The increase was consistent with the assembly motif shown in scheme 1 where a polymer chain separates the QDs in the assemblies. However, increase in the polymer concentration didn't change the inter-particle spacing significantly. A single uniform peak for all the QDs

aggregates suggests that QDs were regularly dispersed within the polymer matrix.

7.2.3 Fluorescence energy transfer in quantum dot – polymer assembly

Figure 7.4a shows the emission and absorption spectra of ZnSe QDs and poly(MMA-*co*-DAP-*co*-Fl). The peaks in the absorption and emission spectra of the polymer were largely due to the flavin unit. The plots in Figure 7.4a show clear spectral overlap between ZnSe QDs emission and flavin absorption. Figure 7.4b shows steady-state fluorescence spectra of Thy-QDs alone and in presence of the poly(MMA-*co*-DAP-*co*-Fl). The concentration of Thy-QDs were kept constant while the concentation of poly(MMA-*co*-DAP-*co*-Fl) was increased in the nanocomposite. Due to the high binding constant between thymine and DAP (~500-1000),[14] the concentration of polymer was chosen 10-100 times more than QDs. The data are consistent with progressive quenching of the Thy-QDs emission and a systematic enhancement of the poly(MMA-*co*-DAP-*co*-Fl) emission as concentration of poly(MMA-*co*-DAP-*co*-Fl) increases from 0.1 mM to 1.0 mM. These results strongly suggest that FRET is the primary mechanism for the reported observations where QDs and flavin serve as energy donor and acceptor in the nanocomposite, respectively. The calculation of the Forster distance and measured FRET distances at different poly(MMA-*co*-DAP-*co*-Fl):Thy-QDs ratios is given in the experimental section. In contrast to Thy-QDs, no quenching upon addition of the poly(MMA-*co*-DAP-*co*-Fl) to the MeThy-QDs (Figure 7.4c) indicated no interactions between MeThy-QDs and flavin. The control experiments confirmed that hydrogen-bonding was responsible for bringing Thy-QDs and flavin in proximity. The enhancement of flavin emission in Figure 7.4b was result of the increment of flavin concentration as well as FRET from Thy-QDs. However, the increase in flavin fluorescence in Figure 7.4c was only due to increasing polymer concentration since no quenching of QDs fluorescence was observed. The TEM and fluorescence results show the ability to manipulate the interaction between the host and guest through choice of recognition elements in “plug

and play" systems.

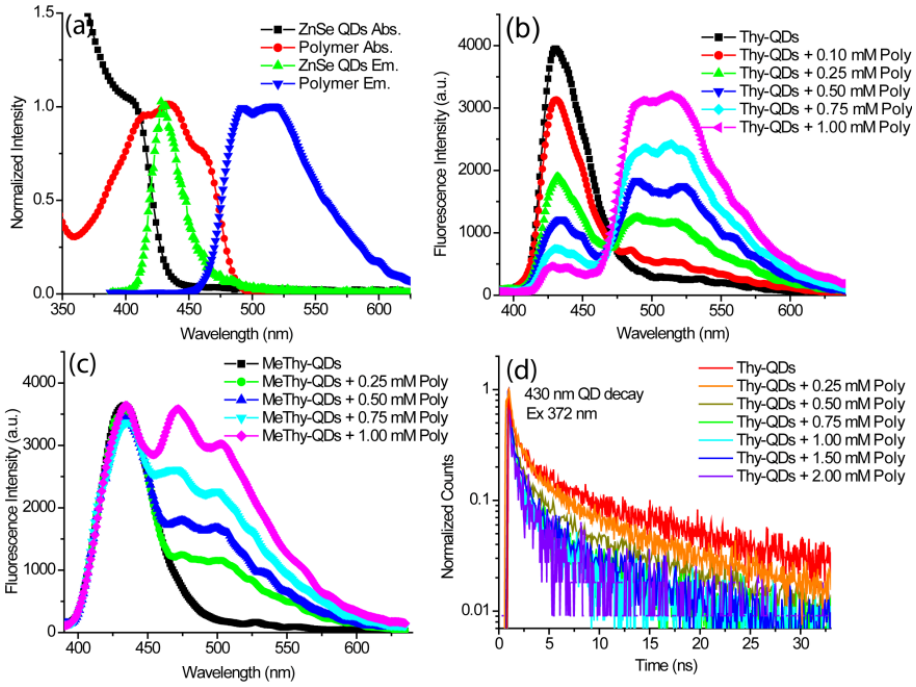

Figure 0.4 (a) Absorption and emission spectra of Thy-QDs and poly(MMA-*co*-DAP-*co*-Fl). Steady-state fluorescence spectra of (b) Thy-QDs and (c) MeThy-QDs alone and in presence of poly(MMA-*co*-DAP-*co*-Fl) at excitation 360 nm. (d) Time resolved photoluminiscence decay curves of Thy-QDs alone and in presence of poly(MMA-*co*-DAP-*co*-Fl) at excitation 372 nm and emission 430 nm.

Energy transfer is expected to substantially alter the exciton lifetime properties of the donor. To investigate this phenomenon, we carried out time-resolved photoluminescence measurements for Thy-QDs in absence and presence of the poly(MMA-*co*-DAP-*co*-Fl) (Figure 7.4d). The lifetimes were calculated by fitting the decay curves as a multiexponential decay. As expected, the average lifetime of the QDs (measured at 430 nm) decreased upon addition of poly(MMA-*co*-DAP-*co*-Fl) (Table 7.2). This is a classic behaviour for an energy donor-acceptor pair, confirming our observation of FRET, based on the steady-state emission data.

A comparison of the average exciton lifetimes (τ) of the donor alone and in presence of an

acceptor molecule, provides information on the FRET efficiency (*E*) which can be calculated as:[16]

$$E = 1 - \tau_{DA}/\tau_{D} \qquad [1]$$

where τ_D and τ_{DA} are the average lifetimes of donor (Thy-QDs) in the absence and presence of the acceptor (poly(MMA-*co*-DAP-*co*-Fl)), respectively (Table 7.2). The change in *E* values show that the energy transfer efficiencies were readily tuned by controlling the molar ratio between the QDs and polymer. The detailed information about the lifetime measurements is given in the experimetal section.

Table 0-2 The average lifetimes and energy transfer efficiencies of Thy-QDs in the absence and presence of poly(MMA-*co*-DAP-*co*-Fl).

Sample	τ (ns)	*E*
Thy-QDs	2.55	0
Thy-QDs + 0.25 mM Poly	1.67	0.34
Thy-QDs + 0.50 mM Poly	1.08	0.57
Thy-QDs + 0.75 mM Poly	0.37	0.85
Thy-QDs + 1.00 mM Poly	0.32	0.87
Thy-QDs + 1.50 mM Poly	0.28	0.89

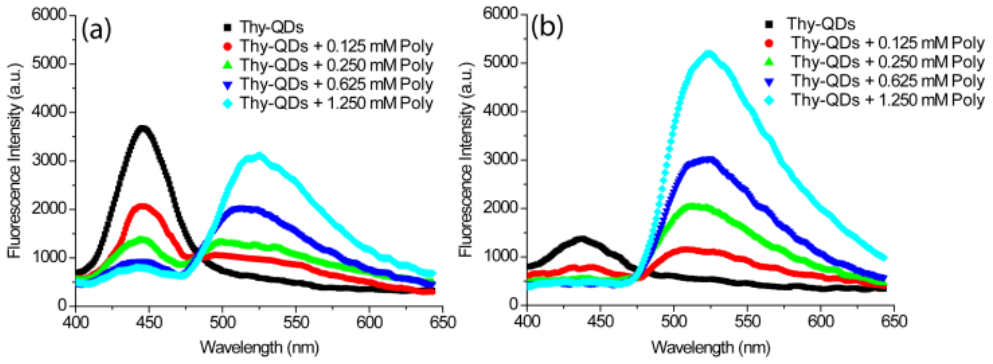

Figure 0.5 Steady-state fluorescence spectra of Thy-QDs poly(MMA-*co*-DAP-*co*-Fl) nano-composite thin films (a) before and (b) after annealing at 100 ºC for 8 hours.

The versatility of this "plug and play" strategy was successfully extended to bulk materials. Using spin casting, thin films of Thy-QDs and QDs/polymer nanocomposite were prepared. Steady-state fluorescence spectra of as-spun thin films also showed the same trend as that observed in solution, i.e., the decrease in Thy-QDs fluorescence with increase in poly(MMA-*co*-DAP-*co*-Fl) (Figure 7.5a). The energy transfer in the solid state indicated that we were able to trap the hydrogen-bonded host-guest complexes in thin films. Previously, we have shown the use of thymine-diaminotriazine hydrogen bonding as a recognition motif on the nanopatterned polymer surfaces [13b] which also suggests hydrogen bonding remains intact in the solid state. The spin cast films were annealed under vacuum at 100 ºC for 8 hours. The drop in QDs emission and the increase in flavin emission were found to be significantly higher in the annealed films (Figure 7.5b). The post-annealing steady-state fluorescence results indicate that annealing of the nanocomposite caused rearrangement of QDs and flavin in the polymer matrix that enhanced the energy transfer from QDs to flavin. This behavior is in contrast to normal nanocomposite materials that exhibit increased phase segregation upon annealing. The structural characteristics of Thy-QDs assemblies in polymer matrix didn't change significantly after annealing as observed in SAXS (Figure 2b).

7.3 Experimental Section

7.3.1 Synthesis of the flavin polymer

Ethyl 2-bromoisobutyrate (EBIB) was used as the initiator for the ATRP reaction that was performed in DMSO at 40°C with a Cu(I)Cl/Cu(II)Br_2/PMDETA catalyst system. GPC analysis was used to monitor the reaction progress and provided number average molecular weight (M_n) of 10200 for the copolymer with narrow distribution (PDI < 1.11). Proton peak integration of the ^{1}H NMR of the copolymer was used to determine the percentage ratio of each constituent monomer unit that was then used to calculate the approximate number of flavin, MMA and DAP moieties.

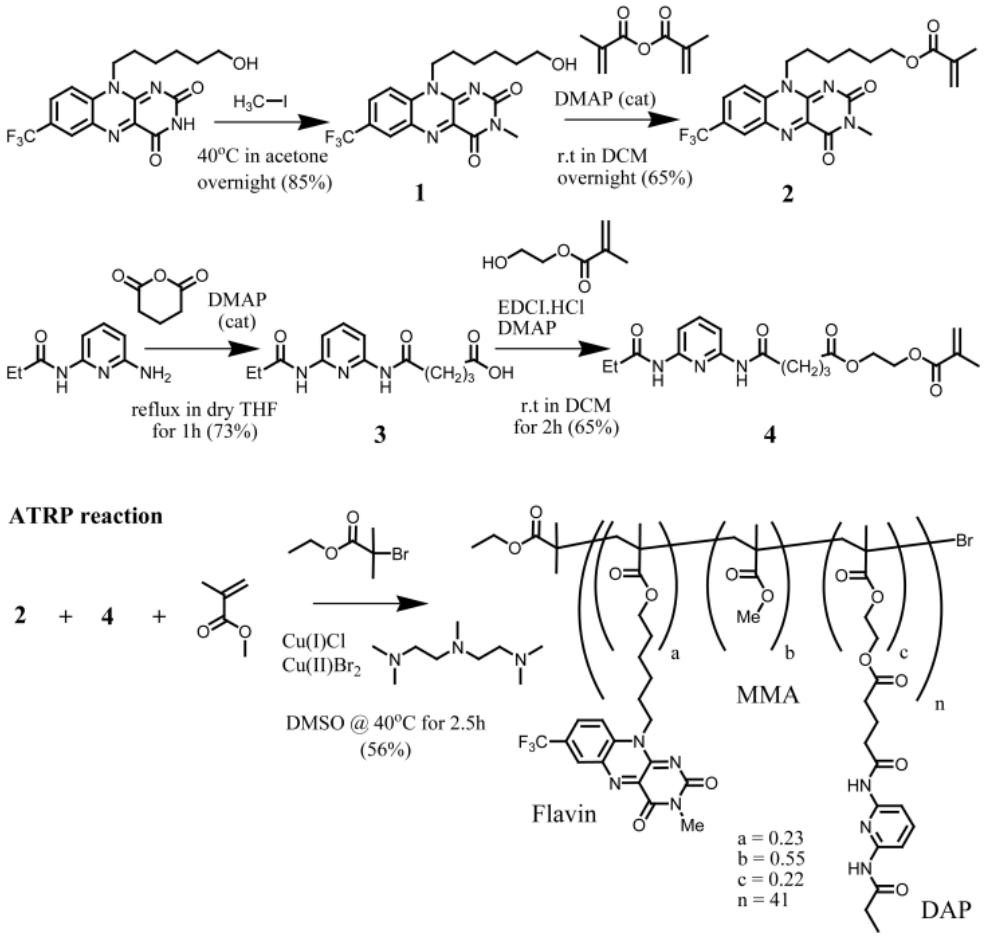

Scheme 0-2 Synthesis of poly(MMA-*co*-DAP-*co*-Fl).

7.3.2 Synthesis of Thymine functionalized ZnSe QDs

ZnSe QDs were synthesized according to previous reports.[15]

Ligand exchange on ZnSe QDs: Thymine functionalized alkanethiol (40mg) and dodecanethiol (60mg) were mixed in 2mL anhydrous DCM. 20mg HDA functionalized ZnSe QDs (precipitated by methanol) were dissolved in this ligand solution followed by adding another 3mL DCM. The reaction mixture was stirred under N_2 gas for 2 days at 40ºC. The ZnSe QDs (Thy-QDs) were purified applying hexane-methanol precipitation procedure and redispersed in DCM for further use. For control experiment, N(3)-methylthymine-functionalized ZnSe QDs were prepared following the same procedure.

7.3.3 Preparation of QDs/polymer nanocomposite

10 μM Thy-QDs solution was added in the poly(MMA-*co*-DAP-*co*-Fl) solutions of different concentration (0.25 mM to 2.0 mM). The volume of both the polymer and QDs were kept same (1 mL) in each mixture. Addition of the poly(MMA-*co*-DAP-*co*-Fl) to Thy-QDs in non-competitive solvents such as dichloromethane (DCM) and chloroform resulted in the slow formation of precipitate. After 8 hours, the precipitate was separated and redispersed for further characterertization.

7.3.4 Preparation of QDs/polymer nanocomposite thin films

A glass substrate was sonicated in isopropyl alcohol for 30 minutes and dried in vacuum for 1 hour to remove residual solvent. A DCM solution of Thy-QDs or QDs/polymer nanocomposite was spin-coated at 500 rpm for 180 seconds onto the substrate. The spin casted films were annealed under vacuum at 100 ºC for 8 hours since the glass transition temperature of the polymer was found 70 ºC via differential scanning calorimetry.

7.3.5 Instrumental characterization

TEM images were acquired on a JEOL 7C operating at 80 keV. Absorption spectra were recorded on HP 8452A diode array spectrophotometer. Photoluminescence was recorded on a Photon Technology International fluorescence spectrometer with Felix 32. Fluorescence lifetimes were measured using an Edinburgh Instruments time-correlated single photon counting (TCSPC) system. The picosecond pulsed diode laser (LDH-P-C-375) was used as 372 nm excitation light source. The detection system consisted of a high speed MicroChannel Plate PhotoMultiplier Tube (MCP-PMT, Hamamatsu R3809U-50) and TCSPC electronics. The repetition rate was 200 kHz. The laser pulse duration was ~110 ps (FWHM). For SAXS, Cu Kα X-rays (1.54 Å) were generated in an Osmic MaxFlux source with a confocal multilayer optic (OSMIC, Inc.). Images were taken with a Molecular Metrology, Inc., camera

consisting of a three pinhole collimation system, 150 cm sample-to-detector distance (calibrated using silver behenate), and a two-dimensional, multiwire proportional detector (Molecular Metrology, Inc.).

7.3.6 Calculation of FRET efficiency

Forster distance and measured FRET distance between QDs and flavin in Thy-QDs / poly(MMA-co-DAP-co-Fl) assemblies FRET efficiency (E) was calculated by

$$E = 1 - \tau_{DA}/\tau_D \qquad [1]$$

Where τ_D and τ_{DA} were the average lifetimes of donor (Thy-QDs) in the absence and presence of the acceptor (poly(MMA-co-DAP-co-Fl)), respectively.

Forster Distance (R_0) was calculated by

$$R_0 = \left(\frac{[9000 \text{ x } (\ln 10)]k_p^2}{128\,\pi^2 n_D^4 N_A} Q_y I \right)^{1/6} \qquad [2]$$

where QY is the quantum yield of the donor; nD is the refractive index of the medium (1.4), N_A is Avogadro's number; k_p^2 is the orientation factor (2/3) and I is the integral of the donor–acceptor spectral overlap over all wavelengths.

Measured FRET distance (r) between QDs and flavin was calculated using the single-donor-multiple acceptor FRET model where E can be expressed as

$$E = \frac{nR_0^6}{nR_0^6 + r^6} \qquad [3]$$

where n is the average number of acceptor molecules interacting with one single donor. R0 is the Forster radius and r is the measured FRET distance.

7.4 Conclusions

We have shown that recognition-mediated self-assembly between ZnSe QDs and a

complementary polymer featuring DAP and flavin moieties is possible in solution and solid states. The assembly process was based upon three point hydrogen bonding between thymine moities attached to the QDs and the DAP moities of the polymer. Due to the spectral overlap and close proximity of the QDs and flavin units in the assembly, FRET was observed from QDs to flavin. The assembly formation and FRET were controlled through the choice of recognition elements, with the FRET efficiency being tuned by controlling QD/polymer ratio in the assembly. Importantly similar properties were extended to solid state as thin films of QDs/polymer nanocomposite also displayed significant FRET. This methodology of to produce self-assembled structures both in solution and solid state, provides a powerful tool for the creation of highly structured multifunctional materials and devices.

7.5 References

1(a) Murray C. B.; Kagan, C. R. *Annu. Rev. Mater. Sci.*, **2000**, *30*, 545-610. (b) Rabani, E.; Reichman, D. R.; Geissler P. L.; Brus, L. E. *Nature*, **2003**, *426*, 271.

2 (a) Kinge, S.; Crego-Calama M.; Reinhoudt, D. N. *ChemPhysChem*, **2008**, *9*, 20. (d) Grzelczak, M.; Vermant, J.; Furst E. M.; Liz-Marzan, L. M. *ACS Nano*, **2010**, *4*, 3591.

3(a) Boal, A. K.; Ilhan, F.; DeRouchey, J. E.; Thurn-Albrecht, T.; Russell, T. P.; Rotello, V. M. *Nature*, **2000**, *404*, 746. (b) Shenhar, R.; Norsten, T. B.; Rotello, V. M. *Adv. Mater.*, **2005,** *17*, 657. (c) Arumugam, P.; Xu, H.; Srivastava, S.; Rotello, V. M. *Polym. Int.*, **2007**, *56*, 461.

4(a) Corbierre, M. K.; Cameron, N. S.; Sutton, M.; Mochrie, S. G. J.; Lurio, L. B.; Ruhm, A.; Lennox, R. B. *J. Am. Chem. Soc.*, **2001**, *123*, 10411. (b) Park, S.; Lim, J. H.; Chung, S. W.; Mirkin, C. A. *Science*, **2004**, *303*, 348. (c) Lin, Y.; Boker, A.; He, J. B.; Sill, K.; Xiang, H. Q.; Abetz, C.; Li, X. F.; Wang, J.; Emrick, T.; Long, S.; Wang, Q.; Balazs, A.; Russell, T. P.; *Nature*, **2005**, *434*, 55. (d) Balazs, A. C.; Emrick, T.; Russell, T. P. *Science*, **2006**, *314*, 1107. (e) Yang, S.; Wang, C.-F.; Chen, S. *J. Am. Chem. Soc.*, **2011**, *133*, 8412.

5 Ofir, Y.; Samanta, B.; Rotello, V. M. *Chem. Soc. Rev.*, **2008**, 37, 1814.

6(a) Sun, B. Q.; Marx, E.; Greenham, N. C. *Nano Lett.*, **2003**, *3*, 961. (b) Dayal, S.; Kopidakis, N.; Olson, D. C.; Ginley, D. S.; Rumbles, G. *J. Am. Chem. Soc.*, **2009**, *131*, 17726. (c) Zorn, M.; Bae, W. K.; Kwak, J.; Lee, H.; Lee, C.; Zentel, R.; Char, K. *ACS Nano*, **2009**, *3*, 1063.

7(a) Sun, S. H.; Anders, S.; Hamann, H. F.; Thiele, J. U.; Baglin, J. E. E.; Thomson, T.; Fullerton, E. E.; Murray, C. B.; Terris, B. D. *J. Am. Chem. Soc.*, **2002**, *124*, 2884. (b) Korth, B. D.; Keng,

P.; Shim, I.; Bowles, S. E.; Tang, C.; Kowalewski, T.; Nebesny, K. W.; Pyun, J. *J. Am. Chem. Soc.*, **2006**, *128*, 6562.

8 Akcora, P.; Liu, H.; Kumar, S. K.; Moll, J.; Li, Y.; Benicewicz, B. C.; Schadler, L. S.; Acehan, D. ; Panagiotopoulos, A. Z.; Pryamitsyn, V.; Ganesan, V.; Ilavsky, J.; Thiyagarajan, P.; Colby, R. H.; Douglas, J. F. *Nat. Mater.*, **2009**, *8*, 354.

9 Shenhar, R.; Rotello, V. M. *Acc. Chem. Res.*, **2003**, *36*, 549.

10 South, C. R.; Burd, C.; Weck, M. *Acc. Chem. Res.*, **2007**, *40*, 63.

11(a) Ilhan, F.; Gray, M.; Rotello, V. M. *Macromolecules*, **2001**, *34*, 2597-2601. (b) Boal, A. K.; Galow, T. H.; Ilhan, F.; Rotello, V. M. *Adv. Funct. Mater.*, **2001**, *11*, 461.

12(a) Frankamp, B. L.; Uzun, O.; Ilhan, F.; Boal, A. K.; Rotello, V. M. *J. Am. Chem. Soc.*, **2002**, *124*, 892. (b) Boal, A. K.; Frankamp, B. L.; Uzun, O.; Tuominen, M. T.; Rotello, V. M. *Chem. Mater.*, **2004**, *16*, 3252. (c) Uzun, O.; Frankamp, B. L.; Sanyal, A.; Rotello, V. M. *Chem. Mater.*, **2006**, *18*, 5404.

13(a) Nandwana, V.; Subramani, C.; Eymur, S.; Yeh, Y.-C.; Tonga, G. Y.; Tonga, M.; Jeong, Y.; Yang, B.; Barnes, M. D.; Cooke, G.; Rotello, V. M. *Int. J. Mol. Sci.*, **2011**, *12*, 6357. (b) Subramani, C.; Dickert, S.; Yeh, Y. C.; Tuominen, M. T.; Rotello, V. M. *Langmuir*, **2011**, *27*, 1543.

14 Beijer, F. H.; Sijbesma, R. P.; Vekemans, J. A. J. M.; Meijer, E. W.; Kooijman, H.; Spek, A. L. *J. Org. Chem.*, **1996**, *61*, 6371.

15 Hines, M. A.; Guyot-Sionnest, P. *J. Phys. Chem. B*, **1998**, *102*, 3655.

16 Lakowicz, J. R. *Principles of Fluorescence Spectroscopy*, 2nd Edn., Kluwer Academic/ Plenum Publishers, New York, 1999, 238–264.

CHAPTER 8

FLAVIN AS A PHOTO-ACTIVE ACCEPTOR FOR EFFICIENT ENERGY AND CHARGE TRANSFER IN A MODEL DONOR-ACCEPTOR SYSTEM

8.1 Introduction

In organic bulk heterojunction photovoltaic (PV) devices, carefully selected donor and acceptor molecules with appropriate optical and electronic properties are keys to effective light absorption, charge separation, and transport in the solar energy conversion process.[1,2] For the initial step of the PV process, broad absorption spectrum overlap with the solar spectrum and high absorption coefficients are desirable for effective solar energy harvesting.[3] It has been shown that the secondary energy harvesting by acceptors due to energy transfer from donor to acceptor can substantially increase the efficiency of the solar cell,[4,5,6] which promotes the need for the further development of photo-active acceptor molecules.

Although a wide variety of donor-incorporating molecules and polymers have been utilized in the construction of organic solar cells, comparatively few acceptor systems have been developed. For example, the fullerene based acceptor [6,6]-phenyl-C61-butyric acid methyl ester (PCBM) has become ubiquitous in contemporary PV devices, however, its inherent drawbacks (e.g. poor light absorption characteristics) are likely to remain a limitation for the development of next generation systems with significantly higher efficiencies.[7] Other acceptor systems have also been investigated including: perylenediimides,[8] vinazenes,[9] quinacridones,[10] 9,9'-bifluorenylidenes,[11] pentacenes,[12] carbon nanotubes,[13] diketopyrrolopyrroles,[14] and quantum dots.[15] However, these systems have generally failed to provide similar efficiencies to PCBM-based PV systems and thus there is a need for new

acceptor systems to be developed that can at least rival the properties and efficiencies of this benchmark acceptor.

Flavins are redox active molecules that serve as enzyme cofactors, performing redox reactions and working as electron shuttles in the metabolic cycle. [16, 17] Furthermore, flavin has a photo-active center that is thought to be the most likely candidate for the photo receptor pigment in the ubiquitous "blue light" photoreceptive processes such as the photoaccumulation of unicellular algae, the photoresponse of fungal sporangiophores and the DNA repair by photolyase.[18] It has been demonstrated that the optical and redox properties of flavin can be easily tuned through simple synthetic modification of substituents attached to this heterocycle. A variety of flavin derivatives with different LUMO energies and band gaps have been synthesized.[19] Despite the relative ease with which precise adjustments can be made to the properties of flavin derivatives, however, it is surprising that the photovoltaic properties have only received limited attention.[20, 21]

To explore the future application of flavins as photo-active acceptors in PV systems, we report the investigation of the photoinduced excitation energy (ET) and charge transfer (CT) properties of an oligothiophene-flavin (OT4-flavin) donor-acceptor (D-A) model system. In particular, we report a solution phase investigation of these transfer processes in compound dyad to assess the feasibility of this D-A pair for future elaboration into PV devices.[22, 23, 24, 25, 26] Photophysical studies showed very high efficiencies of ET and CT from the oligothiophene (OT4) donor to flavin acceptor, which effectively leads to a charge transfer state formed in the dyad. It is believed that the photo-activity of flavin plays a very important role for the effective formation of charge transfer state through combined ET and CT processes.

8.2 Result and Discussion

8.2.1 Synthesis of the thiophene-flavin dyad

The synthesis of the D-A dyad **6** is outlined in Scheme 1. We utilize the *N*3 position of flavin due to the convenient synthetic protocols available to introduce functionality into this position. In this study, flavin bearing a linker molecule with an azide group, compound **5** (*N3*-flavin-azide), was synthesized by reacting 7,8-dimethyl-isobutylflavin **3** with the 1-(2-azidoethoxy)-2-bromoethane **4** in the presence of K_2CO_3 in dry DMF. The donor molecule **2** was obtained by removing the triisopropylsilyl (TIPS) protecting group from compound **1** (see the experimental section for details). Then, compound **2** was easily coupled with compound **5** under Cu(I)-catalyzed azide–alkyne cycloaddition (CuAAc) reaction conditions to afford the dyad **6** (N3-OT4-flavin dyad). The ease of substitution at the *N*3 position of the flavin may provide a general synthetic strategy for a series of D-A dyads using flavin and its derivatives, and can open new avenues for the systematic investigation of ET and CT processes in these systems.

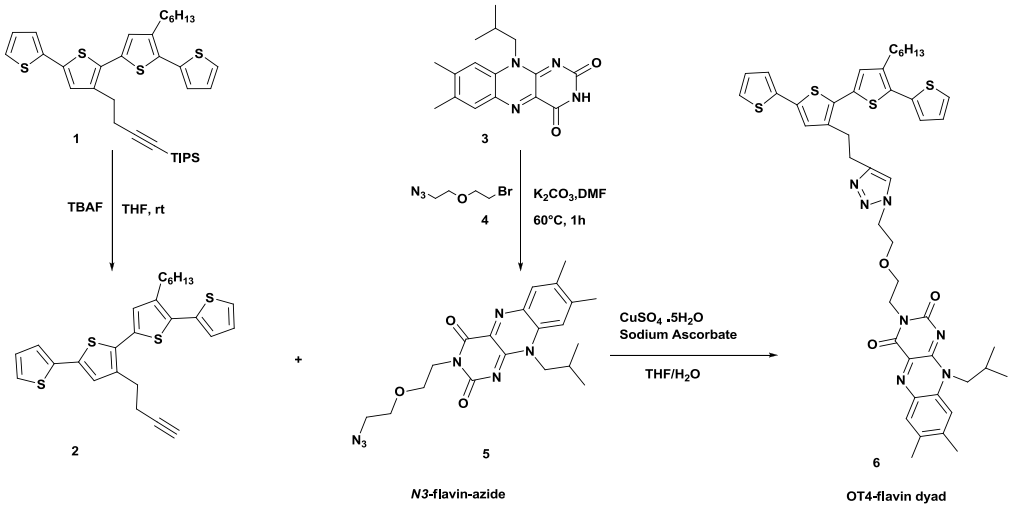

Scheme 0-1 Synthesis of oligothiophene(OT4)-flavin dyad.

8.2. Steady state absorption and fluorescence spectroscopy characterization

We first investigated the steady state absorption of the dyads by UV-Vis spectroscopy. The absorption spectra of OT4-flavin, *N*3-flavin-azide and OT4-TIPS are shown in Figure 8.1. The main absorption peak of flavin is around 450 nm and OT4 is 370 nm. The spectrum of *N*3-OT4-flavin can be considered as a linear combination of *N*3-flavin-azide and OT4-TIPS, which spans the UV and blue-green part of their spectrum. There is no extra peak appearing in the spectrum, which provides evidence for the lack of molecular orbital reorganization between the flavin and OT4 in the ground electronic state.

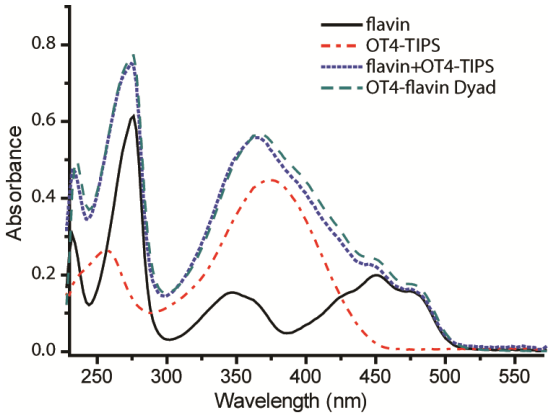

Figure 0.1 UV-Vis spectroscopy of *N*3-OT4-flavin, *N*3-flavin-azide, and OT4-TIPS.

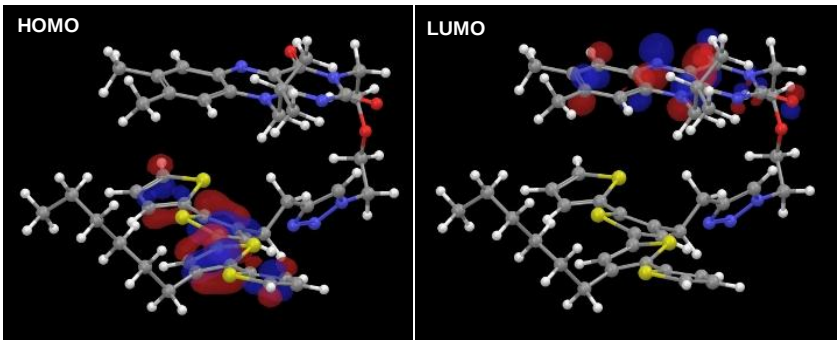

Figure 0.2 Molecular orbitals of the Thiophene-flavin dyad obtained by ab initio calculation. The conformation of the molecule was obtained by molecule conformational search. The distance between flavin and Thiophene is estimated to be around 8 Å.

Molecular dynamic simulation (MD) and quantum mechanical ab initio calculations were used to further examine the electronic communication between flavin and OT4 in the dyad. As shown in Figure 8.2, the conformational search using MD simulation (continuum solvation model in chloroform) revealed a stable conformation where flavin and OT4 adopt a stacked configuration, which is possibly due to π-π stacking interaction between flavin and OT4. Meanwhile, no strong molecular orbital coupling or reorganization between flavin and OT4 was observed, which is consistent with the UV spectroscopy result. This further confirmed that flavin and OT4 molecules in the dyad are discrete and can be treated independently.

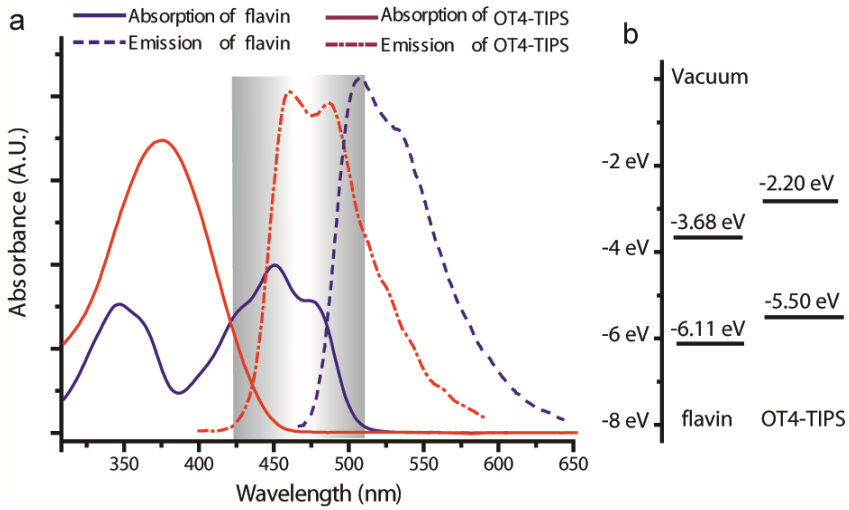

Figure 0.3 a) Absorption and emission spectra of *N*3-flavin-azide and OT4-TIPS. *N*3-flavin-azide and OT4-TIPS were excited at 450nm and 370nm respectively. Note the overlap between the emission of OT4 with the absorption of flavin. b) The energy diagram of HOMO and LUMO of flavin and OT4.

Ab initio calculations also show that the bridge, hydrocarbon and triazole feature large HOMO-LUMO gaps of 8 eV and 6 eV respectively, and do not affect the electronic spectra of D and A in the energy range close to their HOMO and LUMO levels. This excludes a through-bond charge transfer coupling of D and A in the electronic ground state of the dyad.

To explore possible ET or CT between OT4 and flavin in the dyad, we examined the linear absorption and emission spectra of *N*3-flavin-azide and OT4-TIPS (Figure 8.3a). The overlap

between the emission spectrum of OT4 and the absorption spectrum of flavin indicates that Förster resonance energy transfer (FRET) is possible from OT4 to the flavin. A calculation of the Förster distance for this dyad yields an R_0 of 30.1 Å based on the spectroscopy results. This is quite a large value, which implies a possible very efficient energy transfer considering the stacking conformation of the dyad (Figure 8.2). We estimated the HOMO and LUMO energy levels of OT4 and flavin by combing the oxidation potential (HOMO) of OT4-TIPS and reduction potential (LUMO) of *N*3-flavin-azide using cyclic voltammetry and the energy gaps estimated by UV-Vis absorption spectra. As shown schematically in Figure 8.3(b), the HOMO and LUMO of OT4 are offset upward relative to that of flavin respectively. This arrangement makes ET from OT4*$\rightarrow$flavin thermodynamically possible.

The ET and CT process in the dyads were investigated by steady state fluorescence spectroscopy of the dyad. We first examined the emission spectrum using excitation at 385 nm, since at this wavelength OT4 has a strong absorption where the extinction of flavin is at a minimum.

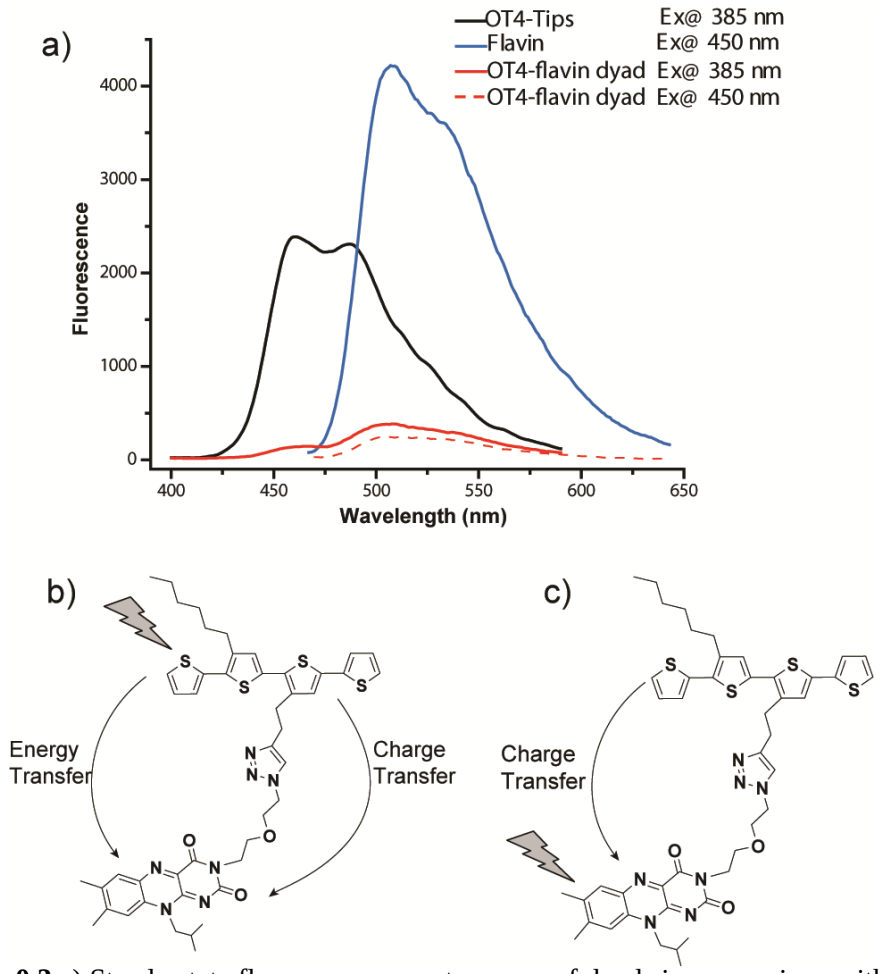

Figure 0.3 a) Steady state fluorescence spectroscopy of dyads in comparison with OT4 and flavin, and the schematic representation of ET and CT processes when OT4 b) or flavin c) are excited.

As shown in Figure 8.4(a), the fluorescence of OT4 in the dyad is quenched strongly, as much as 97%, indicating a very efficient deactivation of its excited state. We believe that both ET and CT processes from OT4 to flavin accounts for the fluorescence quenching of OT4 moiety in the dyad since the spectral overlap and energy level offset of the donor and acceptor (Figure 8.3b) make both processes possible.

Although it is hard to separate the ET and CT processes from OT4* to flavin using steady-state spectroscopy, the ET process can be explored by fluorescence excitation spectroscopy by examining the excitation efficiency of flavin compared to the dyad. We collected the emission at

650 nm corresponding to the emission of flavin only and scanned the excitation wavelength from 330 nm to 530 nm. As shown in Figure 8.5(a), excitation into the OT4 moiety results in lower emission from the flavin, consistent with highly efficient CT compared to ET to the flavin itself. The dyad emission has been multiplied 42x for comparison with the flavin emission.

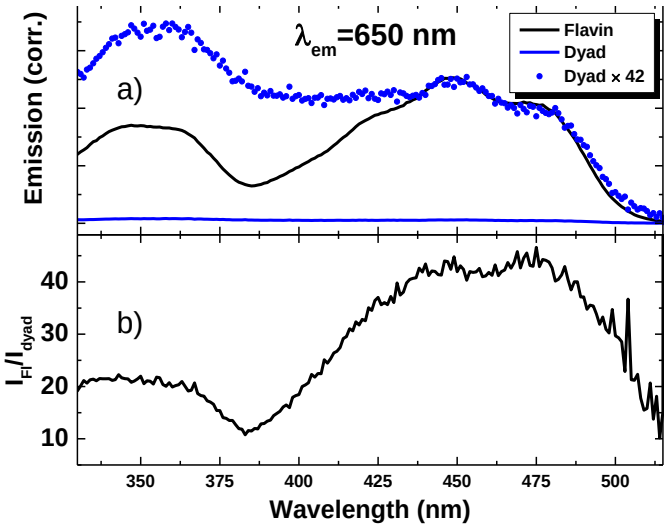

Figure 0.4 a) Fluorescence excitation spectra of *N3*-flavin-azide (black line) and OT4-flavin dyad (blue line) with emission at 650 nm. The quenched dyad emission is multiplied by a factor of 42 for visual presentation (•). b) The ratio I_{Fl}/I_{dyad}.

If OT4* acted as a perfect ET donor, the excitation spectrum would show a much larger emission around 360 nm where the OT4 has its maximal extinction. However, only a small enhancement is seen. The ratio of Fl emission to dyad emission is shown in Figure 8.5(b), quantifying this observation.

As a photo-active acceptor, the flavin chromophore in the dyad can be selectively excited using 450 nm light. We also observed strong quenching of flavin fluorescence (Figure 8.4 a and c). Since the possibility of FRET from flavin to OT4 can be excluded because it is endergonic, we hypothesized that flavin fluorescence quenching in the dyad is due to the CT from OT4 to the flavin. This is an important result since it means that the light absorption in both donor and

acceptor can induce charge transfer in the dyad, which should significantly increase the charge separation efficiency.

8.2.3 Dynamics characterized by time resolved fluorescence spectroscopy

To further investigate and quantitatively measure CT from OT4 to flavin, we performed time-resolved fluorescence measurements. The dyads were excited mainly through the OT4 molecule using a 404 nm pulsed laser. The flavin fluorescence signal at >550 nm was collected using an optical filter (Figure 8.6). The flavin emission showed a decay time of 7.2 ns. In contrast, the excited states of flavin decayed much faster in the dyads. These results support our assumption that the low fluorescence intensity of flavin in the dyad, when OT4 was excited, is due to the deactivation of flavin* rather than the low efficiency of FRET from OT4 to flavin. Identical results were obtained when using 440 nm laser excitation in which flavin is primarily excited. This implies that the behaviour of flavin in both cases is the same and that deactivation of the flavin excited state is due to hole transfer from flavin to OT4.

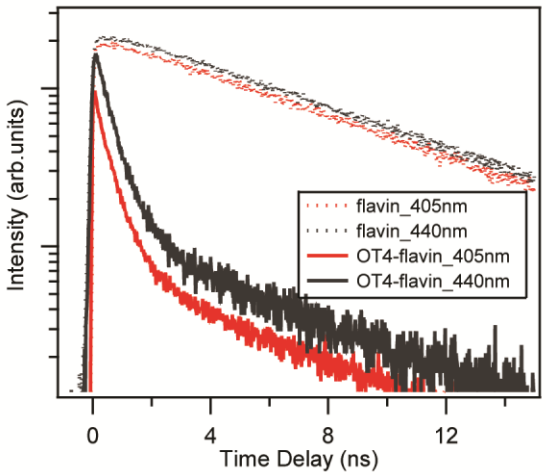

Figure 0.5 Time-resolved fluorescence decay of flavin and OT4-flavin dyad excited at different wavelengths showing essentially identical decay profiles.

Fitting the decay curve of the dyad to a single exponential curve gave a decay time of 478 ps, indicating a very fast deactivation process (here a low amplitude long-lived decay component,

<4%, was ignored). Assuming CT, the charge transfer efficiency (η_{CT}) then can be calculated by the equations[27] :

$$\eta_{CT} = \frac{k_{CT}}{k_{Fl-Thio}} = \frac{k_{Fl-Thio} - k_{Fl}}{k_{Fl-Thio}}$$

$$k_{Fl} = \frac{1}{\tau_{Fl}}$$

$$k_{Fl-Thio} = \frac{1}{\tau_{Fl-Thio}}$$

where *k* is the decay kinetic constant, τ is decay life time and the subscript Fl and Fl-Thio are flavin and OT4-flavin dyads respectively. Using these relations and the values in Figure 8.6, we calculated that the charge transfer rate constants and efficiencies of the OT4-flavin dyad are as large as 1.96×10^9 s^{-1}, or 93.4%, a very efficient charge transfer process in the dyad.

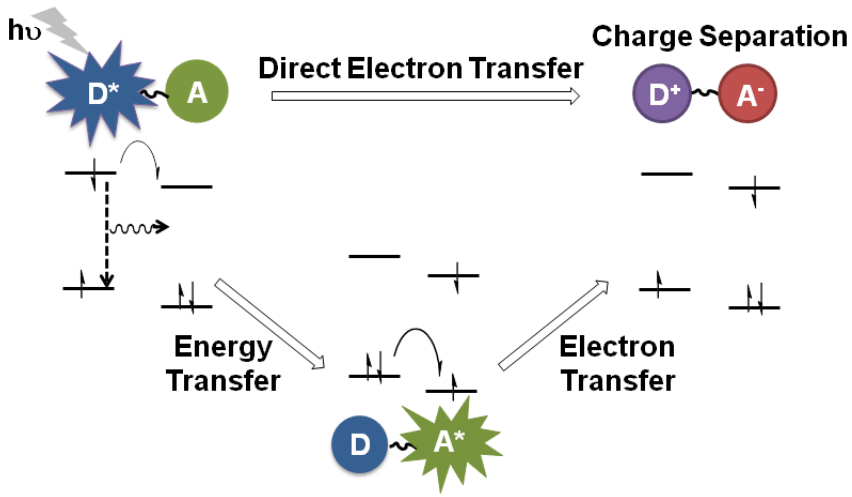

Figure 0.6 Scheme representation of ET and CT processes that can take place in the OT4-flavin D-A dyads upon excitation of the OT4 chromophore.

The above analysis actually suggests a secondary CT process in the dyad following FRET from the OT4 to the flavin. In Figure 8.7, we summarize the possible energy and CT processes in the OT4-flavin dyad. After OT4 was excited, it can undergo both energy transfer and charge transfer.

The latter process leads directly to the charge separation state. Energy transfer, on the other hand, is followed by the excitation of flavin with a secondary CT thereafter, which generates charge separation as well. We believe that both primary and secondary CT are taking place in the dyad and that this is responsible for the highly efficient quenching.

8.2.4 Charge separation state observed by transient spectroscopy

The charge transfer process was confirmed by using broadband subpicosecond transient absorption spectroscopy to identify the ion radicals formed in the dyad molecule after CT. The dyad was pumped using 0.6 μJ pulse of 390 nm and the transient absorption spectrum recorded using a white-light continuum (400 – 710 nm) at pump-probe delays of up to 4 ns. Note that at this excitation wavelength and extinctions, the OT4 has six times the absorption of the flavin.

As shown in Figure 8.8, the absorption peak of the OT4 radical cation, $OT4^{\bullet+}$, can be seen clearly at around 648 nm after only about 2 ps.[28] A global target analysis of the transient absorption data suggests that this fast time constant is due to electron transfer from OT4* to the ground state flavin moiety, producing the anionic flavosemiquinone, which has a modest absorption maximum at 490 nm.[29] This radical pair, $OT4^{\bullet+}$:$Fl_{SQ}^{\bullet-}$ recombines in about 435 ps. A relatively fast FRET process is in competition with the 2 ps ET channel, resulting in Fl_{OX}*. This FRET life time is about 50 ps. The quantum yield for fast electron transfer is $\Phi_{ET1} = k_{CT}/(k_{CT}+k_{FRET}) = 0.96$. The FL_{OX}* species undergoes electron transfer as an acceptor with OT4 as the donor in about 29 ps, again leading to $OT4^{\bullet+}$:$Fl_{SQ}^{\bullet-}$. These results clearly confirm the formation of the charge separation states in our D-A dyad system, which is a critical criterion for the possible practical applications of the D-A pair in the solar cell construction.

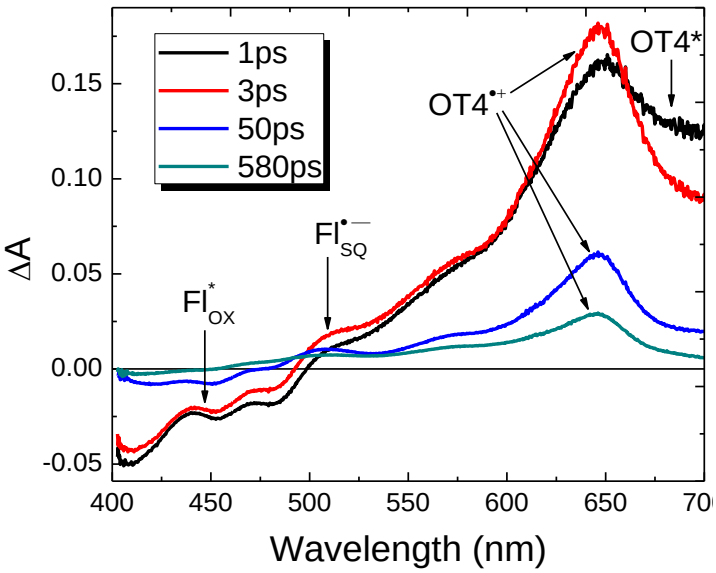

Figure 0.7 Transient absorption spectra of the OT4-*N*3-flavin dyad with excitation at 390 nm. Charge separation takes place in picoseconds.

8.3 Experimental Section

8.3.1 Synthesis of the dyad

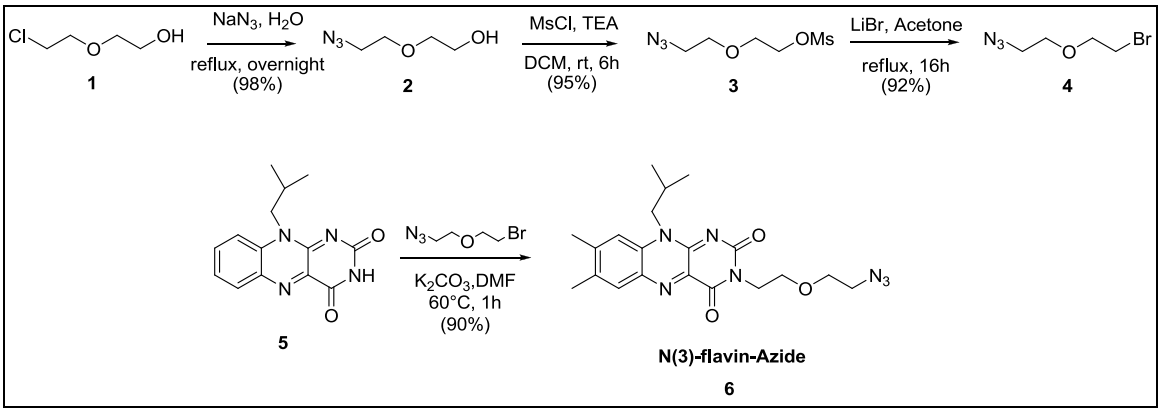

Scheme 0-2 Synthetic scheme for the synthesis of compound **6**

Synthesis of compound **2:** 2-(2-Chloroethoxy)ethanol (**1**) (40 mmol) and sodium azide (20 mmol) in 100 ml H_2O are refluxed overnight. Upon cooling the reaction mixture was extracted with CH_2Cl_2 (3 x 25 ml), the organic layers were combined, washed with brine, anhydrous Na_2SO_4, filtered, and and concentrated under reduced pressure. Yield: 98%.

Synthesis of compound **3:** To a solution of **2** (30 mmol) and Et_3N (60 mmol) in dry CH_2Cl_2 (50 ml) at 0 ^{0}C, MsCl (45 mmol) was added dropwise. Then, reaction was runned at rt for 6h. The reaction mixture was washed with H_2O. Aqueous phase was extracted with CH_2Cl_2 (3 x 25 ml), the organic layers were combined, washed with brine, anhydrous Na_2SO_4, filtered, and concentrated under reduced pressure. Yield: 95%.

Synthesis of compound **4:** Compound **3** (28.5 mmol) and LiBr (84.5 mmol) are refluxed in acetone for 16 h. The reaction mixture was evaporated and washed with H_2O. Aqueous phase was extracted with CH_2Cl_2 (3 x 25 ml), the organic layers were combined, washed with brine, anhydrous Na_2SO_4, filtered, and concentrated under reduced pressure. Yield: 92%. ^{1}H NMR (400 MHz, $CDCl_3$): δ 3.80 (t, J= 6.2 Hz, 2H), 3.68 (t, J= 5.0 Hz), 3.46 (t, J= 6.2 Hz, 2H), 3.39 (t, J=5.0, 2H).

Synthesis of compound **6: N(3)-Flavin-Azide:**

To a solution of 7,8-dimethoxy-N(10)-isobutylisoalloxazine[30] **5** (1 mmol) and K_2CO_3 (4 mmol) in DMF (5 ml) at 60 ^{0}C was added **4** (2 mmol) and the reaction was allowed to proceed overnight. Upon cooling, the reaction was quenched with H_2O and extracted with $CHCl_3$ (3 x 25 ml). The organic layers were combined, washed with brine, anhydrous Na_2SO_4, filtered, and reduced under reverse pressure onto silica gel. The crude product was then purified using flash column chromatography (15:1 CH_2Cl_2/THF) yielding **6.** Yield: 90%. MS(ESI): *m/z* for calcd for $C_{20}H_{25}N_7O_3$ $[M+H]^+$: 412.4679, found 412.0 ^{1}H NMR (400 MHz, $CDCl_3$): δ 8.07 (s, 1H), 7.40 (s, 1H), 4.62 (b, 2H), 4.40 (t, J=5.6 Hz, 2H), 3.89 (t, J=5.7 Hz, 2H), 3.75 (t, J=5.0 Hz, 2H), 3.35 (t, J=4.9 Hz, 2H), 2.56 (s, 3H), 2.48 (m, 1H), 2.46 (s, 3H), 1.06 (d, J=6.7 Hz, 6H).

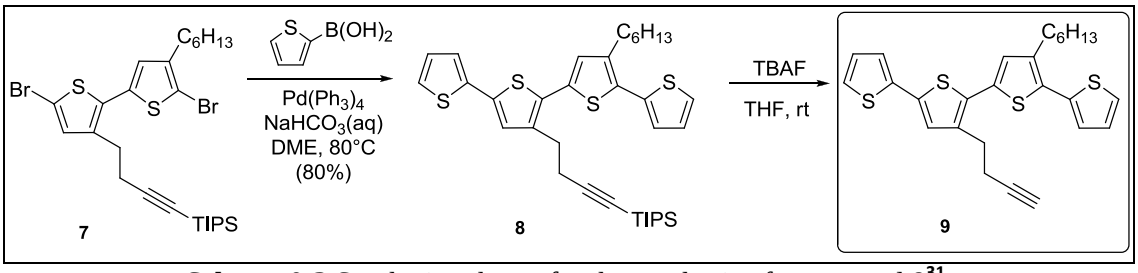

Scheme 0-3 Synthetic scheme for the synthesis of compound **9**[31].

Synthesis of compound **9:** Suzuki coupling of **7**[32] with commercially available 2-thiophene boronic acid gave **8** in 70% yield. Deprotection of trisopropylsilyl group using TBAF gave **9** in 99% yield. Compound **9** was used without further purification to synthesize dyad OT4-flavin.

Synthesis of **Oligothiophene-flavin** dyad (**OT4-flavin**): The dyad OT4-flavin was synthesized through the Cu(I)-catalyzed azide–alkyne cycloaddition (CuAAc) reaction[33] between quarter thiophene (**9)** and N(3)-Flavin-Azide (**6)**. To a round bottom flask, was added $CuSO_4.5H_2O$ (0.185 mmol) and sodium ascorbate (1.0 mmol) followed by the addition of tetrahydrofuran (THF) (15 mL). To this stirred solution, water (5.0 mL) was added followed by the addition of N(3)-Flavin-Azide **(6)** (3.7 mmol) and compound **6** (1.8 mmol). The reaction was stirred for 24 h. The reaction was quenched with water and extracted with ethyl acetate (2x25 mL). The combined organics were washed with water (2x25 mL), brine solution, dried over Na_2SO_4, filtered, and concentrated under reduced pressure. Purification of the residue by silica gel chromatography afforded **OT4-flavin**. Yield: 80%. ^{1}H NMR (400 MHz, $CDCl_3$): δ 7.97 (s, 1H), 7.51 (s, 1H), 7.32 (dd, J=1.1 Hz, J= 3.9 Hz, 1H), 7.27 (s, 1H), 7.23 (dd, J=1.0 Hz, J= 4.0 Hz, 1H), 7.16 (dd, J=1.0 Hz, J= 2.5 Hz, 1H), 7.12 (dd, J=1.1 Hz, J= 2.4 Hz, 1H), 7.09-7.06 (m, 1H), 7.05-7.01 (m, 1H), 6.93 (s, 1H), 6.91 (s, 1H), 4.50 (t, J= 4.8 Hz, 2H), 4.48 (b, 2H), 4.34 (t, J= 5.2 Hz, 2H), 3.82 (t, J= 4.9 Hz, 2H), 3.78 (t, J= 5.2 Hz, 2H), 3.08-2.98 (m, 2H), 2.97-2.87 (m, 2H), 2.73 (t, J= 7.9 Hz, 2H), 2.47 (s, 3H), 2.42-2.34 (m, 1H), 2.33 (s, 3H), 1.74-1.56 (m, 2H), 1.44-1.24 (m, 6H), 0.98 (d, J= 6.7 Hz, 6H), 0.89 (t, J= 6.9 Hz, 3H). MS(ESI): *m/z* for calcd for $C_{46}H_{51}N_7O_3S_4$ $[M+H]^+$: 901.1898, found 900.6130. ^{13}C NMR ($CDCl_3$, ppm): δ 160.1, 155.6, 149.4, 149.3, 146.6, 140.0,

138.6, 138.4, 137.5, 137.1, 137.1, 137.0, 136.9, 136.6, 135.0, 131.2, 129.2, 128.3, 127.2, 127.1, 126.8, 126.7, 126.6, 125.1, 125.6, 124.5, 121.5, 114.9, 69.1, 68.4, 50.3 50.2, 41.0, 34.8, 32.6, 29.3, 29.1, 28.1, 26.9, 25.1 22.7, 20.7, 19.4, 14.6.

8.3.2 Steady state characterization

UV/Vis spectra were taken on a HP 8452A spectrometer and Fluorescence spectra were measured with a PTI QuantaMaster fluorimeter using a 1 cm cuvette. The energy gaps were determined from the onset of the longest wavelength absorption band of flavin and OT4.

The flavin reduction and OT4 redox potentials were determined by cyclic voltammetry on a Cypress System potentiostat with a three-electrode system using a platinum working electrode, a platinum wire as the counter electrode, and a silver wire as a pseudo-reference electrode in dichloromethane solution using tetrabutylammonium perchlorate (TBAP) as the supporting salt. The ferrocene–ferricenium couple was used to calibrate and translate the redox potentials into the HOMO of OT4 and LUMO of flavin relative to vacuum.[34]

8.3.3 Molecular dynamics and ab intio calcuation

The conformational search was performed by MacroModel (Schrodinger, Inc.) using the OPLS_2005 force field and mixed torsional/low-mode sampling method with chloroform as the solvent in continuum solvation model.

The ab initio calculations were performed using Jaguar (Schrodinger, Inc.) with the initial conformation determined by a conformational search. Geometry optimizations and single point energy calculations were carried out using the B3LYP functional and 6-31G* basis set.

8.3.4 Dynamic fluorescence spectroscopy

For the time resolved fluorescence measurements, the samples were excited using 405 nm/ 440nm pulsed diode laser with a repetition rate of 40 MHz and pulse width of 50 ps. The collected flavin fluorescence was filtered through a long-pass optical filter (550nm), detected

with an avalanche photodiode (APD, id Quantique id100-50) for photon counting, and analyzed with a time-correlated single photon counting (TCSPC) system (PicoQuant PicoHarp 300). The laser and detector systems provided a 70 ps time resolution in time-resolved fluorescence measurements.

8.3.5 Transient absorption spectrscopy

The optical layout and laser system used for ultrafast transient absorption spectroscopy has been previously described. The samples had optical densities of 0.4-0.6 in the 2 mm path length of the quartz cuvette, which was thermostatted at 20°C. The pump and probe beams were focused with beam diameters of ~ 250 and ~100 μm respectively, and a relative angle of 3°. The transmission of the sample was probed at the magic angle (54.7 °). The chirp on the white-light continuum (WLC) beam was measured using the Kerr effect where the dyad sample in the cuvette was replaced with a napthelene-toluene solution. The primarily electronic response of the napthalene molecule gave the instrument response function with high fidelity. The chirp of the entire WLC pulse evolved within 1 ps. The data analysis was truncated at early times to avoid coherent artifacts and stimulated Raman scattering by included time points only after the chirp fully developed (> 1ps). The fitted lifetimes were found to be robust for starting time point between 1-4 ps.

8.4 Conclusions

We demonstrate in this study a D-A model system using flavin as a photo-active acceptor. The OT4 donor and flavin are covalently linked by an inert hydrocarbon and triazole linker molecule using click chemistry. Photophysical investigations of the D-A dyad revealed very efficient ET and CT processes between flavin and OT4. Quenching rates of 1.96×10^{9} s^{-1} and efficiencies of 93.4% were estimated using dynamic fluorescence spectroscopy, but transient absorption shows that the initial electron transfer event takes place in about 3 ps. A mechanism including the combined energy and electron transfer processes and secondary hole transfer process is proposed

to explain the effective formation of a charge-separated state, where the photo-activity of the flavin has played an important role. These results suggested that flavin is a promising photo-active acceptor candidate for solar energy conversion and storage. Our strategy has opened an avenue for a series of investigations of the energy and charge transfer properties using various flavin derivatives.

8.5 References

1 Sun, S.-S.; *Mater. Sci. Eng. B*, **2005**, *116*, 251.

2 Kooistra, F. B.; Knol, J.; Kastenberg, F.; Popescu, L. M.; Verhees, W. J. H.; Kroon, J. M.; Hummelen, J. C.; *Org. Lett.*, **2007**, *9*, 551.

3 Shoaee, S.; Clarke, T. M.; Huang, C.; Barlow, S.; Marder, S. R.; Heeney, M.; McCulloch, I.; Durrant, J. R. *J. Am. Chem. Soc.*, **2010**, *132*, 12919.

4 Liu, Y.; Summers, M. A.; Edder, C.; Fréchet, J. M. J.; McGehee, M. D. *Adv. Mater.*, **2005**, *17***,** 2960.

5 Lloyd, M. T.; Lim, Y.-F.; Malliaras, G. G. *Appl. Phys. Lett.*, **2008**, *92*, 143308.

6 Driscoll, K.; Fang, J.; Humphry-Baker, N.; Torres, T.; Huck, W. T. S.; Snaith, H. J.; Friend, R. H. *Nano Lett.*, **2010**, *10***,** 4981.

7 (a) Gunes, S.; Neugebauer, H.; Sariciftci, N. S.; *Chem. Rev.*, **2007**, *107*, 1324.(b) Beaujudge P. M.; Fréchet, J. M. *J. Am. Chem. Soc*., **2011**,*133*, 20009. (c) Anthony, J. E. *Chem. Mater.*, **2011**, *23*, 583.

8 (a) Shin, W. S.; Jeong, H. H.; Kim, M.-K.; Jin, S.-H.; Kim, M. R.; Lee, J. K.; Lee, J. W. J.; Gal, Y.-S. *J. Mater. Chem*., **2006**, *16*, 384. (b) Dittmer, J. J.; Marseglia E. A.; Friend, R. H. *Adv. Mater.*, **2000**,*12*, 1270.

9 Woo, C. H.; Holcombe, T. W.; Unruh, D. A.; Sellinger, A.; Fréchet, J. M. J. *Chem. Mater*., **2010**, *22*, 1673.

10 Zhou,T.; Jia, T.; Kang, B.; Li, F.; Fahlman, M.; Wang, Y. *Adv. Energy Mater.*, **2011**, *1*, 431.

11 Brunetti, F. G,; Gong, X.; Tong, M.; Heeger A. J.; Wudl, F.; *Angew. Chem., Int. Ed*., **2010**, *49*, 532.

12 Lim, Y.-F.; Shu, Y.; Parkin, S. R.; Anthony, J. E.; Malliaras, G. G. *J. Mater. Chem.*, **2009**, *19*, 3049.

13 (a) D'Souza, F.; Ito, O. *Chem. Rev.* **2012**, *41*, 86. (b) Guldi, D. M.; Sgobba, V.; *Chem. Commun.*, **2011**, *47*, 606.

14 Sonar, P.; Ng, G.-M.; Lin, T. T.; Dodabalapur, A.; Chen, Z.-K. *J. Mater. Chem.,* **2010**, 20, 3626.

15 (a) Liu, J.; Tanaka, T.; Sivula, K.; Alivisatos, A. P.; Fréchet, J. M. J. *J. Am. Chem. Soc.*, **2004,** *126*, 6550. (b) Zhou, Y.; Li, Y.; Zhong, H.; Hou, J.; Ding, Y.; Yang, C.; Li, Y. *Nanotechnology,* **2006**, *17*, 4041. (c) Sun, B.; Marx, E.; Greenham, N. C. *Nano Lett.,* **2003**, *3*, 961. (d) Dayal, S.; Kopidakis, N.; Olson, D. C.; Ginley, D. S.; Rumbles, G. *Nano Lett.,* **2009**, *10*, 239.

16 Hemmerich, P.; Veeger, C.; Wood, H. C. S. *Angew. Chem. Int. Ed.*, **1965**, *4*, 671.

17 Muller, F.; Chemistry and Biochemistry of Flavoenzymes, CRC Press, Boca Raton, Volume I., 1991.

18 Heelis, P. F. *Chem. Soc. Rev.*, **1982**, *11*, 15.

19 Legrand, Y.-M.; Gray, M.; Cooke, G.; Rotello, V. M. *J. Am. Chem. Soc.*, **2003,** *125*, 15789.

20 Hermann, D. T.; Schindler, A. C.; Polborn, K.; Gompper, R.; Stark, S.; Parusel, A. B. J.; Grabner, G. ; Köhler, G. *Chem. Eur. J.*, **1999,** *5*, 3208.

21 Murakami, M.; Ohkubo, K.; Fukuzumi, S. *Chem. Eur. J.*, **2010**, *16*, 7820.

22 Pullerits, T.; Sundström, V. *Acc. Chem. Res.*, **1996**, *29*, 381.

23 Clarke, T. M.; Durrant, J. R. *Chem. Rev.*, **2010**, *110*, 6736.

24 Deibel, C.; Strobel, T.; Dyakonov, V. *Adv. Mater.*, **2010**, *22*, 4097.

25 Organic Photovoltaics: Materials, Device Physics, and Manufacturing Technologies, edited by Christoph Brabec, Vladimir Dyakonov and Ullrich Scherf, Wiley-VCH Verlag GmbH, 2008.

26 Mayer, A.; Scully, S.; Hardin, B.; Rowell, M.; Mcgehee, M. *Mater.Today,* **2007,** *10*, 28.

27 Justin Thomas, K. R.; Thompson, A. L.; Sivakumar, A. V.; Bardeen, C. J.; Thayumanavan, S.; *J. Am. Chem. Soc.*, 2005, **127**, 373.

28 Emmia, S. S.; Angelantonioa, M. D.; Beggiatoa, G.; Poggic, G.; Geria, A.; Pietropaolob, D.; Zottid, G. *Radiat. Phys. Chem.,* **1999**, *53*, 263.

29 Niemz, A.; Imbriglio, J.; Rotello, V. M. *J. Am. Chem. Soc.*, **1997**, *119*, 887.

30 Legrand, Y-M.; Gray, M.; Cooke, G.; Rotello, V. M. *J. Am. Chem. Soc.* **2003**, *125*, 15789–15795

31 Bheemaraju, A.; Pourmand, M.; Yang, B.; Surampudi, S. K.; Benanti, T. L.; Achermann, M.; Barnes, M. D.; Venkataraman, D. *J. Macromol. Sci. A* **2011**, *48*, 986–993

32 Benanti, T. L.; Kalaydjian, A.; Venkataraman, D. *Macromolecules* **2008**, *41*, 8312–8315.

33 Kolb, H. C.; Finn, M. G.; M. G. Sharpless, M. G. *Angew. Chem. Int. Ed*. **2001**, *40*, 2004–2021

34 Cardona, C. M.; Li, W.; Kaifer, A. E.; Stockdale, D.; Bazan, G. C. *Adv. Mater.*, **2011**, *23*, 2367.

BIBLIOGRAPHY

Abdallah, D. J.; Weiss, R. G. *Adv. Mater.* **2000**, *12*, 1237.

Andrew, N. S.; Eugenii, K.; Itamar, W. *Chemphyschem* **2000**, *1*, 18.

Anthony, J. E. *Chem. Mater.*, **2011**, *23*, 583.

Arango, A.C.; Oertel, D.C.; Xu, Y.; Bawendi, M.G.; Bulović, V. *Nano Lett.* **2009**, *9*, 860.

Arumugam, P.; Patra, D.; Samanta, B.; Agasti, S. S.; Subramani, C.; Rotello, V. M. *J. Am. Chem. Soc.* **2008**, *130*, 10046-10047.

Arumugam, P.; Xu, H.; Srivastava, S.; Rotello, V. M. *Polym. Int.* **2007**, *56*, 461–466.

Badia, A.; Cuccia, L.; Demers, L.; Morin, F.; Lennox, R.B. *J. Am. Chem. Soc.* **1997**, *119*, 2682.

Beaujudge, P. M.; Fréchet, J. M. *J. Am. Chem. Soc*., **2011**,*133*, 20009.

Beloborodov, I.; Lopatin, A.; Vinokur, V.; Efetov, K. *Rev. Mod. Phys.* **2007**, *79*, 469–518.

Benanti, T. L.; Kalaydjian, A.; Venkataraman, D. *Macromolecules* **2008**, *41*, 8312–8315.

Bera, D.; Qian, L.; Tseng, T.-K.; Holloway, P. H. *Materials* **2010**, *3*, 2260–2345.

Bergbreiter, D. E.; Chance, B. S. *Macromolecules* **2007**, *40*, 5337.

Bergbreiter, D. E.; Sprinivas, B.; Xu, G.-f.; Aguilar, G. ; Ponder, B. C.; Gray, H. N.; Bandella, A. in *Symposium on Polymer Surfaces and Interfaces: Characterization, Modification and Application* (Eds.: K. L. Mittal, K.-W. Lee), Utrecht, Netherlands, Boston, MA, **1997**, pp. 3.

Berthold, K.; Hopfel, R.A.; Gornik, E. *Appl. Phys. Lett.* **1985**, *46*, 626.

Bheemaraju, A.; Pourmand, M.; Yang, B.; Surampudi, S. K.; Benanti, T. L.; Achermann, M.; Barnes, M. D.; Venkataraman, D. *J. Macromol. Sci. A* **2011**, *48*, 986–993

Bigioni, T. P.; Lin, X.-M.; Nguyen, T. T.; Corwin, E. I.; Witten, T. a; Jaeger, H. M. *Nat. Mater.* **2006**, *5*, 265–70.

Binder, W. H.; Kluger, C.; Straif, C. J.; Friedbacher, G. *Macromolecules* **2005**, *38*, 9405.

Binder, W. H.; Petraru, L.; Roth, T.; Groh, P. W.; Pálfi, V. S.; Ivan, K. B. *Adv. Funct. Mater.* **2007**, *17*, 1317.

Binks, B. *Curr. Opin. Colloid Interface Sci.* **2002**, *7*, 21–41.

Binks, B. P. *Phys. Chem. Chem. Phys.* **2007**, *9*, 6298-6299.

Binks, B. P.; Clint, J. H.; Fletcher, P. D. I.; Lees, T. J. G.; Taylor, P. *Langmuir* **2006**, *22*, 4100-4103.

Binks, B. P.; Horozov, T. S. In *Colloidal Particles at Liquid Interfaces*; Cambridge University Press, **2006**.

Binks, B. P.; Lumsdon, S. O. *Langmuir* **2000**, *16*, 8622-8631.

Bishop, K. J. M.; Wilmer, C. E.; Soh, S.; Grzybowski, B. a *Small* **2009**, *5*, 1600–30.

Boal, A. K.; Ilhan, F.; DeRouchey, J. E.; Thurn-Albrecht, T.; Russell, T. P.; Rotello, V. M. *Nature* **2000**, *404*, 746.

Böker, A.; He, J.; Emrick, T.; Russell, T. P. *Soft Matter* **2007**, *3*, 1231.

Böker, A.; Lin, Y.; Chiapperini, K.; Horowitz, R.; Thompson, M.; Carreon, V.; Xu, T.; Abetz, C.; Skaff, H.; Dinsmore, a D.; Emrick, T.; Russell, T. P. *Nat. Mater.* **2004**, *3*, 302–6.

Bourlinos, A. B.; Herrera, R.; Chalkias, N.; Jiang, D.D.; Zhang, Q.; Archer, L.A.; Giannelis, E. P. *Adv. Mater.* **2005**, *17*, 234;

Bourlinos, A.B.; Ray Chowdhury, S.; Herrera, R.; Jiang, D. D.; Zhang, Q.; Archer, L.A.; Giannelis, E. P. *Adv. Funct. Mater.* **2005**, *15*, 1285;

Brabec, Christoph; Organic Photovoltaics: Materials, Device Physics, and Manufacturing Technologies, Vladimir Dyakonov and Ullrich Scherf, Wiley-VCH Verlag GmbH, 2008.

Braybrook, J. H.; Hall, L. D. *Prog. Polym. Sci.* **1990**, *15*, 715.

Bresme, F.; Oettel, M. *J. Phys. Condens. Mat.* **2007**, *19*, 413101.

Brunetti, F. G,; Gong, X.; Tong, M.; Heeger A. J.; Wudl, F.; *Angew. Chem., Int. Ed.*, **2010**, *49*, 532.

Brunsveld, L.; Folmer, B. J. B.; Meijer, E. W.; Sijbesma, R. P.; *Chem. Rev.* **2001**, *101*, 4071.

Brust, M. D.; Schiffrin, J.; Whyman, R.; *J. Chem. Soc., Chem. Commun.* **1994**, 801.

Brust, M.; Fink, J.; Bethell, D.; Schiffrin, D. J.; Kiely, C. *J. Chem. Soc. Chem. Commun* **1995**, 1655.

Brust, M.; Walker, M.; Bethell, D.; Schiffrin, D. J.; Whyman, R. *J. Chem. Soc., Chem. Commun.* **1994**, 801.

Butt, H.-J.; Graf, K.; Kappl, M. *Physics and Chemistry of Interfaces*, 2nd ed.; Wiley-VCH, **2006**.

Cao, H.; Yu, Z. N.; Wang, J.; Tegenfeldt, J. O.; Austin, R. H.; Chen, E.; Wu, W.; Chou, S. Y. *Appl. Phys. Lett.* **2002**, *81*, 174;

Cardenas-valera, A. E.; Bailey, A. I. *Colloids Surf., A* **1995**, *97*, 1-12.

Cardona, C. M.; Li, W.; Kaifer, A. E.; Stockdale, D.; Bazan, G. C. *Adv. Mater.*, **2011**, *23*, 2367.

Caruso, F.; Caruso, R. A.; Möhwald, H. *Science* **1998**, *282*, 1111–1114.

Cedeno, C. C.; Seekamp, J.; Kam, A. P.; Hoffmann, T.; Zankovych, S.; Torres, C. M. S.; Menozzi, C.; Cavallini, M.; Murgia, M.; Ruani, G.; Biscarini, F.; Behl, M.; Zentel, R.; Ahopelto, J. *Microelectron. Eng.* **2002**, *61*, 25.

Chen, H.; Yuan, L.; Song, W.; Wu, Z.; Li, D. *Prog. Polym. Sci.* **2008**, *33*, 1059.

Cheng, J. Y.; Ross, C. A.; Smith, H. I.; Thomas, E. L. *Adv. Mater.* **2006**, *18*, 2505.

Cheng, X.; Hong, Y. T.; Kanicki, J.; Guo, L. J. *J. Vac. Sci. Technol. B* **2002**, *20*, 2877;

Choi, C. L.; Alivisatos, a P. *Ann. Rev. Phys. Chem.* **2010**, *61*, 369–89.

Choi, J. J.; Luria, J.; Hyun, B.-R.; Bartnik, A. C.; Sun, L.; Lim, Y.-F.; Marohn, J. a; Wise, F. W.; Hanrath, T. *Nano Lett.* **2010**, *10*, 1805–11.

Chou, S. Y. *Proc. IEEE* **1997**, *85*, 652;

Chou, S. Y.; Krauss, P. R.; Renstrom, P. J. *Science* **1996**, *272*, 85.

Chowdhury, D.; Maoz, R.; Sagiv, J. *Nano Lett.* **2007**, *7*, 1770;

Clarke, T. M.; Durrant, J. R. *Chem. Rev.*, **2010**, *110*, 6736.

Creran, B.; Yan, B.; Moyano, D. F.; Gilbert, M. M.; Vachet, R. W.; Rotello, V. M. *Chem. Commun.* **2012**, *48*, 4543.

Crespilho, F.; Zucolotto, V.; Jr, O. O.; Nart, F. *Int. J. Electrochem. Sci* **2006**, *1*, 194–214.

Crespo-Biel, O.; Ravoo, B. J.; Reinhoudt, D. N.; Huskens, J. *J. Mater. Chem.* **2006**, *16*, 3997.

Crossley, S.; Faria, J.; Shen, M.; Resasco, D. E. *Science* **2010**, *327*, 68-72.

Csucs, D.; Falconnet, G.; Grandin, H. M.; Textor, M.; *Biomaterials* **2006**, *27*, 3044.

D'Souza, F.; Ito, O. *Chem. Rev.* **2012**, *41*, 86.

Daniel, M. C.; Astruc, D. *Chem. Rev.* **2004**, *104*, 293–346.

Dayal, S.; Kopidakis, N.; Olson, D. C.; Ginley, D. S.; Rumbles, G. *Nano Lett.*, **2009**, *10*, 239.

De, M.; Ghosh, P. S.; Rotello, V. M. *Adv. Mater.* **2008**, *20*, 4225–4241.

De, M.; Miranda, O. R.; Rana, S.; Rotello, V. M. *Chem. Comm.* **2009**, 2157-2159.

De, M.; You, C.-C.; Srivastava, S.; Rotello, V. M. *J. Am. Chem. Soc.* **2007**, *129*, 10747-10753.

Dealy, J.M.; Larson, R.G. Structure and Rheology Of Molten Polymers - From Structure To Flow Behavior and Back Again, Hanser Publishers **2006**

Decher, G. *Science* **1997**, *277*, 1232–1237.

Deibel, C.; Strobel, T.; Dyakonov, V. *Adv. Mater.*, **2010**, *22*, 4097.

Deng, J.; Wang, L.; Liu, L.; Yang, W. *Prog. Polym. Sci.* **2009**, *34*, 156.

Dickinson, E. *Curr. Opin. Colloid Interface Sci.* **2010**, *15*, 40-49.

Dinsmore, A. D. *Nat. Mater.* **2007**, *6*, 921–2.

Dinsmore, A. D.; Hsu, M. F.; Nikolaides, M. G.; Marquez, M.; Bausch, A. R.; Weitz, D. A. *Science* **2002**, *298*, 1006-1009.

Dittmer, J. J.; Marseglia E. A.; Friend, R. H. *Adv. Mater.*, **2000**,*12*, 1270.

Driscoll, K.; Fang, J.; Humphry-Baker, N.; Torres, T.; Huck, W. T. S.; Snaith, H. J.; Friend, R. H. *Nano Lett.*, **2010**, *10***,** 4981.

Driscoll, K.; Fang, J.; Humphry-Baker, N.; Torres, T.; Huck, W. T. S.; Snaith, H. J.; Friend, R. H. *Nano Lett.*, **2010**, *10***,** 4981.

Du, K.; Glogowski, E.; Emrick, T.; Russell, T. P.; Dinsmore, A. D. *Langmuir* **2010**, *26*, 12518-12522.

Duan, H. W.; Wang, D. Y.; Sobal, N. S.; Giersig, M.; Kurth, D. G.; Mohwald, H. *Nano Lett.* **2005**, *5*, 949-952.

Duan, H. W; Wang, D.; Kurth, D. G.; Möhwald, H. *Angew. Chem. Int. Ed.* **2004**, *43*, 5639–42.

E. Foster, G. Kearns, S. Goto, J. E. Hutchison, *Adv. Mater.* **2005**, *17*, 1542;

Eigler, D. M.; Schweizer, E. K.; *Nature* **1990**, *344*, 524;

Emmia, S. S.; Angelantonioa, M. D.; Beggiatoa, G.; Poggic, G.; Geria, A.; Pietropaolob, D.; Zottid, G. *Radiat. Phys. Chem.*, **1999**, *53*, 263.

Erb, R. M.; Son, H. S.; Samanta, B.; Rotello, V. M.; Yellen, B. B. *Nature* **2009**, *457*, 999–1002.

Estroff, L. A.; Hamilton, A. D. *Chem. Rev.* **2004**, *104*, 1201.

Eurenius, L. ; Haggland, C.; Olsson, E.; Kasemo, B.; Chakarov, D. *Nat. Photon.* **2008**, *2*, 360;

Falconnet, D. ; Pasqui, D.; Park, S. ; Eckert, R.; Schift, H. ; Gobrecht, J.; Barbucci, R. ; Textor, M. ; *Nano Lett.* **2004**, *4*, 1909.

Fogleman, E. A.; Yount, W. C.; Xu, J.; Craig, S. L. *Angew. Chem. Int. Ed.* **2002**, *41*, 4026.

Frederick, M. T.; Amin, V. A.; Cass, L. C.; Weiss, E. A. *Nano lett.* **2011**, *11*, 5455–60.

Friedman, P. W. A. R. S. *Molecular Quantum Mechanics*; 5th ed.; Oxford University Press: Oxford, 2011; p. 592.

Fujii, S.; Aichi, A.; Muraoka, M.; Kishimoto, N.; Iwahori, K.; Nakamura, Y.; Yamashita, I. *J. Colloid Interface Sci.* **2009,** *338*, 222-228.

Fyfe, M. C. T.; Stoddart, J. F. *Acc. Chem. Res.* **1997**, *30*, 393.

Gao, T.; Rosen, M. J. *J. Colloid Interface Sci*. **1995**, *172*, 242-248.

Garbassi, F.; Morra, M.; Occhiello, E. *Polymer Surfaces from Physics to Technology*, Wiley, Chichester, England **1994**.

Ghose, A. K.; Crippen, G. M. *J. Comput. Chem.* **1986**, *7*, 565-577.

Ghosh, A.; Basak, S.; Wunsch, B. H.; Kumar, R.; Stellacci, F. *Angew. Chem. Int. Ed.* **2011**, *50*, 7900–5.

Glinsner, T.; Hangweier, P.; Luesebrink, H.; Dorsey, P.; Homola, A.; Wachenschwanz, D. *Solid State Technol.* **2005**, *48*, 51;

Goddard, J. M.; Hotchkiss, J. H. *Prog. Polym. Sci.* **2007**, *32*, 698.

Granot, E.; Patolsky, F.; Willner, I. *J. Phys. Chem. B* **2004**, *108*, 5875–5881.

Greenwood, O. D.; Boyd, R. D.; Hopkins, J.; Badyal, J. P. S. in *International Symposium on Polymer Surface Modification: Relevance to Adhesion* (Ed.: K. L. Mittal), Utrecht, Netherlands : VSP, 1996, Las Vegas, Nevada, **1993**, pp. 17.

Grzelczak, M.; Vermant, J.; Furst, E. M.; Liz-Marzán, L. M. *ACS nano* **2010**, *4*, 3591–605.

Guldi, D. M.; Sgobba, V.; *Chem. Commun.*, **2011**, *47*, 606.

Gunes, S.; Neugebauer, H.; Sariciftci, N. S.; *Chem. Rev.*, **2007**, *107*, 1324.

Guo, L. J. *Adv. Mater.* **2007**, *19*, 495.

Guo, L. J.; Cheng, X. ; Chou, C. F.; *Nano Lett.* **2004**, *4*, 69

Guo, L. J.; Cheng, X.; Chao, C. Y. *J. Mod. Opt.* **2002**, *49*, 663

H.Nakanishi, K.J.M. Bishop, B.Kowalczyk, A.Nitzan, E.A. Weiss, K.V. Tretiakov, M.M . Apodaca, R. Klajn, J.F. Stoddart, B.A. Grzybowski, *Nature* **2009**, *460*, 371.

Halas, N.; Lal, S.; Chang, W.; Link, S.; Nordlander, P. *Chem. Rev.* **2011**, *111*, 3913–3961.

Hammond, P. T. *Materials Today* **2012**, *15*, 196.

Hanrath, T. *J. Vac. Sic. Technol. A* **2012**, *30*, 030802.

He, J.; Niu, Z.; Tangirala, R.; Wan, J.-Y.; Wei, X.; Kaur, G.; Wang, Q.; Jutz, G.; Boeker, A.; Lee, B.; Pingali, S. V.; Thiyagarajan, P.; Emrick, T.; Russell, T. P. *Langmuir* **2009,** *25*, 4979-4987.

Heelis, P. F. *Chem. Soc. Rev.*, **1982**, *11*, 15.

Hemmerich, P.; Veeger, C.; Wood, H. C. S. *Angew. Chem. Int. Ed.*, **1965**, *4*, 671.

Hermann, D. T.; Schindler, A. C.; Polborn, K.; Gompper, R.; Stark, S.; Parusel, A. B. J.; Grabner, G. ; Köhler, G. *Chem. Eur. J.*, **1999,** *5*, 3208.

Hermanson, K. D.; Huemmerich, D.; Scheibel, T.; Bausch, A. R. *Adv. Mater.* **2007,** *19*, 1810-1815.

Hermanson, K. D.; Lumsdon, S. O.; Williams, J. P.; Kaler, E. W.; Velev, O. D. *Science* **2001**, *294*, 1082–6.

Hervés, P.; Pérez-Lorenzo, M.; Liz-Marzán, L. M.; Dzubiella, J.; Lu, Y.; Ballauff, M. *Chem. Soc. Rev.* **2012**, *41*, 5577–87.

Herzig, E. M.; White, K. A.; Schofield, A. B.; Poon, W. C. K.; Clegg, P. S. *Nat. Mater.* **2007**, *6*, 966–71.

Hirst, R.; Smith, D. K.; Feiters, M. C.; Geurts, H. P. M.; Wright, A. C. *J. Am. Chem. Soc.* **2003**, *125*, 9010.

Hof, F.; Craig, S. L.; Nuckolls, C.; Julius Rebek, J. *Angew. Chem. Int. Ed.* **2002**, *41*, 1488.

Hoff, J. D.; Cheng, L. J.; Meyhofer, E.; Guo, L. J.; Hunt, A. J. *Nano Lett.* **2004**, *4*, 853;

Hu, M.-S.; Chen, H.-L.; Shen, C.-H.; Hong, L.-S.; Huang, B.-R.; Chen, K.-H.; Chen, L.-C.; *Nat. Mater.* **2006**, *5*, 102;

Hua, X. Y.; Rosen, M. J. *J. Colloid Interface Sci.* **1988**, *124*, 652-659.

Huang, C.; Dong, B.; Lu, N.; Yang, B.; Gao, L.; Tian, L.; Qi, D.; Wu, Q.; Chi, L. *Small* **2009**, *5*, 583.

Huskens, J.; Deij, M. a; Reinhoudt, D. N. *Angew. Chem. Int. Ed.* **2002**, *41*, 4467–71.

Ilhan, F.; Galow, T. H.; Gray, M.; Clavier, G.; Rotello, V. M. *J. Am. Chem. Soc.* **2000**, *122*, 5895.

Ilhan, F.; Gray, M.; Blanchette, K.; Rotello, V. M. *Macromolecules* **1999**, *32*, 6159.

Imada, M.; Fujimori, A.; Tokura, Y. *Rev. Mod. Phys.* **1998**, *70*, 1039–1263.

Indira, T.; Lakshmi, P. *Int. J. Phar. Sci. Nanotech.* **2010**, *3*, 1035.

Jeon, N. L.; Finnie, K.; Branshaw, K.; Nuzzo, R. G. *Langmuir* **1997**, *13*, 3382.

Jin, Y.; Friedman, N. *J. Am. Chem. Soc.* **2005**, *127*, 11902;

Jones, R. B.; Gordus, A.; Krall, J. A.; MacBeath, G. *Nature* **2006**, *439*, 168.

Jong, W. H. De; Borm, P. J. A. *Inter. J. Nanomed.* **2008**, *3*, 133–49.

Justin Thomas, K. R.; Thompson, A. L.; Sivakumar, A. V.; Bardeen, C. J.; Thayumanavan, S.; *J. Am. Chem. Soc.*, 2005, **127**, 373.

Kalsin, A. M.; Fialkowski, M.; Paszewski, M.; Smoukov, S. K.; Bishop, K. J. M.; Grzybowski, B. *Science* **2006**, *312*, 420–4.

Kane, J.; Ong, J.; Saraf, R. F. *J. Mater. Chem.* **2011**, *21*, 16846.

Kao, P. C.; Chu, S. Y.; Chen, T. Y.; Zhan, C. Y.; Hong, F. C.; Chang, C. Y.; Hsu, L. C.; Liao, W. C.; Hon, M. H. *IEEE Trans. Electron Devices* **2005**, *52*, 1722.

Kaur, G.; He, J.; Xu, J.; Pingali, S. V.; Jutz, G.; Boeker, A.; Niu, Z.; Li, T.; Rawlinson, D.; Emrick, T.; Lee, B.; Thiyagarajan, P.; Russell, T. P.; Wang, Q. *Langmuir* **2009,** *25*, 5168-5176.

Kempen, H. van; Dubois, J. G. A.; Gerritsen, J. W.; Schmid, G. *Phys. B* **1995**, *204*, 51–56.

Kim, J.-W.; Lee, D.; Shum, H. C.; Weitz, D. A. *Adv. Mater.* **2008**, *20*, 3239-3243.

Kim, W.J.; Kim, S. J.; Lee, K-S.; Samoc, M.; Cartwright, A. N.; Prasad, P. N.; *Nano Lett.* **2008**, *8*, 3262;

Kinge, S.; Crego-Calama, M.; Reinhoudt, D. N.; *Chemphyschem* **2008**, *9*, 20.

Kittel, Charles; *Introduction to Solid State Physics*; 8th ed.; John Wiley & Sons: Weinheim, 2004; p. 704.

Klajn, R.; Bishop, K.J.M.; Fialkowski, M.; Paszewski, M.; Campbell, C.J.; Gray, T.P.; Grzybowski, B.A. *Science* **2007**, *316*, 261.

Ko, S.H.; Park, I.; Pan, H.; Grigoropoulos, C.P.; Pisano, A.P.; Luscombe, C.K.; Frechet, J. M. J. *Nano Lett.* **2007**, *7*, 1869.

Kolb, H. C.; Finn, M. G.; M. G. Sharpless, M. G. *Angew. Chem. Int. Ed*. **2001**, *40*, 2004–2021

Kooistra, F. B.; Knol, J.; Kastenberg, F.; Popescu, L. M.; Verhees, W. J. H.; Kroon, J. M.; Hummelen, J. C.; *Org. Lett.*, **2007**, *9*, 551.

Kotov, N. A.; Dekany, I.; Fendler, J. H. *J. Phys. Chem.* **1995**, *99*, 13065–13069.

Kumar,A. M. S.; Sivakova, S.; Fox, J. D.; Green, J. E.; Marchant, R. E.; Rowan, S. J. *J. Am. Chem. Soc.* **2008**, *130*, 1466.

Kushner, A. M.; Gabuchian, V.; Johnson, E. G.; Guan, Z. *J. Am. Chem. Soc.* **2007**, *129*, 14110.

Kutuzov, S.; He, J.; Tangirala, R.; Emrick, T.; Russell, T. P.; Boker, A. *Phys. Chem. Chem. Phys.* **2007**, 6351-6358.

Leatherdale, C.; Kagan, C.; Morgan, N.; Empedocles, S.; Kastner, M.; Bawendi, M. *Phy. Rev. B* **2000**, *62*, 2669.

Lee, K. W.; Kowalczyk, S. P.; Shaw, J. M.; *Macromolecules* **1990**, *23*, 2097.

Lee, K.-B.; Kim, E.-Y.; Mirkin, C. A.; Wolinsky, S. M.; *Nano Lett.* **2004**, *4*, 1869.

Lee, L. A.; Wang, Q. *Nanomedicine* **2006,** *2*, 137-49.

Legrand, Y.-M.; Gray, M.; Cooke, G.; Rotello, V. M. *J. Am. Chem. Soc.*, **2003,** *125*, 15789.

Lemaur, V.; Steel, M.; Beljonne, D.; Brédas, J.-L.; Cornil, J. *J. Am. Chem. Soc.*, **2005**, *127*, 6077.

Li, M.; Yamato, K.; Ferguson, J. S.; Singarapu, K. K.; Szyperski, T.; Gong, B. *J. Am. Chem. Soc.* **2008**, *130*, 491.

Li, X. L.; Jia, Y.; Cao, A. Y. *ACS Nano* **2010**, *4*, 506;

Lim, S. I.; Zhong, C.-J. *Acc. Chem. Res.* **2009**, *42*, 798.

Lim, Y.-F.; Shu, Y.; Parkin, S. R.; Anthony, J. E.; Malliaras, G. G. *J. Mater. Chem.*, **2009**, *19*, 3049.

Lin, Y.; Skaff, H.; Boker, A.; Dinsmore, A. D.; Emrick, T.; Russell, T. P. *J. Am. Chem. Soc.* **2003**, *125*, 12690-12691.

Link, S.; El-Sayed, M. A. *Annu. Rev. Phy. Chem.* **2003**, *54*, 331.

Liu, D.-P.; Li, G.-D.; Su, Y.; Chen, J.-S. *Angew. Chem., Int. Ed.* **2006**, *45*, 7370.

Liu, H.; Mun, B.; Thornton, G.; Isaacs, S.; Shon, Y.-S.; Ogletree, D.; Salmeron, M. *Phy. Rev. B* **2005**, *72*, 155430.

Liu, J.; Tanaka, T.; Sivula, K.; Alivisatos, A. P.; Fréchet, J. M. J. *J. Am. Chem. Soc.*, **2004,** *126*, 6550.

Liu, X.; Fu, L.; Hong, S.; Dravid, V. P.; Mirkin, C. A.; *Adv. Mater.* **2002**, *14*, 231.

Liu, Y.; Summers, M. A.; Edder, C.; Fréchet, J. M. J.; McGehee, M. D. *Adv. Mater.*, **2005**, *17***,** 2960.

Lloyd, M. T.; Lim, Y.-F.; Malliaras, G. G. *Appl. Phys. Lett.*, **2008**, *92*, 143308.

Love, J. C.; Estroff, L. A.; Kriebel, J. K.; Nuzzo, R. G.; Whitesides, G. M. *Chem. Rev.* **2005**, *105*, 1103-1169.

Lu, A.-H.; Salabas, E. L.; Schüth, F. *Angew. Chem. Int. Ed.* **2007**, *46*, 1222.

Lu, N.; Gleiche, M.; Zheng, J.; Lenhert, S.; Xu, B.; Chi, L.; Fuchs, H.; *Adv. Mater.* **2002**, *14*, 1812;

Lu, X.; Rycenga, M.; Skrabalak, S. E.; Wiley, B.; Xia, Y. *Ann. Rev. Phys. Chem.* **2009**, *60*, 167–92.

Lu, Z.; Yin, Y. *Chem. Soc. Rev.* **2012**, *41*, 6874–87.

Luo, W.; Chan, E. W.; Yousaf, M. N. *J. Am. Chem. Soc.* **2010**, *132***,** 2614;

Luo, X.; Morrin, A.; Killard, A. J.; Smyth, M. R. *Electroanalysis* **2006**, *18*, 319–326.

MacBeath, G.; Schreiber, S. L. *Science* **2000**, *289*, 1760.

Mahalingam, V.; Onclin, S.; Péter, M.; Ravoo, B. J.; Huskens, J.; Reinhoudt, D. N. *Langmuir* **2004**, *20*, 11756–62.

Martin, J. I.; Nogues, J.; Liu, K.; Vicent, J. L.; Schuller, I. K. *J. Magn.Magn. Mater.* **2003**, *256*, 449;

Mayer, A.; Scully, S.; Hardin, B.; Rowell, M.; Mcgehee, M. *Mater.Today*, **2007,** *10*, 28.

McAlpine, M. C.; Friedman, R. S.; Lieber, C. M. *Nano Lett.* **2003**, *3*, 443.

McClelland, G. M.; Hart, M. W.; Rettner, C. T.; Best, M. E.; Carter, K. R.; Terris, B. D. *Appl. Phys. Lett.* **2002**, *81*, 1483.

Mele, E.; Di Benedetto, F.; Persano, L.; Cingolani, R.; Pisignano, D. *Nano Lett.* **2005**, *5*, 1915.

Miller, R.; Fainerman, V. B.; Makievski, A. V.; Kragel, J.; Grigoriev, D. O.; Kazakov, V. N.; Sinyachenko, O. V. *Adv. Colloid Interface Sci.* **2000**, *86*, 39-82.

Miranda, O.R.; Chen, H. T.; You, C. C.; Mortenson, D. E.; Yang, X. C.; Bunz, U. H. F.; Rotello, V. M.; *J. Am. Chem. Soc.* **2010,** 132, 5285.

Moores, A.; Goettmann, F. *New J. Chem.* **2006**, *30*, 1121.

Mott, N. *Proc. R. Soc. Lond. A* **1982**, *382*, 1–24.

Moyano, D. F.; Rotello, V. M. *Langmuir* **2011**, *27*, 10376-10385.

Mulder, A.; Huskens, J.; Reinhoudt, D. N. *Org. Biomol. Chem.* **2004**, *2*, 3409–24.

Muller, F.; Chemistry and Biochemistry of Flavoenzymes, CRC Press, Boca Raton, Volume I., 1991.

Murakami, M.; Ohkubo, K.; Fukuzumi, S. *Chem. Eur. J.*, **2010**, *16*, 7820.

Murray, C.; Kagan, C. R.; Bawendi, M. G. *Ann. Rev. Mater.* **2000**, *30*, 545–610.

Murray, R. W. *Chem. Rev.* **2008**, *108*, 2688;

Nie, Z.; Kumacheva, E. *Nat. Mater.* **2008**, *7*, 277.

Niemz, A.; Imbriglio, J.; Rotello, V. M. *J. Am. Chem. Soc.*, **1997**, *119*, 887.

Nikolic, M. S.; Krack, M.; Aleksandrovic, V.; Kornowski, A.; Foerster, S.; Weller, H. *Angew. Chem. Int. Ed.* **2006**, *45*, 6577-6580.

Nuzzo, R. G.; Smolinsky, G.; *Macromolecules* **1984**, *17*, 1013.

Ofir, Y.; Moran, I. W.; Subramani, C.; Carter, K. R. V. M. Rotello, *Adv. Mater.* **2010**, *22*, 3608;

Palermo, V.; Samorì, P. *Angew. Chem. Int. Ed.* **2007**, *46*, 4428–32.

Paraschiv, V.; Zapotoczny, S.; Jong, M. R. de; Vancso, G. J.; Huskens, J.; Reinhoudt, D. N. *Adv. Mater.* **2002**, *14*, 722.

Park, J.; Joo, J.; Kwon, S. G.; Jang, Y.; Hyeon, T. *Angew. Chem. Int. Ed.* **2007**, *46*, 4630–4660.

Park, J.-I.; Lee, W.-R.; Bae, S.-S.; Kim, Y. J.; Yoo, K.-H.; Cheon, J.; Kim, S. *J. Phys. Chem. B* **2005**, *109*, 13119–23.

Park, M.-H.; Ofir, Y.; Samanta, B.; Arumugam, P.; Miranda, O. R.; Rotello, V. M. *Adv. Mater* **2008**, *20*, 4185.

Park, S. Y.; Lytton-Jean, A. K. R.; Lee, B.; Weigand, S.; Schatz, G. C.; Mirkin, C. a *Nature* **2008**, *451*, 553–6.

Patra, D.; Malvankar, N.; Chin, E.; Tuominen, M.; Gu, Z.; Rotello, V. M. *Small* **2010**, *6*, 1402-1405.

Patra, D.; Ozdemir, F.; Miranda, O. R.; Samanta, B.; Sanyal, A.; Rotello, V. M. *Langmuir* **2009**, *25*, 13852-13854.

Patra, D.; Pagliuca, C.; Subramani, C.; Samanta, B.; Agasti, S. S.; Zainalabdeen, N.; Caldwell, S. T.; Cooke, G.; Rotello, V. M. *Chem. Commun.* **2009**, 4248-4250.

Patra, D.; Sanyal, A.; Rotello, V. M. *Chem. Asian J.* **2010**, *5*, 2442-2453.

Phizicky, E.; Bastiaens, P. I. H.; Zhu, H.; Snyder, M. ; Fields, S. *Nature* **2003**, *422*, 208.

Pieranski, P. *Phys. Rev. Lett.* **1980**, *45*, 569-572.

Pileni, M. P. *J. Phys. Chem. B* **2001**, *105*, 3358–3371.

Pisignano, D.; Persano, L.; Mele, E.; Visconti, P.; Anni, M.; Gigli, G.; Cingolani, R.; Favaretto, L.; Barbarella, G.; *Synth. Met.* **2005**, *153*, 237;

Pisignano, D.; Persano, L.; Raganato, M. F.; Visconti, P.; Cingolani, R.; Barbarella, G.; Favaretto, L.; Gigli, G.; *Adv. Mater.* **2004**, *16*, 525;

Pollino, J. M.; Stubbs, L. P.; Weck, M. *J. Am. Chem. Soc.* **2004**, *126*, 563.

Prabhakar A.; Mukherji, S. *Lab Chip* **2010**, *10*, 3422;

Pullerits, T.; Sundström, V. *Acc. Chem. Res.*, **1996**, *29*, 381.

Quaroni, L.; Chumanov, G. *J. Am. Chem. Soc.* **1999**, *121*, 10642–10643.

Rekharsky, M. V.; Inoue, Y. *Chem. Rev.* **1998**, *98*, 1875–1918.

Roberts, I. *Lipids* **1985**, *20*, 243.

Rodriguez, R.; Herrera, R.; Archer, L.A.; Giannelis, E.P. *Adv. Mater.* **2008**, *20*, 4353; e) Jespersen, M. L.; Mirau, P. A.; von Meerwall, E.; Vaia, R.A.; Rodriguez, R.; Giannelis, E.P. *ACS Nano* **2010,** *4*, 3735.

Rosen, M. J. *Surfactants and Interfacial Phenomena*, 3rd ed.; Wiley-Interscience, **2004**.

Rozkiewicz, D. I.; Kraan, Y.; Werten, M. W. T.; Wolf, F. A. d.; Subramaniam, V.; Ravoo, B. J.; Reinhoudt, D. N. *Chem. Eur. J.* **2006**, *12*, 6290.

Rozkiewicz, D.I.; Jańczewski, D.; Verboom, W.; Ravoo, B. J.; Reinhoudt, D. N. *Angew. Chem., Int. Ed.* **2006**, *45*, 5292.

Saha, K.; Agasti, S. S.; Kim, C.; Li, X.; Rotello, V. M. *Chem. Rev.* **2012**, *112*, 2739–2779.

Salaita, K.; Wang, Y.; Mirkin, C. A. *Nat Nano* **2007**, *2*, 145–55.

Samanta, B.; Yang, X.-C.; Ofir, Y.; Park, M.-H.; Patra, D.; Agasti, S. S.; Miranda, O. R.; Mo, Z.-H.; Rotello, V. M. *Angew. Chem. Int. Ed.* **2009**, *48*, 5341-5344.

Sangeetha, N. M.; Maitra, U. *Chem. Soc. Rev.* **2005**, *34*, 821.

Sankhe, A.Y.; Booth, B. D.; Wiker, N. J.; Kilbey, S. M. *Langmuir* **2005**, *21*, 5332;

Sargent, E. H. *Adv. Mater.* **2008**, *20*, 3958.

Schedelbeck, G. *Science* **1997**, *278*, 1792–1795.

Schönherr, H.; Hruska, Z.; Vancso, G. J. *Macromolecules* **1998**, *31*, 3679.

Serpe, M. J.; Craig, S. L. *Langmuir* **2007**, *23*, 1626.

Shevchenko, E. V.; Talapin, D. V.; Schnablegger, H.; Kornowski, A.; Festin, O.; Svedlindh, P.; Haase, M.; Weller, H. *J. Am. Chem. Soc.* **2003**, *125*, 9090–101.

Shi, N. E.; Dong, H.; Yin, G.; Xu, Z.; Li, S. H. *Adv. Funct. Mater.* **2007**, *17*, 1837.

Shin, W. S.; Jeong, H. H.; Kim, M.-K.; Jin, S.-H.; Kim, M. R.; Lee, J. K.; Lee, J. W. J.; Gal, Y.-S. *J. Mater. Chem.*, **2006**, *16*, 384.

Shipway, A. N.; Katz, E.; Willner, I. *ChemPhysChem* **2000**, *1*, 18–52.

Shoaee, S.; Clarke, T. M.; Huang, C.; Barlow, S.; Marder, S. R.; Heeney, M.; McCulloch, I.; Durrant, J. R. *J. Am. Chem. Soc.*, **2010**, *132*, 12919.

Silva, R.; Muniz, E. C.; Rubira, A. F. *Langmuir* **2009**, *25*, 873.

Sivaramakrishnan, S.; Chia, P.-J.; Yeo, Y.-C.; Chua, L.-L.; Ho, P. K. H. *Nat Mater.* **2007**, *6*, 149.

Skaff, H.; Lin, Y.; Tangirala, R.; Breitenkamp, K.; Boker, A.; Russell, T. P.; Emrick, T. *Adv. Mater.* **2005**, *17*, 2082-2086.

Sonar, P.; Ng, G.-M.; Lin, T. T.; Dodabalapur, A.; Chen, Z.-K. *J. Mater. Chem.*, **2010**, 20, 3626.

Song, J.; Gunst, U.; Arlinghaus, H. F.; Vancso, G. J. *Appl. Surf. Sci.* **2007**, *253*, 9489.

Soreni-Harari, M.; Yaacobi-Gross, N.; Steiner, D.; Aharoni, A.; Banin, U.; Millo, O.; Tessler, N. *Nano lett.* **2008**, *8*, 678–84.

South, C. R.; Burd, C.; Weck, M. *Acc. Chem. Res.* **2007**, *40*, 63.

Srivastava, S.; Samanta, B.; Jordan, B. J.; Hong, R.; Xiao, Q.; Tuominen, M. T.; Rotello, V. M. *J. Am. Chem. Soc.* **2007**, *129*, 11776–80.

Stanley, R. J.; MacFarlane, A. W. IV *J. Phys. Chem. A*, **2000**, *104*, 6989.

Steigerwald, M. L.; Brus, L. E. *Acc. Chem. Res.* **1990**, *23*, 183–188.

Subramani, C.; Dickert, S.; Yeh, Y.-C.; Tuominen, M. T.; Rotello, V. M. *Langmuir* **2011,** *27*, 1543;

Subramani, C.; Ofir, Y.; Patra, D.; Jordan, B. J.; Moran, I. W.; Park, M.-H.; Carter, K. R.; Rotello, V. M.; *Adv. Funct. Mater.* **2009**, *19*, 2937.

Sun, B.; Marx, E.; Greenham, N. C. *Nano Lett.*, **2003**, *3*, 961.

Sun, S. *Adv. Mater.* **2006**, *18*, 393–403.

Sun, S.; Zeng, H.; Robinson, D. B.; Raoux, S.; Rice, P. M.; Wang, S. X.; Li, G. *J. Am. Chem. Soc.* **2004**, *126*, 273.

Sun, S.-S.; *Mater. Sci. Eng. B,* **2005**, *116*, 251.

Talapin, D. V.; Murray, C. B. *Science* **2005**, *310*, 86–9.

Talapin, D. V.; Rogach, A. L.; Kornowski, A.; Haase, M.; Weller, H. *Nano Lett.* **2001**, *1*, 207–211.

Talapin, D.V.; Lee, J.-S.; Kovalenko, M. V.; Shevchenko, E.V. *Chem. Rev.* **2010**, *110*, 389.

Taleb, A.; Petit, C.; Pileni, M. P. *J. Phys. Chem. B* **1998**, *102*, 2214–2220.

Tans, S. J.; Dekker, C.; *Nature* **2000**, *404*, 834;

Tao, A. R.; Habas, S.; Yang, P. *Small* **2008**, *4*, 310–325.

Tao, N. J. *Nat. Nano.* **2006**, *1*, 173–81.

Templeton, A. C.; Wuelfing, M. P.; Murray, R. W. *Acc. Chem. Res.* **2000**, *33*, 27.

ten Brinke, G.; Ruokolainen, J.; Ikkala, O. in *Hydrogen Bonded Polymers, Vol. 207*, **2007**, pp. 113.

Terrill, R. H.; Postlethwaite, T. A.; Chen, C.-H; Poon, C.-D.; Terzis, A.; Chen, A.; Hutchison, J. E.; Clark, M. R.; Wignall, G. *J. Am. Chem. Soc.* **1995**, *117*, 12537.

Thibault, R. J.; Uzun, O.; Hong, R.; Rotello, V. M. *Adv. Mater.* **2006**, *18*, 2179.

Tricoli, A.; Pratsinis, S. E. *Nature Nanotech*. **2010**, *5*, 54;

Trindade, T.; O'Brien, P.; Pickett, N. L. *Chem. Mater.* **2001**, *13*, 3843.

Upadhyayula, V. K. K. *Anal. Chim. Acta.* **2012**, *715*, 1–18.

Uzun, O.; Sanyal, A.; Nakade, H.; Thibault, R. J.; Rotello, V. M. *J. Am. Chem. Soc.* **2004**, *126*, 14773.

Vanmaekelbergh, D.; Liljeroth, P. *Chem. Soc. Rev.* **2005**, *34*, 299–312.

Wang, B.; Wang, M.; Zhang, H.; Sobal, N. S.; Tong, W.; Gao, C.; Wang, Y.; Giersig, M.; Wang, D.; Moehwald, H. *Phys. Chem. Chem. Phys.* **2007**, *9*, 6313-6318.

Wang, G. R.; Wang, L.; Rendeng, Q.; Wang, J.; Luo, J.; Zhong, C.-J. *J. Mater. Chem.* **2007**, *17*, 457;

Wang, H.-T.; Nafday, O. a.; Haaheim, J. R.; Tevaarwerk, E.; Amro, N. a.; Sanedrin, R. G.; Chang, C.-Y.; Ren, F.; Pearton, S. J. *Appl. Phys. Lett.* **2008**, *93*, 143105.

Warren, S.C.; Banholzer, M. J.; Slaughter, L. S.; Giannelis, E. P.; DiSalvo, F. J.; Wiesner, U. B. *J. Am. Chem. Soc.* **2006**, *128*, 12074;

Wei, D.; Baral, J. K.; Osterbacka, R.; Ivaska, A. *J. Mater. Chem.* **2008**, *18*, 1853.

Werts,M. H. V.; Lambert, M.; Bourgoin, J.-P.; Brust, M. *Nano Lett.* **2002**, *2*, 43.

Wessels, J. M.; Nothofer, H.-G.; Ford, W. E.; Wrochem, F. von; Scholz, F.; Vossmeyer, T.; Schroedter, A.; Weller, H.; Yasuda, A. *J. Am. Chem. Soc.* **2004**, *126*, 3349–56.

Whitesides, G. M.; Mathias, J. P.; Seto, C. T. *Science* **1991**, *254*, 1312.

Wilson, D. S.; Nock, S. *Angew. Chem. Inter. Ed.* **2003**, *42*, 494.

Wollenweber, C.; Makievski, A. V.; Miller, R.; Daniels, R. *Colloids Surf., A* **2000**, *172*, 91-101.

Woo, C. H.; Holcombe, T. W.; Unruh, D. A.; Sellinger, A.; Fréchet, J. M. J. *Chem. Mater*., **2010**, *22*, 1673.

Wu, W.; Cui, B.; Sun, X. Y.; Zhang, W.; Zhuang, L.; Kong, L. S.; Chou, S. Y. *J. Vac. Sci. Technol. B* **1998**, *16*, 3825;

Xia, D.; Brueck, S. R. J. *Nano Lett.* **2004**, *4*, 1295.

Xia, Y. N.; Whitesides, G. M.; *J. Am. Chem. Soc.* **1995**, *117*, 3274;

Xia, Y.; Whitesides, G. M. *Angew. Chem. Int. Ed.* **1998**, *37*, 550.

Yaacobi-Gross, N.; Garphunkin, N. *ACS Nano* **2012**, 3128–3133.

Yan, M.; Harnish, B. *Adv. Mater.* **2003**, *15*, 244.

Yang, X.-C.; Samanta, B.; Agasti, S. S.; Jeong, Y.; Zhu, Z.-J.; Rana, S.; Miranda, O. R.; Rotello, V. M. *Angew. Chem. Int. Ed.* **2011**, *50*, 477-481.

Yin, J.; Hu, P.; Luo, J.; Wang, L.; Cohen, M. F.; Zhong, C.-J. *ACS Nano* **2011**, *5*, 6516;

Yin, Y.; Alivisatos, A. P. *Nature* **2005**, *437*, 664–70.

You, C. C.; Miranda, O. R.; Gider, B.; Ghosh, P. S.; Kim, I. B.; Erdogan, B.; Krovi, S. A.; Bunz, U. H. F.; Rotello, V. M.; *Nat. Nanotechnol*. **2007,** 2, 318.

Yount, W. C.; Loveless, D. M.; Craig, S. L.; *J. Am. Chem. Soc.* **2005**, *127*, 14488.

Zabet-Khosousi, A.; Dhirani, A.-A. *Chem. Rev.* **2008**, *108*, 4072–4124.

Zabet-Khosousi, A.; Trudeau, P.-E.; Suganuma, Y.; Dhirani, A.-A.; Statt, B. *Phys. Rev. Lett.* **2006**, *96*, 2–5.

Zhang, Y.; Gu, H.; Yang, Z.; Xu, B. *J. Am. Chem. Soc.* **2003**, *125*, 13680.

Zheng, H.; Lee, I.; Rubner, M. F.; Hammond, P. T. *Adv. Mater.* **2002**, *14*, 569.

Zhou, Y.; Li, Y.; Zhong, H.; Hou, J.; Ding, Y.; Yang, C.; Li, Y. *Nanotechnology*, **2006**, *17*, 4041.

Zhou,T.; Jia, T.; Kang, B.; Li, F.; Fahlman, M.; Wang, Y. *Adv. Energy Mater.*, **2011**, *1*, 431.

Zirbs, R.; Kienberger, F.; Hinterdorfer, P.; Binder, W. H. *Langmuir* **2005**, *21*, 8414–21.